

MONITORING SMALL SCALE EXPLOSIVE ACTIVITY AS A PRECURSOR  
TO PERIODS OF HEIGHTENED VOLCANIC UNREST

By

Anna K. Worden

RECOMMENDED:



Dr. Douglas Christensen

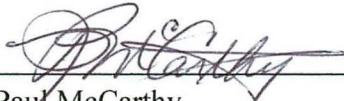


Dr. Peter Webley



Dr. Jonathan Dehn

Advisory Committee Chair



Dr. Paul McCarthy

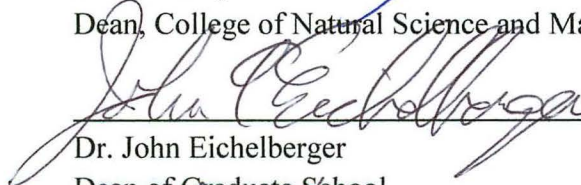
Chair, Department of Geology and Geophysics

APPROVED:



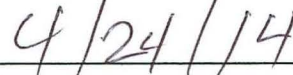
Dr. Paul Layer

Dean, College of Natural Science and Mathematics



Dr. John Eichelberger

Dean of Graduate School



Date



MONITORING SMALL SCALE EXPLOSIVE ACTIVITY AS A PRECURSOR  
TO PERIODS OF HEIGHTENED VOLCANIC UNREST

A  
THESIS

Presented to the Faculty  
of the University of Alaska Fairbanks

in Partial Fulfillment of the Requirements  
for the Degree of

MASTER OF SCIENCE

By  
Anna K. Worden, B.S.

Fairbanks, Alaska

May, 2014

## **Abstract**

Volcanic activity can pose a threat to the public and infrastructure. This threat is mitigated by monitoring volcanoes and volcanic activity. In many places this can be hindered by remote location and high cost. Satellite remote sensing is a tool that can be used to safely monitor volcanic activity and aid in the mitigation of hazards and the implementation of hazard preparedness. Small scale explosive activity is often a precursor to periods of heightened volcanic activity. This activity is typified by distinct small explosions that eject hot material onto the flanks of a volcano and can be detected as thermal anomalies by satellite sensors. The aim of this study is to develop a monitoring tool to detect changes in the frequency of small explosions leading up to periods of activity with ash plumes and other volcanic activity. Development of this method was carried out on Stromboli Volcano in Italy, a very reliably eruptive volcano with a wide variety of other monitoring instrumentation collecting data. Once developed, the method was applied to three remote volcanoes in the North Pacific: (1) Chuginadak (Mt. Cleveland) and (2) Shishaldin in Alaska, USA; and (3) Karymsky Volcano in Kamchatka, Russia. The results produced at all four of these volcanoes showed distinct trends in activity, unique to each volcano, prior to periods of heightened eruptive activity. The method provides a baseline for the detection of precursory activity and these trends can be used on other volcanoes undergoing similar types and patterns of eruptive activity.



## Table of Contents

	Page
Signature Page .....	i
Title Page .....	iii
Abstract .....	v
Table of Contents .....	vii
List of Figures .....	xi
List of Tables .....	xiii
Acknowledgements .....	xv
Chapter One - Introduction .....	1
1.1 Background .....	1
1.2 Remote Sensing as a Monitoring Tool .....	1
1.3 Activity of Interest: Small Scale Explosive Activity .....	2
1.4 Aim of Research .....	2
1.5 Experimental Setting (Volcanoes) .....	3
Chapter Two – Frequency Based Detection and Monitoring of Small Scale Explosive Activity .....	7
2.1 Abstract .....	7
2.2 Introduction .....	8
2.2.1 Background .....	9
2.2.2 Small Scale Explosive Activity – Strombolian Explosions .....	10
2.2.3 Source and Transience of Thermal Anomalies .....	12
2.2.3.1 Thermal Source .....	12
2.2.3.2 Spatial Distribution .....	14
2.2.3.3 Cooling Rate .....	14
2.3 Materials and Methods .....	16
2.3.1 Materials .....	16
2.3.1.1 Satellite Data .....	16

2.3.1.2 Thermal Camera Imagery.....	18
2.3.1.3 Other Data .....	21
2.3.2 Methods.....	23
2.3.2.1 Database Retrieval.....	23
2.3.2.2 Development of Processing Routine .....	25
2.3.2.3 Statistical Analysis .....	27
2.3.2.4 Thermal Camera and Satellite Comparisons .....	28
2.4 Results.....	30
2.4.1 Spatter Field Measurements .....	30
2.4.1.1 Spatter Field Thermal Flux.....	31
2.4.2 Results of Statistical Analysis .....	32
2.5 Discussion.....	33
2.5.1 Feasibility of Method .....	33
2.5.2 Factors for a Statistically Valid Methodology .....	35
2.5.2.1 Continuous and Continually Populated Dataset.....	36
2.5.2.2 Appropriate Satellite Resolutions (Spatial and Temporal).....	37
2.5.2.3 Recorded History of Volcano.....	37
2.5.2.4 Ground Based Monitoring Systems .....	38
2.5.3 Potential for Future Work.....	38
2.6 Conclusion .....	38
2.7 Acknowledgements.....	39
2.8 References.....	39
Chapter Three – Frequency Based Satellite Monitoring of Small Scale Explosive	
Activity at Remote North Pacific Volcanoes.....	51
3.1 Abstract.....	51
3.2 Introduction.....	52
3.3 Background.....	53
3.3.1 Volcanoes that Exhibit Small Scale Explosive Activity .....	54
3.3.1.1 Chuginadak (Mt. Cleveland), Alaska.....	55

3.3.1.2 Shishaldin, Alaska .....	57
3.3.1.3 Karymsky, Kamchatka .....	60
3.3.2 Thermal Anomalies: Determination of Source and Transient Nature .....	62
3.3.2.1 Small Scale Explosive Activity .....	62
3.3.2.2 Thermal Source .....	62
3.3.2.3 Spatial Distribution.....	63
3.3.2.4 Cooling Rate.....	64
3.4 Available Data and Methodologies Applied.....	65
3.4.1 Available Data.....	65
3.4.1.1 Satellite Remote Sensing.....	65
3.4.1.2 Other Data Available for Study.....	66
3.4.2 Methodology Applied to Satellite Data.....	68
3.4.2.1 Description of Satellite Method .....	68
3.4.2.2 Database Retrieval.....	69
3.4.2.3 Processing Routines Applied to Satellite Data.....	71
3.4.2.4 Statistical Analysis .....	73
3.5 Results.....	73
3.5.1 Chuginadak (Mt. Cleveland), Alaska .....	73
3.5.2 Shishaldin, Alaska .....	74
3.5.3 Karymsky, Kamchatka .....	75
3.6 Discussion.....	76
3.6.1 Trends in Activity.....	76
3.6.1.1 Cleveland.....	77
3.6.1.2 Shishaldin .....	78
3.6.1.3 Karymsky .....	78
3.6.2 Factors for a Statistically Valid Methodology .....	79
3.6.2.1 Dataset Population.....	81
3.6.2.2 Spatial and Temporal Resolution .....	81



3.6.2.3 Recorded History.....	82
3.6.2.4 Ground-Based Observations and Monitoring.....	82
3.7 Conclusion .....	83
3.8 Acknowledgements.....	84
3.9 References.....	85
Chapter Four – Conclusions.....	101
4.1. Summary of Findings .....	101
4.2. Method Development .....	102
4.3. Method Application.....	104
4.4. Future Work.....	105
References.....	107

## List of Figures

	Page
1.1 Map of Stromboli Volcano .....	4
1.2 Map of the North Pacific volcanic region.....	5
2.1 Location map of a) Stromboli Volcano, Italy .....	10
2.2 Loose, brittle backfill sitting atop the magma column .....	13
2.3 Cooling curve of two explosions from crater NE1. ....	15
2.4 Theoretical (a) and actual (b) pixel and field of view (FOV) size.....	19
2.5 Schematic diagram showing the geometries of FLIR.....	20
2.6 Database from Universita de Firenze.....	23
2.7 Frequency plot for satellite based estimated activity .....	33
2.8 Scaled comparison of the thermal camera detected explosions.....	35
3.1 Map of the North Pacific volcanic region.....	55
3.2 a) Location map of Mt. Cleveland .....	56
3.3 a) Location map of Shishaldin Volcano.....	58
3.4 Location map of Karymsky Volcano .....	61
3.5 Plot of estimated number of explosions per week .....	74
3.6 Plot of estimated number of explosions per week .....	75
3.7 Plot of estimated number of explosions per week .....	76
3.8 The strongest trends in activity .....	79
4.1 The strongest trends in activity .....	102



**List of Tables**

	Page
2.1 Detection statistics for multiple methods.....	22
2.2 Available data/images of Stromboli Volcano .....	24
2.3 Band math products .....	25
2.4 Results from multiple steps of the processing routine .....	27
2.5a Radiance values for two points in time.....	31
2.5b Detection thresholds for MODIS and ASTER sensors.....	31
3.1 Comparison of the spatial, spectral, and temporal resolutions .....	69
3.2 Summary of the available data for Shishaldin, Cleveland, and Karymsky .....	70
3.3 Band math products available for AVHRR data.....	71



## Acknowledgements

This thesis would not be possible without the support and help of a number of people. Firstly, a debt of gratitude must be paid to my committee. My advisor Jon Dehn introduced me to volcano remote sensing and took me under his wing to begin this thesis. He has been a constant for fun, learning, and adventures as he has accompanied me and sent me to volcanoes around the world. Peter Webley has proved himself invaluable in my understanding of satellites and sensors and has provided guidance throughout the writing process. Doug Christensen gave me my first Alaskan field work experience; hauling batteries to seismic stations. Doug was always there to answer questions, offer advice, and buy a beer. Thanks also to the staff and students at the University of Alaska Fairbanks department of Geology and Geophysics and Geophysical Institute who provided encouragement, support, and guidance during my time here.

Thanks to the numerous people I was able to meet through my field work in Italy: Andrew Harris (Université Blaise Pascal - Clermont Ferrand); Maurizio Ripepe, Dario delle Donna, Georgio Lacanna, and Emmanuel Marchetti (Universita di Firenze); Diego Coppola and Davide Piscopo (Universita degli studi di Torino); Catherine & Corrado, Mario 9-Fingers, and ZaZa (Stromboli Island)

Funding and support was given by the United States Geological Survey - Alaska Volcano Observatory. The researchers there aided by providing up to date data and analysis and were always welcome to helping students study Alaskan volcanoes.

My fiancé Chris, parents Greg and Katherine, and brother Carl have always supported me and offered words of encouragement. And finally, my Uncle Dick. I grew up hearing his stories of being a volcanologist and they must have stuck around long enough to persuade me to follow in his footsteps. I truly do not think I would be studying what I am today if he had not taken the time to entertain a young niece with his tales.

## **Chapter One**

### **Introduction**

#### **1.1 Background**

Volcanic activity can pose a threat to population centers, air traffic, and human infrastructure (Neal et al., 1997). Monitoring this activity offers a chance to implement safety plans and warn the public about what dangers a particular volcano poses. Many methods of monitoring are used on volcanoes around the world. Seismic networks are used to monitor the level of earthquake activity near volcanoes, as well as subsurface processes such as fluid movement and rock fracturing (McNutt, 1996). Infrasonic arrays can detect explosions and other acoustic signals (Fee and Matoza, 2013). Field based cameras and field observations can detect changes in snow cover, ground temperature, steaming, and other visual cues that may develop prior to an eruption. The one thing all these methods have in common is a requirement for a person to be near a volcano; which can be a dangerous prospect at an active volcano. For many volcanoes this can also be a very costly endeavor. For this reason, the development of monitoring methods based on remote sensing data from sensors aboard satellites is a beneficial and valuable enterprise.

#### **1.2 Remote Sensing as a Monitoring Tool**

Satellite remote sensing is a tool commonly used to monitor volcanic activity (Dehn et al., 2000; Harris et al., 2000; Dean et al., 2002; Webley et al., 2009; Dehn and Harris, 2014), though the focus is usually on viewing and analyzing images after some delay to detect activity. There has not been a great deal of work done on using satellite remote sensing as a tool to try and forecast what activity might occur in the future.

The mid-infrared wavelengths available on some sensors are especially useful in the detection of thermal activity (Wright et al., 2004; Dehn and Harris, 2014). Hot features, such as deposits from active volcanoes, are detectable in these wavelengths and can be

characterized and tracked by determining the size of the deposit, duration of visibility, and temperature of the material (Harris, 2013).

### **1.3 Activity of Interest: Small Scale Explosive Activity**

Small scale explosive activity is one of the most common types of activity on Earth and can occur at shield, composite, and cinder cone volcanoes (Simkin and Siebert, 1994; Siebert and Simkin, 2002). It can occur in conjunction with fissure eruptions, dome destroying explosions, and other types of activity. This activity can be part of a larger eruptive suite, but can also be an indication of a change in the activity of a volcanic center. It is characterized by small explosions, potentially caused by gas slugs reaching the top of an open volcanic conduit system (Harris and Ripepe, 2007) or a volcanic system breaking the overpressure of a vent plugging dome. These explosions consist of ash, gasses, and juvenile volcanic material being ejected from a single vent. This material is either deposited on the flanks of the volcano or can fall back into the crater and cover the active vent, depending on the geometry of the specific volcano (Patrick et al., 2007). When the hot material is deposited on the flanks of the volcano it is potentially visible to satellites as a thermal anomaly, a feature that is detectably warmer than the typical background temperature. The transient nature of small explosions means that each detected thermal anomaly can be counted as a discrete event when determining the frequency of explosive activity.

### **1.4 Aim of Research**

The ability to monitor volcanic activity is of importance to ensure the safety of populations and infrastructure located near volcanoes. Unfortunately in many locations the ability to monitor volcanoes is hindered by hard to reach locations at remote volcanoes, costly monitoring, and the general unsafe nature of working on or near an active volcano.



The second chapter of this thesis will deal with the development of a monitoring method. This was achieved by working on a reliably eruptive volcano in a relatively easy to access and work area. Easy access to multiple monitoring methods in addition to satellite data from sensors that image the entire Earth provides an opportunity to connect eruptive activity in a way that will be useful at a number of volcanoes.

The third chapter will focus on using the method developed and molding it for specific use at remote volcanoes in the North Pacific, where field measurement can be a difficult, dangerous, and costly undertaking. Three volcanoes were chosen for this portion of the research as each volcano has a distinct geologic setting and activity level.

The fourth chapter will cover the general conclusions of the development process, the application of the methodology to other volcanoes, and the prospect of future work on this topic.

### **1.5 Experimental Setting (Volcanoes)**

A set of volcanoes were chosen based on their characteristic activity as well as the timing of this activity and their specific location and accessibility:

- *Stromboli, Italy*

Stromboli Volcano is located in the Aegean Sea, North of Sicily and is one of the most active volcanoes in the world (Judd, 1881; Rosi et al., 2000) (Figure 1.1).

The summit is composed of a number of active vents nestled within a shallow crater. The eruption currently underway began in 1934 (Barberi et al., 1993) and is characterized by regular explosions every 30 minutes or so with only a few short breaks or changes in activity (Bertagnini et al., 2011).

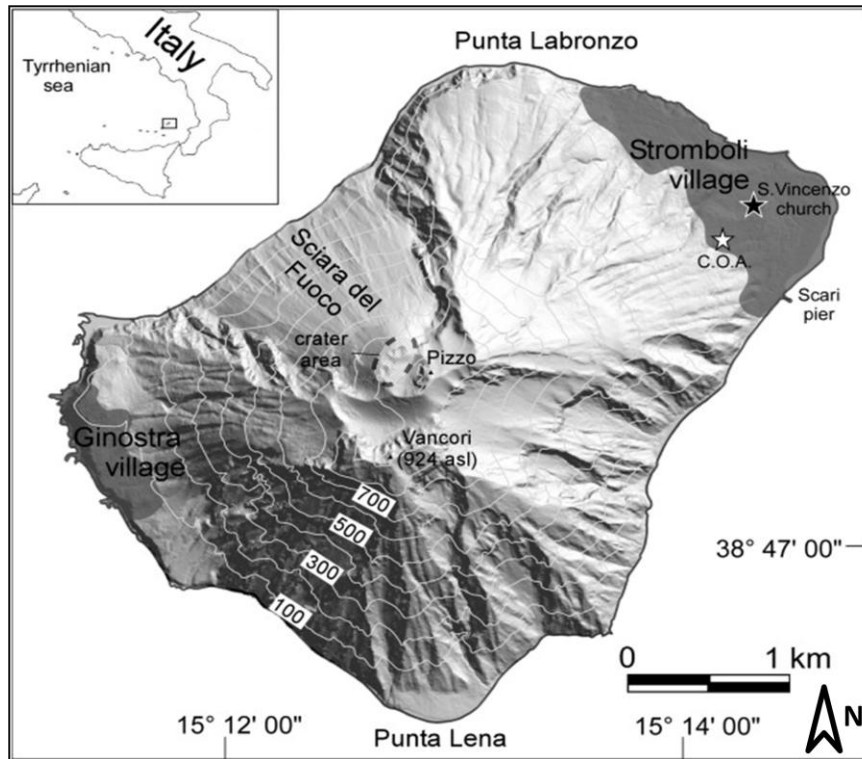


**Figure 1.1:** Map of Stromboli Volcano (modified from Bertolaso et al., 2009).

- *Mt. Chuginadak (Cleveland), Alaska, USA*

Mt. Cleveland is located on the western half of Chuginadak Island in the Aleutian Arc of Alaska (Figure 1.2). It is a stratocone volcano with a single active vent within a moderately shallow summit crater. Though the volcano is quite distant from large population centers, there are a number of small villages nearby. In addition, the airspace above Mt. Cleveland is the daily home to more than 10,000 passengers and millions of dollars in cargo on numerous air traffic routes (Neal et al., 1997). Mt. Cleveland is the most consistently active volcano in the Aleutian Arc (AVO, 2014a; GVP, 2014a) and has produced ash plumes up to 10 km above sea level (a.s.l.) during major eruptions with many lower level plumes occurring throughout its eruptive cycles (GVP, 2006, 2008, 2010). Lava flows, mud flows, dome building and destruction, and small summit explosions have also been reported at Cleveland.

- *Shishaldin, Alaska, USA*

Shishaldin is the highest peak (at 2857 m asl) in the Aleutians as well as one of the most active volcanoes in the arc (Neal et al., 1995) (Figure 1.2). Shishaldin volcano has had 27 recorded eruptions since 1775 including 2 dozen in the 20<sup>th</sup> century (Miller et al., 1998; Neal et al., 2004), most of which have involved small scale explosive activity, ash, and steam emissions (Neal et al., 1995). This volcano is a stratocone with a deep, steep sided summit crater, the site of the single active vent (Dehn et al., 2002). Shishaldin is unique in the set of volcanoes being studied here as it is fairly close to a number of population centers, posing a threat to people and infrastructure should a large eruption occur. Shishaldin is also the only volcano in this sample set with permanent seismic and infrasound networks (Caplan-Auerbach and McNutt, 2003), lending an interdisciplinary approach to volcano monitoring.



**Figure 1.2:** Map of the North Pacific volcanic region with the three volcanoes chosen for this study highlighted (modified from Hansell et al., 2006; Steinbeck and Fuller, 2004).

- *Karymsky, Kamchatka, Russia*

Karymsky volcano is located on the Kamchatka Peninsula (Figure 1.2). The volcano sits on the edge of a lake created by a large eruption nearly 8000 years ago (Braitseva et al., 1995). The stratocone has a single active vent within a shallow summit crater. There are numerous small towns and airports throughout the Kamchatka Peninsula, each within 600 km of the volcano. Karymsky is the most consistently active volcano in the Kamchatka Peninsula (KVERT, 2013; GVP, 2014c) and is a part of a volcanic complex with Academia Nauk and Maly Semiachik. The ongoing activity has been mostly made up of continuous small scale explosive activity accompanied by periods of effusive activity, pyroclastic flows, and frequent ash emissions (Ozerov et al., 2001). Regular explosions have been seen to send ash and gas to an altitude of 2 – 3 km above the vent (Izbekov, 2004). In the case of larger eruptions, ash can travel to heights of up to 10 km asl (KVERT, 2013).

## Chapter Two

### Frequency Based Detection and Monitoring of Small Scale Explosive Activity<sup>1</sup>

#### **2.1. Abstract**

Thermal activity is a common precursor to explosive volcanic activity. The ability to use these thermal precursors to monitor the volcano and obtain early warning about upcoming activity is beneficial for both human safety and infrastructure security. By using a very reliably active volcano, Stromboli Volcano in Italy, a method has been developed and tested to look at changes in the frequency of small scale explosive activity and how this activity changes prior to larger, ash producing explosive events. Thermal camera footage was used to designate parameters for typical explosions at Stromboli (size of spatter field, cooling rate, and frequency of explosions) and this information was applied to characterize explosions in satellite imagery. Satellite data from The National Aeronautics and Space Administration's (NASA) Moderate Resolution Imaging Spectroradiometer (MODIS) and US/Japan designed Advanced Spaceborne Thermal Emission and Reflection Radiometer (ASTER) for numerous periods in 2002 to 2009 were analyzed for thermal features which were used to calculate an estimate of the level of activity during the given time period. The results at Stromboli showed a high level of small scale explosions that stop completely prior to large paroxysmal eruptive episodes. This activity also corresponds well to seismic and infrasonic records at Stromboli, indicating that this thermal infrared monitoring method may be used in conjunction with other detection methods where available, and also indicates that it may be a useful method for volcano monitoring when other methods (e.g. seismic instrumentation, infrasound arrays, etc.) are not available.

---

<sup>1</sup> Worden, A., Dehn, J., Ripepe, M., and Delle Donne, D. (2014). Frequency based detection and monitoring of small scale explosive activity. *Journal of Volcanology and Geothermal Research*. (Submitted to Journal of Volcanology and Geothermal Research).

## 2.2. Introduction

Satellite remote sensing has proved to be a useful tool in the monitoring of volcanoes (Dehn et al., 2000; Harris et al., 2000; Dean et al., 2002; Webley et al., 2009; Dehn and Harris, 2014). This tool becomes especially useful at remote volcanoes where field work is not always feasible or ground observations are not available. Satellite sensors collect data that cover larger areas more frequently than is possible for researchers in the field. This data can be analyzed to monitor activity at volcanoes all over the world, regardless of location, activity, and instrumentation logistics.

In order to use the remote sensing capabilities to their fullest, it is important to develop a method using data/images from a variety of satellite sensors to determine the type and frequency of activity occurring on the ground. In developing this method, the use of a well studied, monitored, and frequently erupting volcano was essential. For this reason, Stromboli Volcano in Italy was chosen as our ‘test-case’. In addition, beginning with a well known and monitored volcano allows for identification of factors that could have a large impact at non-instrumented volcanoes. It is important to have a continuous data set, a known record of eruptive history, good temporal resolution, and appropriate spatial resolutions to get the optimal results with the best data set. A continuous baseline is also very important when considering the detection of changes in eruptive character and frequency. For most volcanoes, there are archives of satellite data available for use in the creation of such baselines; such as at the Alaska Volcano Observatory (AVO) Remote Sensing (RS) (Dean et al., 2002), National Oceanic and Atmospheric Administration (NOAA) Comprehensive Large Array-data Stewardship System (CLASS) website (NOAA CLASS, 2013), National Aeronautical and Space Administration (NASA) Moderate Resolution Imaging Spectroradiometer (MODIS) Rapid Response website (2013), MODVOLC System (Wright et al., 2004) ; it simply requires a consistent method for sorting through the data, analyzing the activity and statistically comparing them. The

aim is to better monitor the volcanoes, improve our understanding of the volcanic processes, and making use of any data made available.

### *2.2.1 Background*

Stromboli Volcano is located in the Aegean Sea, North of Sicily (Figure 2.1). This island has been referred to as the “Lighthouse of the Mediterranean” due to its regular and spectacular eruptive activity over the past 2000-2500 years (Judd, 1881; Rosi et al., 2000). A period of nearly continuous eruptive activity began in 1934 (Barberi et al., 1993) and has only been interrupted for short periods of time, usually associated with a slight change in eruptive behavior (Bertagnini et al., 2011).

The volcanism in the Tyrrhenian region has resulted from a complex series of subduction, rifting, basin formation, and extension (Ferrari and Manetti, 1993). Stromboli is the northernmost island in the Aeolian Arc, a portion of the larger Calabrian Arc, which is largely related to the subduction of the African Plate beneath the Eurasian Plate (Ferrari and Manetti, 1993). During the past 100,000 years the main eruptive centers on Stromboli have been focused in the central part of the cone at about 750-800m a.s.l. (Hornig-Kjarsgaard et al., 1993). The main cone is built up of calc-alkaline, potassic, and most recently, shoshonitic basalts (Francalanci, 1993).

The summit crater of Stromboli is composed of a dynamic complex of active and inactive vents (Chouet et al., 1974; GVN, 1988; GVN, 1990; GVN, 1991a; GVN, 1993; GVN, 1997; GVN, 2003). During the field work for this study (summer of 2010), there were a total of five vents, three of which were explosively active with the remaining two a fairly consistent source of gas puffing and emission (Figure 2.1b). Two vents (North-East crater 1 [NE1] and North-East crater 2 [NE2]) were chosen for focus in this study due to their eruptive nature, frequently depositing spatter fields onto the inner and outer flanks of the volcano.

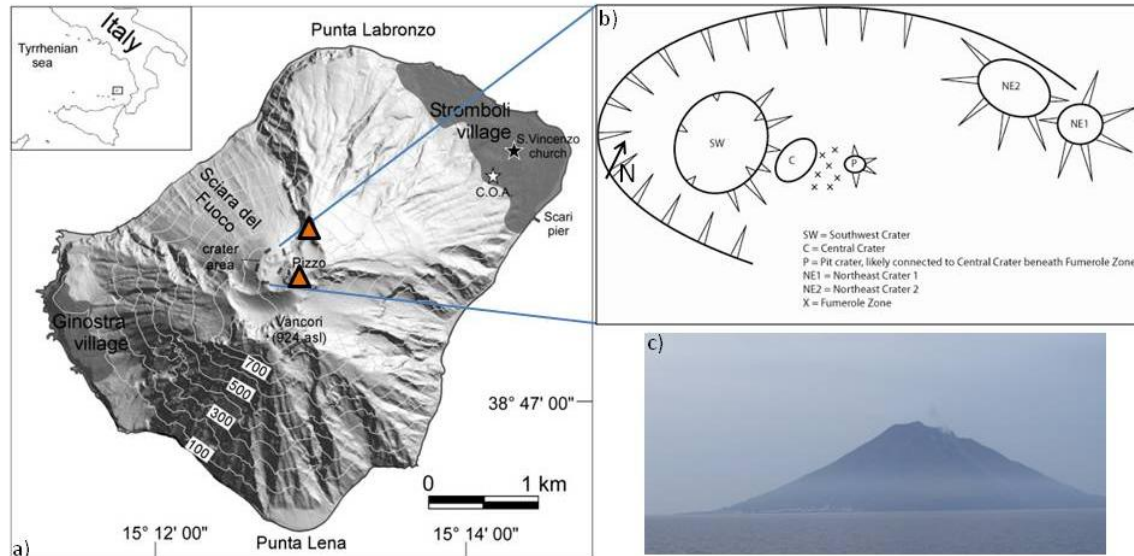


**Figure 2.1:** Location map of a) Stromboli Volcano, Italy (modified from Bertolaso et al., 2009) and b) a detailed sketch of the summit crater area during the 2010 field campaign. Locations of thermal camera deployment are marked with triangles in (a). Both camera locations were chosen to view NE1 and NE2 and were 250-400 meters from the vents. c) Stromboli is a stratovolcano in the Mediterranean Sea with an elevation of 924 m a.s.l.

### 2.2.2 Small Scale Explosive Activity – Strombolian Explosions

Small scale explosive activity is some of the most common volcanic activity on Earth, occurring at a large number of volcanoes around the world (e.g. Pacaya, Guatemala (GVN, 2007); Etna, Italy (Andronico et al., 2005); Paricutin, Mexico (Pioli et al., 2008); Villarrica and Llaima, Chile (Aguilera, 2005)). This type of activity occurs at shield, composite, and cinder cone volcanoes and can occur in conjunction with fissure eruptions, dome destroying explosions, and other types of activity. This activity can be part of a larger eruptive suite, but can also be an indication of a change in the activity of a volcanic center. For this latter reason, it is important to be able to monitor for the introduction or change in the character of small scale explosive activity, as these changes can lead to heightened levels of volcanism which can in turn threaten populations, communities, environments/habitats, and human infrastructure.



Small-scale explosive activity at Stromboli is characterized by transient explosions throwing molten material, as well as entrained edifice material, tens to hundreds of meters above the crater (Blackburn et al., 1976; Patrick et al., 2007; Harris and Ripepe, 2007). These explosions can also contain ash and volcanic gases. The ash portion of small explosions can be a product of fragmented juvenile material, but is more likely due to the mechanical erosion of edifice material or cooled crater infill from previous explosions. There are multiple possible mechanisms for small explosions. Some explosions are due to large gas slugs rising through a volcanic conduit and bursting at a free surface (dubbed strombolian explosions, due to the typical activity seen throughout history at Stromboli Volcano; Lacroix, 1904; Walker, 1973; Wohletz and Heiken, 1992). At other volcanoes, small explosions may be due to a buildup of pressure blowing a small plug or dome out of the vent ;e.g. Cleveland, Alaska, (D. Schneider, Pers. Comm., 2012); Redoubt, Alaska, (S. Prejean, Pers. Comm., 2009); Galeras, Columbia, (Stix et al., 1997); and Soufrière Hills, Montserrat, (Diller et al., 2006). There is also the possibility of a mixture of these two mechanisms, as each volcano has unique activity, crater geometry, magma plumbing system, and magma supply.

In the case of Stromboli Volcano, normal activity is similar to the description of typical strombolian activity above. However, violent strombolian activity and strombolian paroxysms are periods of activity including cessation of small explosions, lava flows, and much larger ash producing explosions (Macdonald, 1972; Barberi et al., 1993; Calvari et al., 2006; Rosi et al., 2006; Ripepe and Harris, 2008). The small explosions at Stromboli have been broken into two classes by Patrick et al. (2007). Type 1 explosions are mainly made up of coarse ballistic particles. Type 2 explosions contain some portion of ash, with Type 2a containing ash and ballistic material, and Type 2b having no ballistic material. These explosion types will be discussed in more detail in following sections.

### 2.2.3 *Source and Transience of Thermal Anomalies*

#### 2.2.3.1 *Thermal Source*

Small scale explosions produce spatter fields of hot, semi-molten bombs and other tephra. These spatter fields are the main component of the thermal signal that can be seen from various satellite platforms and their associated sensors (Dehn et al., 2000). These signals are indicative of a very recent eruption due to the fast cooling rate of material once it is deposited post-eruption. A feature is considered a thermal anomaly if any area of pixels in an image appear to be significantly (or detectably) brighter (and therefore warmer) than the background (Dehn et al., 2000; Dean et al., 2002). When processing data, considerations are made for viewing angle, volcano geometry, and other factors (Dehn and Harris, 2014). The visually detected anomalies indicate larger explosions that can change the radiant temperature of a pixel enough for detection. Smaller explosions are much more common and much harder to detect, though not impossible.

Patrick et al. (2007) describe the types of explosions at Stromboli and characterize them as either Type 1 or Type 2 explosions depending on their character and deposits (Figure 2.2). Type 1 explosions are dominated by coarse ballistic particles, incandescent material, and spatter with no associated ash emission. These explosions are likely the product of gas slug bursts at the surface of the magma column in an open vent scenario. Type 2 explosions are further broken into Type 2a, explosions with an optically thick ash plume in addition to ballistic particles, and Type 2b, explosions with an optically thick ash plume but no accompanying ballistic material. Both 2a and 2b explosions are the result of the bursting gas slug at the surface of the magma column in a choked vent scenario. In these instances, cooled material has filled in the vent area and limits the power of the explosion. This infill will also be the source of the ash portion of the explosion, as the energy released breaks up the material and forces it out of the vent. Types 1 and 2a will produce a spatter field on the volcanoes flanks and may be detectable by satellite sensors, though in Type 2a explosions ash plumes may obscure a sensors' view of the spatter.

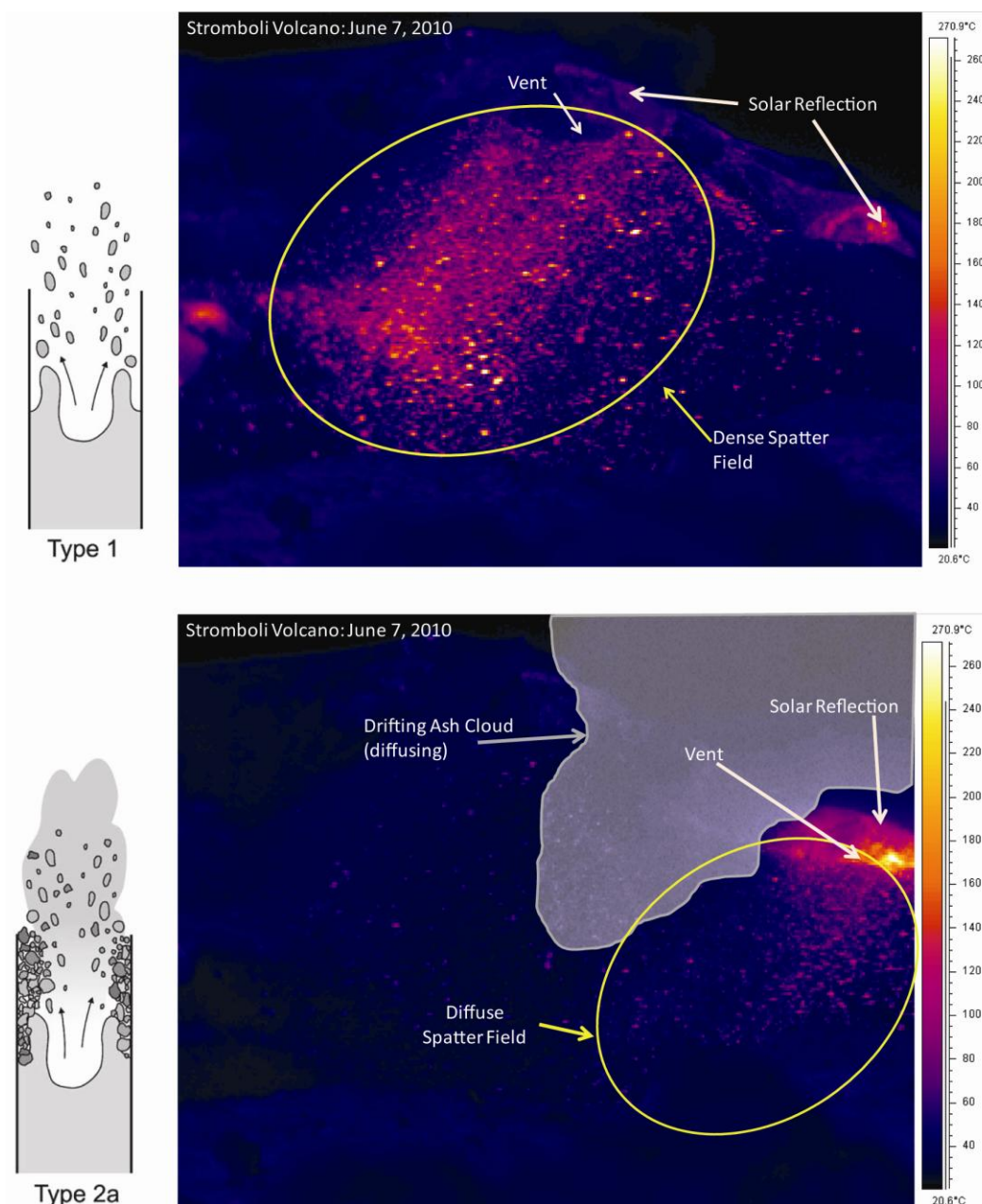


**Figure 2.2:** Loose, brittle backfill sitting atop the magma column is one of two scenarios that can lead to ash-rich strombolian eruptions (the other scenario, rheological changes due to degassing, is not depicted in this figure). Type 1: Gas slug bursts at unobstructed free surface, ejecting coarse ballistics. This will produce a relatively dense spatter field. An example explosion is shown from crater NE2 at Stromboli Volcano, June 7, 2010. Type 2a: High overpressure slug burst produces large scale disruption of backfill, producing ash and ballistics. These explosions were observed to produce a more diffuse and smaller spatter field. Views from sensors may also be obscured by drifting ash cloud. An example explosion is shown from crater NE1 at Stromboli Volcano, June 7, 2010. (Diagrams modified from Patrick et al., 2007).

### *2.2.3.2 Spatial Distribution*

The size of a spatter field is a direct result of the size of the explosion, the existence and amount of pre-eruptive crater infill, crater geometry, and the type of material erupted. For a Type 1 explosion the spatter field will consist of large semi-molten blobs, hot rocks, and other coarse ballistic material and may be quite large, as all the explosive energy is used to deposit this material (Harris and Ripepe, 2007; Patrick et al., 2007; Harris et al., 2013; Figure 2.2, Type 1). Type 2a explosion will likely form a small spatter field, but its size will depend on the amount of eruptive energy used to break through any crater infill. Type 2b explosions, resulting from an explosion through a vent completely choked with infill, will not produce a spatter field at all, as the only material to leave the vent will be gas and ash (Patrick et al., 2007). In these cases, all of the spatter is either constrained beneath the crater infill, or the energy required to break up the crater infill causes too weak an explosion to significantly distribute any juvenile material (Figure 2.2, Type 2a).

The size (or energy capacity) of an explosion will also be a large factor in the size of the resultant spatter field. A small, or low energy, explosion may not make it out of the crater, and therefore not create much of a spatter field. The size of an explosion and depth of crater go hand-in-hand in this respect, as a deeper crater will require an explosion of higher energy to create a detectable spatter field.

### *2.2.3.3 Cooling Rate*

While spatter fields are the source of the thermal signals they will cool quickly due to the high surface area of the bombs and ejecta combined with any environmental effects (such as wind, rain, and crater geometry). Modeled explosions as well as explosions at Stromboli Volcano during the 2010 field campaign were seen to cool below the detection threshold of thermal imagery within seconds to a few minutes (Figure 2.3). This rapid reduction of the thermal signal greatly limits the ability of satellite detection of these events. A spatter field produced from a small scale explosion will only stay hot (relative to its surroundings) for a short amount of time, a minute or two (Harris et al., 2013). As

an example, a volcano with 70 explosions per day will have hot material visible on the surface for approximately 70-140 minutes, or ~5-10% of the day. As this is a very small portion of the day, it is understandable that not all explosions will be detected in satellite imagery. However, by analyzing the number of explosions imaged and observing a volcano with multiple ground based sensors, the percentage of explosions detected in satellite data each day can be determined.

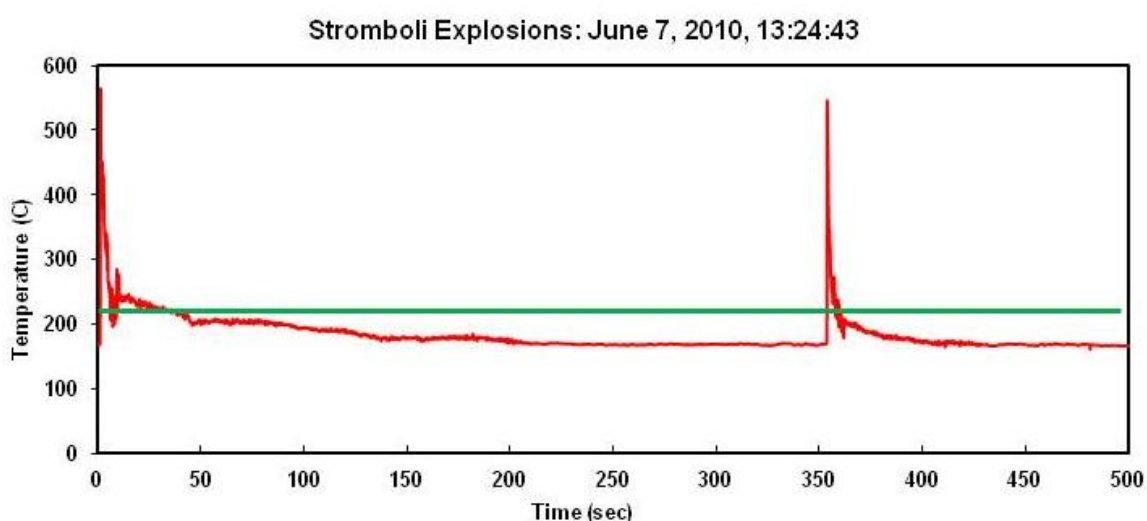


**Figure 2.3:** Cooling curve of two explosions from crater NE1 on June 7, 2010. The green line indicates the thermal detection threshold of the MODIS sensor. Only temperature above this line will be detectable in satellite images.

The duration of an explosion will play a part in determining the cooling rate of the spatter field. In some cases, an explosion would deposit material for up to 30 seconds to one minute. The thermal signal from these explosions would not only include the cooling spatter field, but would incorporate all the time during the explosion when hot material is constantly being supplied. There were very few of these explosions measured at Stromboli during the 2010 field campaign, but they can occur at other volcanoes with different vent geometry and conduit conditions.

## 2.3 Materials and Methods

### 2.3.1 Materials

#### 2.3.1.1 Satellite Data

NASA's MODIS sensor is aboard the polar orbiting Earth Observing System (EOS) satellites Terra and Aqua. MODIS collects data in 36 spectral bands from 0.62 $\mu\text{m}$ -14.385 $\mu\text{m}$ . Two subsets of this spectral window collect images in the thermal- and mid-infrared wavelengths and are used for the detection of thermal features on the ground (Wright et al., 2004; Dehn and Harris, 2014). Bands 20-22 collect data from 3.66 $\mu\text{m}$ -3.989 $\mu\text{m}$  and bands 31 and 32 collect data from 10.78 $\mu\text{m}$ -12.27 $\mu\text{m}$  (NASA MODIS Web, 2013). The MODIS sensors have a temporal resolution that images the entire surface of Earth every one to two days. This provides approximately 3 - 6 images a day at Stromboli (LP DAAC MODIS Overview, 2013).

The Advanced Spaceborne Thermal Emission and Reflection Radiometer (ASTER) is a US/Japan designed sensor also aboard NASA's EOS Terra satellite. As this sensor is co-located with a MODIS sensor, time coincident images can be captured from this satellite. ASTER is equipped to collect data in 15 spectral bands from 0.52 $\mu\text{m}$ -11.65 $\mu\text{m}$ . The short-wave infrared (SWIR) bands (measuring from 1.6 $\mu\text{m}$ -2.43 $\mu\text{m}$ ) are no longer functioning on ASTER with data only available prior to April, 2008 (NASA/JPL, 2009). This data can be used for retrospective analysis of very hot targets. The long-wave (thermal) infrared bands (TIR\_Band 10-14) are still collecting data at 8.125 $\mu\text{m}$ -11.65 $\mu\text{m}$ , which is a spectral window comparable to some of the infrared bands collected by MODIS (Abrams et al., 2002). The ASTER sensor is a tasked sensor, meaning that it only records images when they are requested (Duda et al., 2009). At times of elevated volcanic activity the ASTER sensor can be scheduled to capture imagery of the area (NASA ASTER Urgent Request Protocol) (Duda et al., 2009). This was carried out at

Stromboli in 2003 and 2006 during the larger eruptions which included explosive activity, ash plumes, and lava flows. (LP DAAC ASTER Overview, 2013)

### *Spatial Resolution and Pixel Averaging*

The MODIS data used has a satellite pixel size of 1km at nadir (Figure 2.4a). As the sensor moves from nadir, the pixel size will be distorted (Patrick, 2002; Lillesand et al., 2008). Stromboli Island has a surface area of about 12.5 km and is represented by 12 – 15 pixels (whole and partial) in each MODIS satellite image. For moderate and larger sized explosions, the majority of activity seen historically (GVN, 1989; GVN, 1991b; GVN, 1994; GVN, 2000), this spatial resolution is adequate to detect a thermal signal, though the smallest explosions are likely missed. The size of a spatter field is a direct result of the size of the explosion, the existence or amount of crater infill, crater geometry, and the type of material erupted. Smaller explosions and deep craters will lead to less detectable spatter fields. The angle and velocity at which debris is erupted will impact the size and emplacement of the spatter fields (Figure 2.4b); a smaller eruption angle will produce a smaller field, a low velocity explosion will cover less area and remain close to the vent. The topography of the volcanic edifice will influence a spatter field and how it is imaged by a sensor. Steeply sloping flanks combined with a varying look angle can lead to differing degrees of pixel distortion (Dehn et al., 2002).

The ASTER sensor has a spatial resolution of 90 m (at nadir) in the bands used for the detection of volcanic thermal anomalies (Figure 2.4a). This creates a counter problem from the lower resolution satellites, in that as this resolution is so small it will almost always show hot pixels related to elevated ground temperature unassociated with eruptions, fumaroles, degassing, and cooling material (Harris and Stevenson, 1997). This occurs because the smaller resolution means that more area of each pixel will be filled with the hot target and so the pixel averaging (if any) will result in a much warmer temperature. In some locations, this is a big advantage in detecting thermal activity. However, at Stromboli, it can be a hindrance as the activity is frequent and there are

many constantly active fumarolic vents (Harris and Stevenson, 1997; Harris and Ripepe, 2007).

One important factor to consider when discussing the spatial coverage of the spatter fields is the process of satellite pixel averaging. When a sensor captures an image of an area, it breaks the information into pixels. The MODIS sensor represents thermal information in elliptical pixels of 1 km diameter ( $0.785 \text{ km}^2$  area). This means that the temperatures of any features within that pixels area will be averaged to produce the single temperature value assigned to that pixel. For example, if there is a cool ( $0^\circ\text{C}$ ) background covering  $0.735 \text{ km}^2$  and a small hot ( $500^\circ\text{C}$ ) feature, like a lava flow, covering the remaining  $0.05 \text{ km}^2$ , a pixel temperature value of only  $25^\circ\text{C}$  will occur.

#### *2.3.1.2 Thermal Camera Imagery*

A FLIR (Forward Looking Infrared Radiometer) Systems ThermaCAM™ S40 camera was used from May 29 – June 9, 2010 to record explosions from craters NE1 and NE2 at Stromboli Volcano in Italy (Figure 2.1). The camera uses an uncooled microbolometer to detect and record images in a thermal band at  $7.5 - 13 \mu\text{m}$  and at a temperature range of  $0 - 500^\circ\text{C}$  and frequency of 7.5 Hz. The camera was located at multiple locations at a distance of 250 - 400 meters from the active vents, producing a field of view (FOV) ranging (320 x 240 pixel) from 100 - 150 meters across with a single pixel measuring 33.2-53.1 cm across, respectively (Figure 2.4b and Figure 2.5). The camera was focused so that the FOV would capture the volcano flank and spatter field with little of the image taken up by sky. Approximately 130 explosions were recorded and analyzed.



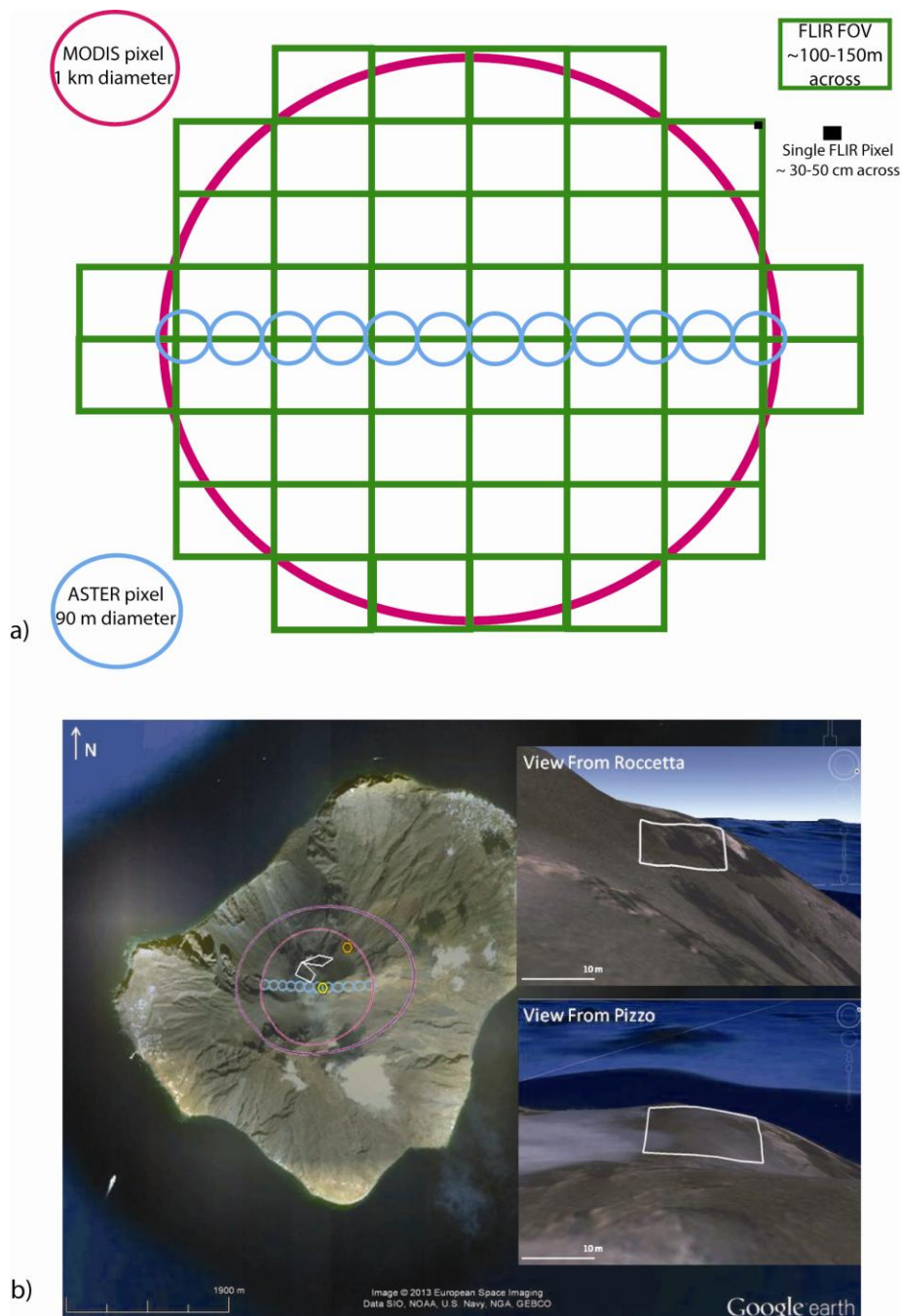


**Figure 2.4:** Theoretical (a) and actual (b) pixel and field of view (FOV) size comparison. (b) Area of MODIS Pixel: at nadir (pink) =  $0.785 \text{ km}^2$ , at  $40^\circ$  sat. zen. (purple) =  $1.74 \text{ km}^2$ . Area of ASTER Pixel at nadir (blue) =  $0.006 \text{ km}^2$ . Area of FLIR Field of View (FOV) (white) =  $\sim 0.017 \text{ km}^2$ . Orange Circle = Rocetta Camera location. Yellow Circle = Pizzo Camera Location. Note the skewing of FLIR pixels when seen from overhead. The views from Rocetta and Pizzo show a rectangular FLIR FOV, but when the view is adjusted to overhead, the rectangles are greatly skewed due to topographic effects.

Thermal camera images were also obtained from periods during the summers of 2002, 2003, and 2008 (see Harris et al., 2005; Calvari et al., 2005; Patrick et al., 2007). Though these images are not used here for specific spatter field analysis (due to frame of view focus), they are used to compare location and magnitude of explosive activity at Stromboli over the years, thus enhancing the temporal resolution of the dataset collected in 2010.

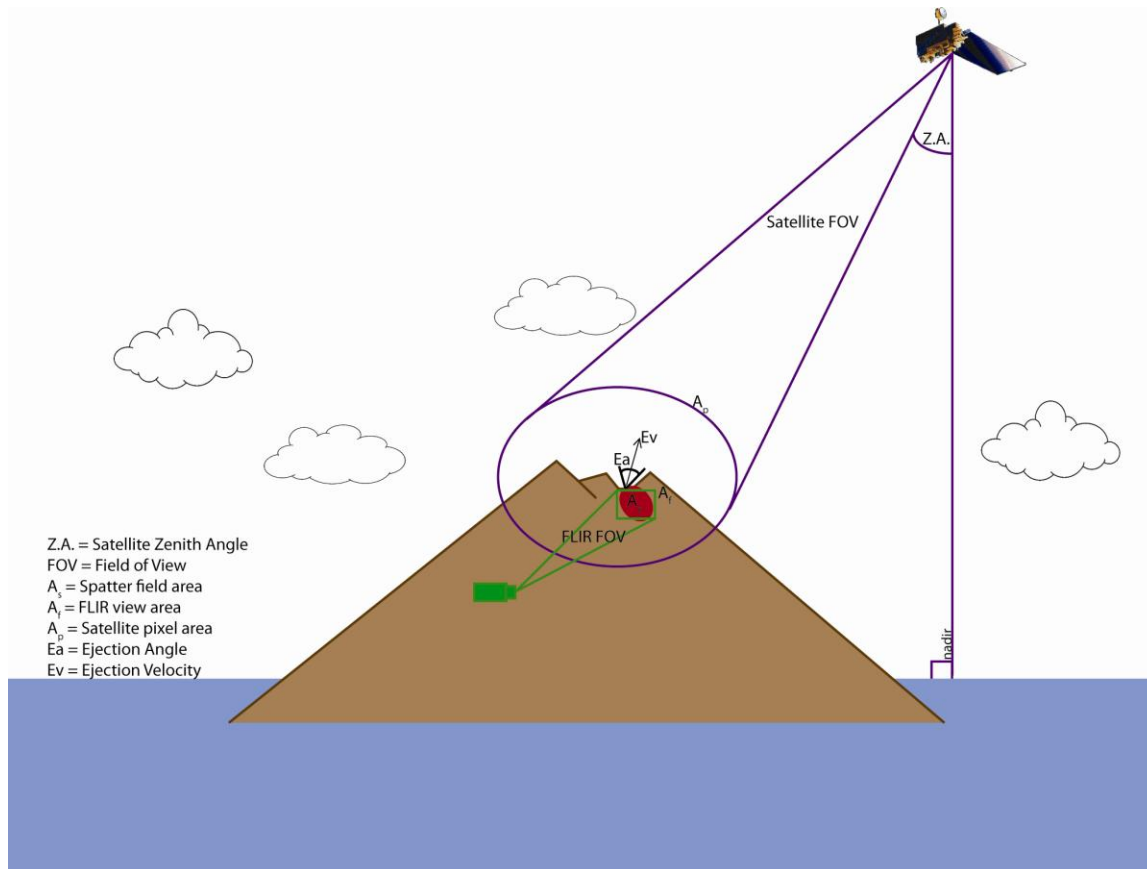


**Figure 2.5:** Schematic diagram showing the geometries of FLIR sensor and satellite sensors as they relate to the work performed at Stromboli Volcano. A satellite will record data/images at a variety of zenith angles, causing different degrees of pixel stretching. Thermal camera images will remain at a constant field of view, though that view will be dependent on the topography of the area of interest. Pixel stretching due to zenith angle can also be seen in Figure 2.2(b).

### *2.3.1.3 Other Data*

At Stromboli Volcano, there is a long, near-continuous, record of seismic and infrasonic activity (Neuberg and Luckett, 1996; Ripepe et al., 2007; Harris and Ripepe, 2007) as well as an analog recording of thermal activity from the north-east (NE) vents since 2003 recorded by the Dipartimento di Scienze della Terra at Universita di Firenze (UF) (Ripepe et al., 2008). The network deployed and utilized by the Scienze della Terra at UF currently operates four seismo-acoustic stations (Neuberg and Luckett, 1996), two thermal imaging cameras (Ripepe et al., 2008), three tilt-meters, one weather station, a five element infrasound array, 2 geochemical/radon sensors, and one wave monitoring sensor located off the coast of Punta dei Corvi (UF, 2011). Data is collected from these sensors and is then reported in an information release by Universita degli Studi di Firenze, Dipartimento di Scienze della Terra. This extensive multi-disciplinary network allows the best use of the limited satellite data for the statistical method of frequency detection, which will be discussed here, along with the known record of explosive activity to map out a comprehensive history of volcanic activity at Stromboli.

The thermal cameras used by UF are focused on the area above the vents to capture explosions, not necessarily the area where the spatter fields are deposited. For this study, no actual data collected by this network is used directly, but the frequency counts from the eruption reports are used to fill in a background data set for Stromboli (see time series in Figure 2.6). This assists the analysis to create a more robust time series as well as to allow detection of changes in activity before, during, and after the two paroxysms to be examined at Stromboli when our satellite datasets are sparse.

The number of explosions per day are reported and counted by using the thermal camera and seismic data each day. Figure 2.6 has been populated by using these daily event counts to create a time series covering all the activity since the implementation of the monitoring system (as set up by UF, Istituto Nazionale di Geofisica e Vulcanologia - Osservatorio Vesuviano, and others). Some trends are clearly evident in this data, such as

the lead up to and occurrence of paroxysmal episodes. Paroxysms cause a complete cessation of small scale explosive activity in both 2003 (April 5) and 2007 (March 15) (Bertagnini et al., 2011). Explosive frequency tends to increase until periods of paroxysmal activity when small explosions completely stop. When explosive activity resumes, there are few explosions per day and numbers increase steadily over time until they reach typical background levels of activity, roughly 75-125 explosions per day (Figure 2.6).

The counts reported by UF are not an absolute number of explosions, as the thermal camera only viewed a portion of the active vents and small explosions can go undetected. Hence, the UF data would give a lower end estimate of the number of explosions. The seismic instruments deployed by UF, INGV, and others (Neuberg et al., 1994; Marchetti and Ripepe, 2005) certainly detect events that are too small to be seen in thermal satellite or FLIR data. These events may in fact not breach the crater rim (occurring within the conduit or under a significant amount of crater infill), resulting in an elevated seismic event count relative to other datasets (Table 2.1).

**Table 2.1:** *Detection statistics for multiple methods at Stromboli showing average number of events per day during periods of possible monitoring. The discrepancy between numbers reflects the capability of different methods in the detection of small scale explosion. Discrepancies consist of (but are not limited to) spatial resolution, temporal resolution, field of view, and instrument sensitivity. (Data compiled from: Stromboli eruption Activity Bulletins from Universita degli Studi di Firenze, Dipartimento di Scienze della Terra; This study; UAF/GINA satellite image database).*

Sensor	Average # of Events per Day
Thermal Camera (UF)	77 (24 hrs/day over 7 years)
Thermal Camera (this study)	146 (extrapolated from 5 days of recorded explosions)
MODIS satellite sensor (this study)	0.35 (available database data)

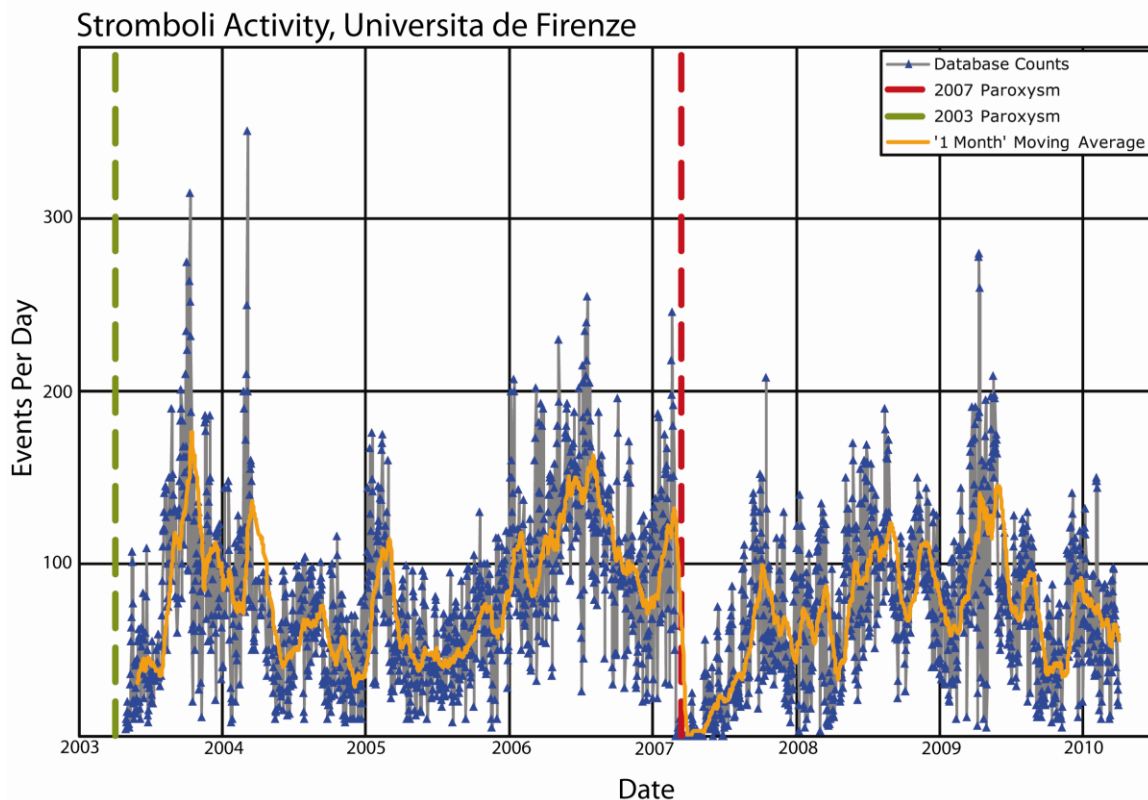


**Figure 2.6:** Database from Universita de Firenze showing the number of explosions recorded per day for a continuous time period spanning 2003-2010. The number of events reported here are from detection with a thermal camera located approximately 400 yards from the active vents. Data collected and combined from: D. Delle Donne (UF), Unpublished data; Bertagnini et al., 2011; Information releases from Italy Civil Protection; Stromboli eruption Activity Bulletins from Universita degli Studi di Firenze, Dipartimento di Scienze delle Terra; Calvari et al., 2006; Rosi et al., 2006; Ripepe and Harris, 2008.

### 2.3.2 Methods

#### 2.3.2.1 Database Retrieval

The University of Alaska, Fairbanks (UAF) and the Geographic Information Network of Alaska (GINA) have a large database of archived satellite imagery from the Advanced Very High Resolution Radiometer (AVHRR) and MODIS sensors, mainly centered on North Pacific volcanoes (Dean et al., 2002). However, there is also a subset of MODIS and ASTER data from Stromboli Volcano including data from the time periods listed in Table 2.2.

When developing a method for detecting changes in frequency of small explosions or explosive activity at a volcano, the ability to sample and analyze from a continuous dataset covering many years is a key component. However, in many cases this is not possible. For Stromboli Volcano, the UAF/GINA catalog consists of a large amount of data over many years, though not continuously. This data was used in this study with the knowledge of the data omissions and the wealth of other instrumentation on the island. Ideally MODIS data would have been collected over the entire 8 years included in this study, though only 22% of these days are available in the archive.

**Table 2.2:** Available data/images of Stromboli Volcano in the UAF/GINA satellite image database.

Sensor	Year	Dates
MODIS	2002	October 23 – December 31
	2004	September 7 – March 30
	2006	Full Year
	2009	February 19 – March 3, May 19, November 29
ASTER	2003	February 23
		March 13
	2006	April 13
		November 16

All metadata for the satellite imagery was accessed and downloaded from UAF/Geophysical Institute (GI)/Alaska Volcano Observatory (AVO) online archive. For Stromboli, this included the satellite identification, date and time of acquisition, but no data about pixel properties. All images were viewed and analyzed in the UAF-GI/AVO online remote sensing webtools 40 x 40 viewer (see description in Dehn et al., 2000; Dean et al., 2002; Webley et al., 2009). This tool shows a 40 pixel by 40 pixel view centered on the georeferenced location of the target volcano. The tool gives information on all spectral bands of each sensor as well as a number of band subtraction products used to indicate ash plumes, removal solar influence, and highlight thermal features, Table 2.3.

**Table 2.3:** *Band math products in UAF-GI/AVO webtools and/or UAF/GINA satellite imagery database. For MODVOLC methods see Wright et al., 2004, BTM method as described in Prata 1989a, 1989b; Corradini et al., 2008; Webley et al., 2009. Solar influence methodology based on method described in Dozier, 1981.*

Name	Band Math	Purpose
20a21	B20 = saturation, then B21	20 unless saturated, then 21
20m31	B20-B31	Mitigate solar influence
20nd32	B20-B32/B20+B32	Similar to MODVOLC method
22nd32	B21-B32/B21+B32	Similar to MODVOLC method
31m32	B31-B32	Ash detection, BTM method

### 2.3.2.2 Development of Processing Routine

Multiple steps were applied to the original dataset in order to cull the data to relevant and viable images. The MODIS data for Stromboli Volcano included information on acquisition date and time, viewing geometry, and spectral bands 12, 17, 20 - 22, and 28 - 32. Further processing is automatically performed to create a number of band math images listed in Table 2.3. The original datasets contained 2065 images recorded over 653 days from 2002 - 2009. In some cases, duplicate images are saved separately. These images are removed to reduce the chance of double identification of thermal features. The remaining images were then subjected to a number of character tests, described below, to ensure the data can be used in a statistical monitoring method.

Each satellite image has a unique set of geometries that can affect the detectability of features on Earth's surface. For this study, the most critical of these geometries is the satellite zenith angle (Figure 2.5) – or the angle from nadir at which the satellite is viewing the volcano. There is a correlation between the satellite zenith angle and the geometry of the actual pixels in any given image (Patrick, 2002; Patrick et al., 2005; Lillesand et al., 2008). As the zenith angle increases the individual pixels become 'stretched'. A MODIS pixel at nadir has a 1 km diameter, but when viewed at a satellite zenith angle of 40°, the pixels dimensions change to roughly 1.7 km by 1.3 km (increasing the pixel area from 0.79 km<sup>2</sup> to 1.74 km<sup>2</sup>). When the zenith angle exceeds 40°, the pixels will overlap to a point where unique data is no longer adequately

represented, as illustrated by Patrick et al. (2005). All data acquired at a satellite zenith angle higher than  $40^\circ$  was removed from the dataset (Patrick et al., 2005; Dehn and Harris, 2014).

The geometry of the volcanic edifice and crater will also dictate viable zenith angles. In cases of a high zenith angle (farther from nadir), the sensor may not be able to detect thermal signals from within a volcanic crater. An ideal zenith angle would be close to zero, or nadir, indicating that the sensor is directly above the volcano. The eruptive vents at Stromboli Volcano each sit in a shallow crater within and around a larger summit depression. Due to the shallowness of the crater a larger zenith angle will still produce useful imagery. All data acquired at a satellite zenith angle higher than  $30^\circ$  was removed from the dataset.

This analysis method required that each image be individually analyzed to ensure that any anomalous feature would be tagged, as well as offering the ability to determine the weather and other atmospheric factors that could affect each image. Weather is a significant hindrance, when viewing thermal infrared data, as the wavelengths in these bands cannot detect thermal signals from the ground surface through clouds or heavy water vapor (Watson and Prakash, 2014). Weather for each image was evaluated on a graded scale as clear (95), mostly clear (75), partly cloudy (50), mostly cloudy (25), cloudy (5), and NAN (0) for any data that was unusable due to pixel corruption and noise. After this step, a weather statistic was calculated by creating a weighted average of the assigned grades and the number of images on a weekly basis. This statistic was then used to calculate the probability of detecting a thermal anomaly in the satellite data and to assist in weighting weather compromised images.

The remaining images were then individually analyzed for thermal anomalies. While thermal anomalies were selected mainly by manual analysis and visual recognition, reviewing of several images verified that observed anomalies tended to be a pixel or



group of pixels with a temperature  $\sim 5 - 10^\circ$  (C) above the background temperature.

Images were grouped by week and the number of thermal anomalies was summed for the entire week. The final dataset consisted of 33.6% of the original images found in the UAF/GINA database and had 227 observed anomalies out of 694 images (Table 2.4).

**Table 2.4:** Results from multiple steps of the processing routine showing the number of MODIS images for Stromboli through steps of data clipping, from initial data to usable image and observed thermal anomalies. SZSwath for Stromboli was set at  $40^\circ$  from nadir and SZCrater at  $30^\circ$ .

Year	Days w/ Data	Initial Images	SZSwath Clip	SZCrater Clip	% of Initial Images	Observed Thermal Anomalies
2002	69	301	132	100	33.2%	37
2003	No Data	No Data	No Data	No Data	No Data	No Data
2004	115	152	87	65	42.7%	9
2005	90	130	56	43	33.1%	12
2006	365	1465	656	482	32.9%	167
2007	No Data	No Data	No Data	No Data	No Data	No Data
2008	No Data	No Data	No Data	No Data	No Data	No Data
2009	14	17	6	4	24%	2
<b>Total</b>	653	2065	937	694	33.6%	227

### 2.3.2.3 Statistical Analysis

Once all of the images had been individually analyzed, the collected information was used to produce a statistical matrix of the estimated number of explosions per day and per week. These calculations and statistical data take into account the weather, the number of observed explosions, the number of passes, residence time of the sensor, and cooling rate of a spatter field.

The first step of the statistical portion of this study was to use the weather grade assigned to each image to calculate a weighted average for a week's worth of data at a time. This weather statistic is used to calculate an estimate for the amount of minutes per week a satellite has a good/clear view of the volcano. This is calculated by multiplying the number of satellite passes per week by the weather statistic, and then multiplying this by

the *residence time* of the spatter field, i.e. the amount of time that a sensor could detect the hot target (Equation 2.1). From this point, the minimum and optimal number of events per week can be determined. The *minimum number of events* per week is the number of observed thermal anomalies in the data. The *optimal number of events* is an estimated number based on the minimum number of events, the amount of good satellite views per week, and the number of minutes in a week (Equation 2.2). The minimum number and optimal number of events are then averaged and this is the estimated *average number of events per week* (Equation 2.3) value that is reported in *Results* and Figure 2.7.

$$\text{Clear View Minutes Per Week} = \left( \left( \#PassesPerWeek \right) \times \left( \frac{\text{WeatherStatistic}}{100} \right) \right) \times \text{ResidenceTime}$$

Equation 2.1

$$\text{Optimal Events Per Week} = \frac{\text{MinimumEventsPerWeek}}{\left( \text{SatelliteMinutesPerWeek} / [24 \times 60 \times 7] \right)}$$

Equation 2.2

$$\text{Average Events Per Week} = \frac{(\text{MinimumEventsPerWeek} + \text{OptimalEventsPerWeek})}{2}$$

Equation 2.3

#### 2.3.2.4 Thermal Camera and Satellite Comparisons

In order to verify the ability of the satellite sensors to detect spatter fields, the thermal flux was calculated for the detectable thresholds of the sensors used and for a selection of spatter fields recorded with the thermal camera. An explosion can only be detected by satellite sensors if the thermal output is high enough to overcome the detection threshold. Each satellite has a different thermal detection threshold, based on wavelength measured, pixel size, and temperature of the target area. The detection capability of the satellite sensor is calculated using a modified Planck function (Equation 2.4) (Kreith and Bohn, 1993).

$$E_{b\lambda} = A_{pix} \times \left\{ \left( \frac{8\pi hc}{\lambda^5} \right) \times \left[ \frac{1}{\left( e^{\frac{hc}{\lambda kT}} - 1 \right)} \right] \right\}$$

Equation 2.4

Where  $E_{b\lambda}$  is the radiance ( $\text{W}\cdot\text{sr}^{-1}\cdot\text{m}^{-2}$ ) measured by the satellite,  $A_{pix}$  is the area ( $\text{m}^2$ ) of the satellite pixel,  $h$  is Planck's constant ( $6.626 \times 10^{-34} \text{ J}\cdot\text{s}$ ),  $c$  is the speed of light ( $3.00 \times 10^8 \text{ m}\cdot\text{s}^{-1}$ ),  $\lambda$  is the wavelength measured ( $1.10 \times 10^{-5} \text{ m}$ ),  $k$  is the Boltzmann constant ( $1.3806 \times 10^{-23} \text{ J}\cdot\text{K}^{-1}$ ), and  $T$  is the temperature (K) of target pixel.

When examining the thermal camera video data a different method is used to calculate the irradiance from the spatter fields. This is performed using the radiant energy equation (Equation 2.5) (Kreith and Bohn, 1993). This number (irradiance) is a measurement of the amount of thermal energy reflected from an object in all directions (Kreith and Bohn, 1993). While each particle in a spatter field will produce a thermal signal, all particles are summed to produce a thermal flux for the entire field. This thermal flux will also include non-thermally anomalous areas (background) and the ambient temperature of this area.

$$Q_r = \sigma \varepsilon \tau \phi A (T_h^4 - T_c^4)$$

Equation 2.5

Where  $Q_r$  is the radiative heat (W) measured by the thermal camera,  $\sigma$  is the Stefan-Boltzmann constant ( $5.6704 \times 10^{-8} \text{ W}\cdot\text{m}^{-2}\cdot\text{K}^{-4}$ ),  $\varepsilon$  is the emissivity (0.95),  $\tau$  is the atmospheric transmissivity (accounted for by FLIR internal corrections for temperature),  $\phi$  is the shape factor (ignored for this work),  $A$  is the area ( $\text{m}^2$ ) of spatter field (including interstitial background area),  $T_h$  is the temperature (K) of hot material, and  $T_c$  is the background temperature (K).

Then equations 2.4 and 2.5 are used to calculate the irradiance and the radiance of a thermal feature. In order to compare the radiance calculated for the satellite sensors thermal detection thresholds and the irradiance (thermal output) calculated for the FLIR data spatter fields, the irradiance is converted from a lambertian (in all directions) reflector to a per steradian (in one specific ray path) reflector (Equation 2.6).

$$E_{b\lambda} = Q_r \cdot \left( \frac{1}{2} \cdot 12.57 \right)$$

Equation 2.6

## 2.4 Results

### 2.4.1 Spatter Field Measurements

During the field campaign, 130 explosions from 2 vents (NE1 and NE2) were recorded using the FLIR thermal camera. The majority of explosions were Type 1 (Patrick et al., 2007, Figure 2.2) and produced spatter fields. There were also a number of Type 2a explosions, also producing spatter fields (Figure 2.2). There were very few Type 2b explosions during the recording period, and as these explosions produce no spatter field, they are not used for this study.

Spatter fields from NE2 ranged from 9 m to 105 m diameter (average diameter of 54 m). The material from an average sized explosion had a spatial distribution of around 2300 m<sup>2</sup> with material covering ~15 - 20% of that area. The explosions that were measured from NE1 range in diameter from 7 m to 135 m (average diameter of 48 m). Spatter fields were mostly located within the crater at Stromboli, though some explosions (mainly from NE1) did send material down the Sciarra del Fuoco (see location in Figure 2.1). Sciarra focused explosions pose a difficulty in measurement due to the obliqueness of the camera angle and because the vast majority of material continually rolls down the slope, dispersing and therefore ‘dimming’ (effectively cooling) the spatter field. This steeper

slope also geometrically constrains the view, making a smaller target for an overhead view (from a satellite).

#### 2.4.1.1 Spatter Field Thermal Flux

The thermal flux was calculated for 38 explosions spread over 4 days from multiple locations and look angles using equations 2.4 and 2.5 (Table 2.5a). Thermal flux was calculated for two periods of time during each explosion; the time of the maximum temperature reading and then again 60 seconds after the point of maximum temperature. This will assist in determining the factor that cooling rate plays in the detection of spatter fields by satellite sensors. The detection thresholds of the satellites used were also calculated in order to determine if spatter fields would be visible (Table 2.5b; Figure 2.3).

**Table 2.5a:** Radiance values for two points in time during the eruption and cooling of spatter fields.

Camera Location	Average Radiance at Maximum Temperature	Average Radiance at 60 Seconds Post-Eruption
Ladybug	$8.46 \times 10^5 \text{ W}\cdot\text{sr}^{-1}\cdot\text{m}^{-3}$	$1.57 \times 10^5 \text{ W}\cdot\text{sr}^{-1}\cdot\text{m}^{-3}$
Pizzo	$3.6 \times 10^6 \text{ W}\cdot\text{sr}^{-1}\cdot\text{m}^{-3}$	$9.61 \times 10^5 \text{ W}\cdot\text{sr}^{-1}\cdot\text{m}^{-3}$
SPSN1	$1.55 \times 10^6 \text{ W}\cdot\text{sr}^{-1}\cdot\text{m}^{-3}$	$1.49 \times 10^5 \text{ W}\cdot\text{sr}^{-1}\cdot\text{m}^{-3}$
SPSN2	$9.83 \times 10^5 \text{ W}\cdot\text{sr}^{-1}\cdot\text{m}^{-3}$	$1.44 \times 10^5 \text{ W}\cdot\text{sr}^{-1}\cdot\text{m}^{-3}$

**Table 2.5b:** Detection thresholds for MODIS and ASTER sensors. Spatter fields must have a radiance which exceeds these thresholds in order to be detected.

Sensor	Detectability Thresholds
MODIS	$2.23 \times 10^5 \text{ W}\cdot\text{sr}^{-1}\cdot\text{m}^{-3}$
ASTER	$1.71 \times 10^3 \text{ W}\cdot\text{sr}^{-1}\cdot\text{m}^{-3}$

When comparing spatter field radiance to the detectable thresholds of the satellite, initially, almost all spatter fields have radiances exceeding satellite thresholds. After sixty seconds, the spatter fields have cooled to a point where only the very largest explosions, generally emplaced on a gently sloping surface, are still observable by satellite detection methods (Figure 2.3).

#### 2.4.2 *Results of Statistical Analysis*

The results of the processing routine are reported in Table 2.4. After data clipping steps, 33% of the original data set was used in the statistical analysis. By plotting the statistical analysis results over time, an estimate of the number of events per week is shown (Figure 2.7). This estimate shows the relative frequency of explosions and can indicate changes in the character of the volcanic activity. The number of estimated events per week is calculated for the periods when satellite data was available; leaving gaps where data was absent (The capability to determine explosive frequency when no satellite data was available was beyond the capabilities of this current study). The weather for the area and two instances of strombolian paroxysms are also plotted in Figure 2.7. These paroxysms represent two periods of time when there was heightened volcanic activity at Stromboli Volcano, resulting in large explosions, ash columns and plumes, and lava flows (Harris et al., 2008; Bertolaso et al., 2009; Bertagnini et al., 2011). The two paroxysms are important as they match up with changes in activity. Prior to each paroxysm regular strombolian activity first increases in frequency and then ceases completely. This occurred in both 2002 - 2003 and 2007 eruptions and may be a key indicator of future paroxysms. If monitoring based on the above method is continued, it may be possible to see when the frequency of explosions changes and determine possible upcoming paroxysmal events. The trends detected using the single-source satellite method (Figure 2.7) match trends in activity seen in the larger source time series (Figure 2.6).

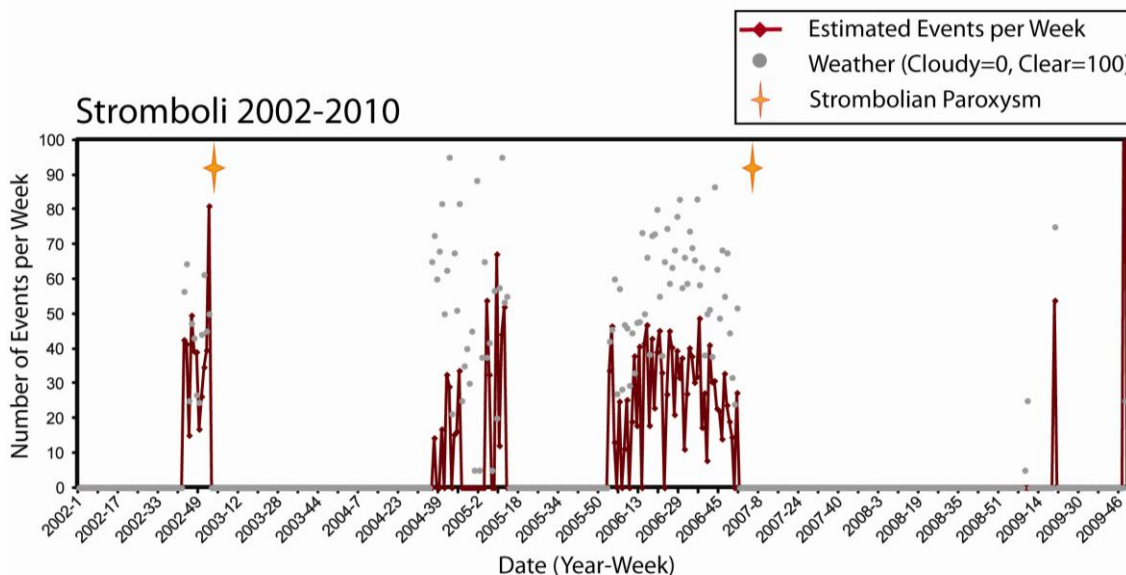


**Figure 2.7:** Frequency plot for satellite based estimated activity from 2002 through 2010. The number of estimated events per week is calculated for the periods when satellite data was available; leaving gaps where data was absent (no effort was made to determine explosive frequency when no satellite data was available). This plot was created with data from 227 thermal anomalies.

## 2.5 Discussion

### 2.5.1 Feasibility of Method

When using period data to determine possible future activity, this method of monitoring volcanic activity proves to be fairly useful. There are a number of requirements in order for high quality data and statistically significant results to be produced and one must acknowledge that all results are averages and/or estimates. This method does not specifically count discrete events at a volcano. However, it should be robust and internally consistent enough to provide a very good indication of the relative change of activity within a volcanic system; be it in frequency, size, temperature, or severity of events.

When used at Stromboli Volcano, the method was able to verify changes in activity prior to strombolian paroxysms and was able to replicate data determined using other ground-based sensors and personal observations and records. The ability to replicate other research methods is particularly useful because it means that this method can be adapted and used at volcanoes where no ground-based systems are present to provide some measure of monitoring, detection, and possibly forecasting. The link was reinforced between the cessation of small scale explosive activity and an impending paroxysm at Stromboli. This pattern was seen in the satellite data for both the 2003 and 2007 events and has been documented for multiple paroxysms in the history of Stromboli.

When the counts of explosions per day collected by UF (collected from thermal camera data) are compared to the average estimated number of explosions determined by the above described satellite method, the results show a correlation of activity frequency in the data (Figure 2.8). The results must be scaled to account for the differing detection thresholds between thermal camera data and satellite derived data. The two sets of data show numerous correlations in peaks of activity. Though the satellite derived result was created using a non-continuous dataset, resulting in gaps where no data is available, for the periods of time when both data sets were populated the relative intensities of explosive activity are complimentary to one another.



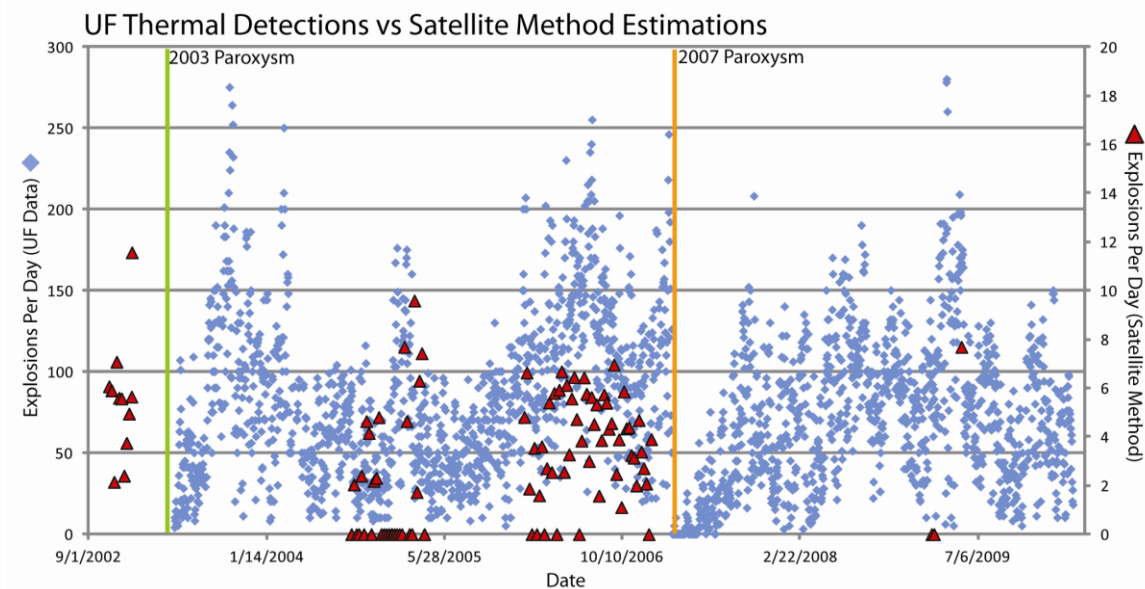


**Figure 2.8:** Scaled comparison of the thermal camera detected explosions and the satellite method estimates of explosions per day. The results have been scaled to reflect the difference in the detection method; thermal camera detection has a lower threshold of detection than the satellite method, and will therefore detect higher activity rates.

Knowledge of the typical type of activity at a volcano is an important factor in the application of this method. As developed here, the method fits best to a volcano with frequent small scale explosive activity. While other infrequent types of activity will not necessarily degrade the information on small explosive frequency, more frequent cases of lava flows and large ash plumes may mask the smaller explosive events; in effect, oversaturating the method with continuous thermal data. Other factors that will affect the validity of application of this method are the availability of a continuous and continually populated dataset, appropriate sensor resolutions, a recorded history of the volcanoes previous activity, and, if available, some ground-based monitoring system (for example; seismic, infrasound, thermal camera, and webcam).

### 2.5.2 Factors for a Statistically Valid Methodology

As mentioned above, there are a number of requirements for this method to produce high quality data, be statistically valid and reliably provide consistent analysis of the volcanic

signals. Though not all factors are vital to the implementation of this method, they each enhance the value of data created.

#### *2.5.2.1 Continuous and Continually Populated Dataset*

At Stromboli Volcano, only a partial dataset was used, with many time gaps in the satellite imagery. This meant a truly continuous time series of eruptive activity was not possible. However, at Stromboli, the presence of other monitoring systems filled in some of the temporal gaps and the well documented history and eruptive activity record indicated that the satellite data that was available covered periods prior to and following the major paroxysms.

At other locations where ground-based systems are not available, such as Cleveland Volcano in Alaska (AVO, 2013), it will be much more important to have a continuous satellite dataset. Any temporal gaps in data at these volcanoes will mean a complete absence of any data, and therefore no conclusions/assessments can be made about the eruptive activity during that time or for a period of time following renewed access to the satellite data. This continuous record is vital in the creation of a baseline of activity at a volcano. This baseline will serve as a reference point to determine if there have been any significant changes in the behavior of the volcano.

One factor, nearly as important as a continuous dataset, is a database that is continually being updated with new data. Having background knowledge of the volcano and its activity levels allows for the creation and population of a historical time series. However, it hinders the ability to build an extensive future extrapolation of activity. With a continually populated database, new images can be analyzed and added to the time series to keep track of the current status of the volcano. As the background data is used to determine indications of changes in activity, the new activity can be analyzed to detect those indicators ahead of eruptive episodes.

### *2.5.2.2 Appropriate Satellite Resolutions (Spatial and Temporal)*

Appropriate spatial and temporal resolutions are needed for the production of a robust time series. Spatial resolution will be mainly dependent upon the target volcano and its activity. Like at Stromboli, a volcano with constant fumarolic activity and frequent small explosions producing spatter fields, a small spatial resolution will not be very useful, as it will tend to show smaller and cooler thermal features than other sensors. A sensor with too coarse a spatial resolution will also be impractical as a small spatter field will be averaged across the larger pixel with too much cool background, and will not be detected as a thermally anomalous pixel.

The temporal resolution of a satellite is important in the creation of a continuous and robust dataset. If satellite overpasses are extremely limited, i.e. single passes with days in between, activity can easily go undetected completely or misidentified. If there is only a single image, a small lava flow may look similar to a spatter field or a small lava dome (Dehn et al., 2000). For the work on Stromboli Volcano, satellite passes were available on an average of ~5 images per day, during the time windows for which ground data has been collected (prior to any data clipping). This number is adequate for the use of our applied monitoring method, though there would be no negative side effects at volcanoes with more frequent passes.

### *2.5.2.3 Recorded History of Volcano*

One final piece that is not necessarily required, but can help to expand a time series, is a well documented history of the activity at a volcano. A written record of prior activity can assist to fill in a time series and give relative timeframes for heightened activity. The database at UAF/GINA only contains satellite data as far back as 1993 for the North Pacific and no further back than 2002 for Stromboli. Fortunately, Stromboli has been a heavily studied and documented volcano. Its activity has been recorded as far back as 6000 B.C. using magnetism and radiocarbon data, and 350 B.C. via historical records (Barberi et al., 1993).

#### *2.5.2.4 Ground Based Monitoring Systems*

At Stromboli Volcano, the wealth of ground based monitoring equipment serves to fill in, verify, and correct much of the data calculated from the satellite statistical method. For this location, the data makes the monitoring system more reliable as well as serving as a methodology check. For most volcanoes on Earth, this abundance of data is not normal, reasonable, or even possible. Short term field campaigns may offer a solution and serve to calibrate and validate satellite data.

#### *2.5.3 Potential for Future Work*

This method has been developed at a very well known and monitored volcano in order to test its feasibility for use at less monitored volcanoes. There are numerous volcanoes around the world that exhibit small explosive activity, and many of these volcanoes are also not suited for ground-based monitoring system deployment. A large number of these volcanoes are located in the North Pacific area, and that is the region that has been chosen for future work and refinement of this method.

## **2.6 Conclusion**

By using a volcano that is heavily monitored and with a comprehensive recorded history a tool for monitoring the frequency of explosive activity has been created in an effort to gain indications to a change in volcanic activity and possible larger eruptions. Using a singular source (space-borne infrared imagery), a time series of eruptive activity for Stromboli was created. This time series is complementary to, and in some cases is able to simulate or duplicate, information gathered from a variety of ground based systems. The frequency of small scale explosions at Stromboli show an increase in number of explosions prior to a cessation of activity which then leads to a large, ash producing paroxysmal eruption. These results highlight the capability of satellite remote sensing to become a single source monitoring tool.

The method described here could be useful in an operational setting. It can be especially useful when applied to remote volcanoes that have the potential to impact populations, infrastructure, and the aviation community. Important factors that will affect the validity of application of this method are the availability of a continuous and continually populated dataset, appropriate sensor resolutions, a recorded history of the volcanoes previous activity, and, if available, some ground-based monitoring system (e.g. seismic, infrasound, thermal camera, and webcam). This method can be first applied using a database of past images and then be continually updated to help track changes in the volcanic setting and any fluctuations in the level of volcanic (thermal) activity.

## **2.7 Acknowledgements**

I would like to thank Andrew Harris for his help both in the field at Stromboli and throughout the writing process. Special thanks to Peter Webley (UAF/GI) for his tireless help throughout the writing and editing process. Also, the help of those working in the Department of Earth Sciences at University of Firenze (Georgio, Dario). Thanks are also due to those working at Stromboli Volcano, both guiding people to the top (Mario and ZaZa) and monitoring the volcano at the Advanced Operations Center (COA).

This project is based on work supported by the United States Geological Survey through the Alaska Volcano Observatory; a NASA Urgent Request Protocol grant for targeting ASTER acquisitions; National Science Foundation (NSF) Interdisciplinary/Collaborative Research under grant no. CMMI-1131799.

J. Dehn, M. Ripepe, and D.della Donne aided in field work, data synthesis, and data analysis for this research.

## 2.8 References

Abrams, M., Hook, S., Ramachandran B. (2002). ASTER User Handbook, Version 2, Jet Propulsion Laboratory, EROS Data Center.

Aguilera, F. (2005). Contrasting styles of volcanic activity as observed by remote sensing: The case of Lascar, Llama and Villarrica volcanoes, Chile. 6<sup>th</sup> Int. Symposium on Andean Geodynamics (Ext. Abstract), 21-25.

Alaska Volcano Observatory (AVO) Website, 2013 -  
<http://www.avo.alaska.edu/volcanoes/volcinfo.php?volcname=Cleveland>

Andronico, D., Branca, S., Calvari, S., Burton, M., Caltabiano, T., Corsaro, R.A., Del Carlo, P., Garfi, G., Lodato, L., Miraglia, L., Murè, F., Neri, M., Pecora, E., Pompilio, M., Salerno, G., Spampinato, L. (2005). A multi-disciplinary study of the 2002-03 Etna eruption: insights into a complex plumbing system. *Bull. Volcanol.*, 27, 314-330.

Barberi, F., Rosi, M., Sodi, A. (1993). Volcanic hazard assessment at Stromboli based on review of historical data. P. Manetti & J. Keller (Ed.), *Acta Vulcanologica*, 3, 173-187.

Bertagnini, A., Di Roberto, A., Pompilio, M. (2011). Paroxysmal activity at Stromboli: lessons from the past. *Bull. Volcanol.*, 73, 1229-1243.

Bertolaso, G., De Bernardinis, B., Bosi, V., Cardaci, C., Ciolli, S., Colozza, R., Cristiani, C., Mangione, D., Ricciardi, A., Rosi, M., Scalzo, A., Soddu, P. (2009). Civil protection preparedness and response to the 2007 eruptive crisis of Stromboli volcano, Italy. *Journal of Volcanology and Geothermal Research*, 182, 269-277.

- Blackburn, E.A., Wilson, L., Sparks, R.S.J. (1976). Mechanisms and dynamics of strombolian activity. *Journal of the Geological Society*, 132, 429-440.
- Calvari, S., Spampinato, L., Lodato, L., Harris, A.J.L., Patrick, M.R., Dehn, J., Burton, M.R., Andronico, D. (2005). Chronology and complex volcanic processes during the 2002-2003 flank eruption at Stromboli volcano (Italy) reconstructed from direct observations and surveys with a handheld thermal camera. *Journal of Geophysical Research*, 110, B02201.
- Calvari, S., Spampinato, L., Lodato, L. (2006). The 5 April 2003 vulcanian paroxysmal explosion at Stromboli volcano (Italy) from field observations and thermal data. *Journal of Volcanology and Geothermal Research*, 149:1-2, 160-175.
- Chouet, B., Hamisevicz, N., McGetchin, R. (1974). Photoballistics of volcanic jet activity at Stromboli, Italy. *Journal of Geophysical Research*, 79 (32), 4961-4976.
- Corradini, S., Spinetti, C., Carboni, E., Tirelli, C., Buongiorno, M. F., Pugnaghi, S., Gangale, G. (2008). Mt. Etna tropospheric ash retrieval and sensitivity analysis using Moderate Resolution Imaging Spectroradiometer measurements. *J. Atmos. Remote Sens.*, 2, 023550.
- Dean, K. G., Dehn, J., Engle, K., Izbekov, P., Papp, K., Patrick, M. (2002). Operational satellite monitoring of volcanoes at the Alaska Volcano Observatory. *Monitoring Volcanic Hotspots using Thermal Remote Sensing*, AJH Harris, M. Wooster and DA Rothery (Eds), *Advances in Environmental Monitoring and Modelling*, 1, 70-97.
- Dehn, J., Dean, K., Engle, K. (2000). Thermal monitoring of North Pacific volcanoes from space. *Geology*, 28(8), 755-758.

Dehn, J., Harris, A.J.L., (2014). Thermal anomalies at volcanoes in satellite imagery. In: Dean & Dehn eds. Atlas of volcanic eruptions from Space, Springer Verlag, New York (in press).

Diller, K., Clarke, A.B., Voight, B., Neri, A. (2006). Mechanisms and conduit plug formation: Implications for vulcanian explosions. Geophysical Research Letters, 33, L20302.

Dozier, J. (1981). A Method for Satellite Identification of Surface Temperature Fields in Subpixel Resolution. Remote Sensing of Environment, 11, 221-229.

Duda, K.A., Ramsey, M., Wessels, R., Dehn, J. (2009). Optical Satellite Volcano Monitoring: A Multi-Sensor Rapid Response System, Geoscience and Remote Sensing, Pei-Gee Peter Ho (Ed.), ISBN: 978-953-307-003-2, InTech, DOI: 10.5772/8303. Available from: <http://www.intechopen.com/books/geoscience-and-remote-sensing/optical-satellite-volcano-monitoring-a-multi-sensor-rapid-response-system>

Ferrari, L., Manetti, P. (1993). Geodynamic framework of the Tyrrhenian volcanism: a review. P. Manetti & J. Keller (Ed.), Acta Vulcanologica, 3, 1-9.

Françalanci, L. (1993). Mineral chemistry of Stromboli volcanic as indicator of magmatic processes. P. Manetti & J. Keller (Ed.), Acta Vulcanologica, 3, 99-113.

Global Volcanism Network (GVN), (1988). Incandescent tephra from several vents, *Scientific Event Alert Network*, **13:11**.

Global Volcanism Network (GVN), (1989). Explosions eject bombs and spatter, *Scientific Event Alert Network*, **14:09**.



Global Volcanism Network (GVN), (1990). Continued Strombolian activity; new vents, *Bulletin of Global Volcanism*, **15:09**.

Global Volcanism Network (GVN), (1991a). Explosive activity from a single crater; strong seismicity, *Bulletin of Global Volcanism*, **16:04**.

Global Volcanism Network (GVN), (1991b). More frequent explosions, *Bulletin of Global Volcanism*, **16:05**.

Global Volcanism Network (GVN), (1993). Explosive activity increases; detailed description of crater, *Bulletin of Global Volcanism*, **18:04**.

Global Volcanism Network (GVN), (1994). Normal Strombolian activity, *Bulletin of Global Volcanism*, **19:03**.

Global Volcanism Network (GVN), (1997). New map of crater terrace, *Bulletin of Global Volcanism*, **22:05**.

Global Volcanism Network (GVN), (2000). Low - to - moderate eruptive activity January - September 2000, *Bulletin of Global Volcanism*, **25:08**.

Global Volcanism Network (GVN), (2003). Lava emissions continue into January; crater morphology changes, *Bulletin of Global Volcanism*, **28:01**.

Global Volcanism Network (GVN), (2007). INSIVUMEH reported that during 4-5 January, Strombolian eruptions from Pacaya produced incandescent material that was expelled at 2-40-second intervals, up to 100 m above the crater. Gas clouds reached an altitude of 2.7 km (8,900 ft) a.s.l. and drifted S. A lava flow 50 m in length pooled near the NE edge of MacKenney Cone, *Instituto Nacional de Sismologia, Vulcanologia, Meteorologia, e Hidrologia (INSIVUMEH)*, **3 January, 2007**.

Harris, A.J.L., Stevenson, D.S. (1997). Thermal observations of degassing open conduits and fumaroles at Stromboli and Vulcano using remotely sensed data. *Journal of Volcanology and Geothermal Research*, 76, 175-198.

Harris, A. J., Flynn, L. P., Dean, K., Pilger, E., Wooster, M., Okubo, C., Wright, R. (2000). Real-time satellite monitoring of volcanic hot spots. *Geophysical Monograph Series*, 116, 139-159.

Harris, A., Dehn, J., Patrick, M., Calvari, S., Ripepe, M., Lodato, L. (2005). Lava effusion rates from hand-held thermal infrared imagery: an example from the June 2003 effusive activity at Stromboli. *Bull Volcanol*, 68, 107-117.

Harris, A., Ripepe, M. (2007). Synergy of multiple geophysical approaches to unravel explosive eruption conduit and source dynamics – A case study from Stromboli. *Chemie der Erde*, 67, 1-35.

Harris, A., Ripepe, M., Calvari, S., Lodato, L., Spampinato, L. (2008). The 5 April 2003 Explosion of Stromboli: Timing of Eruption Dynamics Using Thermal Data. *The Stromboli Volcano: An Integrated Study of the 2002-2003 Eruption*, *Geophysical Monograph Series* 182, 305-316.

Harris, A.J., Delle Donne, D., Dehn, J., Ripepe, M., Worden, A.K. (2013). Volcanic plume and bomb field masses from thermal infrared camera imagery. *Earth and Planetary Science Letters*, 365, 77-85.

Hornig-Kjarsgaard, I., Keller, J., Koberski, U., Stadlbauer, E., Francalanci, L., Lenhart, R. (1993). Geology, stratigraphy and volcanological evolution of the island of Stromboli, Aeolian arc, Italy. P. Manetti & J. Keller (Ed.), *Acta Vulcanologica*, 3, 21-68.

Judd, J.W. (1881), *Volcanoes*. In: Kegan et al. (eds) *What they are and what they teach*. London.

Kreith, F., Bohn, M.S. (1993). *Principles of Heat Transfer*, 5<sup>th</sup> Edition. St. Paul, Minnesota: West Publishing Company.

Lacroix, A. (1904). *Montagne Pelée et ses Éruptions*: Paris, Masson et Cie Éditeurs, pp. 1-662.

Lillesand, T.M., Keifer, R.W., Chipman, J.W. (2008). *Remote Sensing and Image Interpretation*, 6<sup>th</sup> Edition. Hoboken, New Jersey: John Wiley & Sons, Inc.

LP DAAC ASTER Overview – Last visited 2013,  
[https://lpdaac.usgs.gov/products/aster\\_overview](https://lpdaac.usgs.gov/products/aster_overview)

LP DAAC MODIS Overview – Last visited 2013,  
[https://lpdaac.usgs.gov/products/modis\\_overview](https://lpdaac.usgs.gov/products/modis_overview)

Macdonald, G.A. (1972). *Volcanoes*. Prentice-Hall inc., Englewood Cliffs, New Jersey. 510 pp.

Marchetti, E., Ripepe, M. (2005). Stability of the seismic source during effusive and explosive activity at Stromboli Volcano. *Geophysical Research Letters*, 32, L03307.

MODIS Raid Response, Last Viewed 2013 - <http://earthdata.nasa.gov/data/near-real-time-data/rapid-response>

NASA MODIS Web – Technical Specifications, Last Viewed 2013, [modis.gsfc.nasa.gov](http://modis.gsfc.nasa.gov)

NASA/JPL/ASTER User Advisory, (2009), Change in Status Alert, January 12, 2009. <http://asterweb.jpl.nasa.gov/latest.asp>

Neuberg, J., Luckett, R., Ripepe, M., Braun, T. (1994). Highlights from a seismic broadband array on Stromboli Volcano, *Geophysical Research Letters*, 21, 749-752.

Neuberg, J., Luckett, R. (1996). Seismo-volcanic sources on Stromboli volcano. *Annali Di Geofisica*, XXXIX, 377-391.

NOAA CLASS website – Last visited 2013, <http://www.class.ncdc.noaa.gov/saa/products/welcome>

Patrick, M.R. (2002). Numerical Modeling of Lava Flow Cooling Applied to the 1997 Okmok Eruption: Comparison with AVHRR Thermal Imagery, M.S. thesis, University of Alaska Fairbanks, Fairbanks, 141 pp.

Patrick, M.R., Dehn, J., Dean, K. (2005). Numerical modeling of lava flow cooling applied to the 1997 Okmok eruption: Comparison with advanced very high resolution radiometer thermal imagery. *Journal of Geophysical Research*, 110, B02210.

- Patrick, M., Harris, A., Ripepe, M., Dehn, J., Rothery, D., Calvari, S. (2007). Strombolian explosive styles and source conditions: insights from thermal (FLIR) video. *Bull. Volcanology*, 69, 769-784.
- Pioli, L., Erlund, E., Johnson, E., Cashman, K., Wallace, P., Rosi, M., Delgado Granados, H. (2008). Explosive dynamics of violent Strombolian eruptions: The eruption of Parícutin Volcano 1943-1952 (Mexico). *Earth and Planetary Science Letters*, 271, 359-368.
- Prata, A. J. (1989a). Infrared radiative transfer calculations for volcanic ash clouds. *Geophysical Research Letters*, 16(11), 1293-1296.
- Prata, A. J. (1989b). Observations of volcanic ash clouds in the 10-12  $\mu\text{m}$  window using AVHRR/2 data. *International Journal of Remote Sensing*, 10(4-5), 751-761.
- Ripepe, M., Marchetti, E., Ulivieri, G. (2007). Infrasonic monitoring at Stromboli volcano during the 2003 effusive eruption: Insights on the explosive and degassing process in an open conduit system. *Journal of Geophysical Research*, 112, BO9207, 1-13.
- Ripepe, M., Delle Donne, D., Harris, A., Marchetti, E., Ulivieri, G. (2008). Dynamics of Strombolian Activity. *The Stromboli Volcano: An Integrated Study of the 2002-2003 Eruption*, Geophysical Monograph Series 182, 39-48.
- Ripepe, M., Harris, A.J.L. (2008). Dynamics of the 5 April 2003 explosive paroxysm observed at Stromboli by a near-vent thermal, seismic, and infrasonic array. *Geophysical Research Letters*, 35:7, DOI: 10.1029/2007GL032533.
- Rosi, M., Bertagnini, A., Landi, P. (2000). Onset of the persistent activity at Stromboli Volcano (Italy). *Bulletin of Volcanology*, 62, 294-300.

Rosi, M., Bertagnini, A., Harris, A.J.L., Pioli, L., Pistolesi, M., Ripepe, M. (2006). A case history of paroxysmal explosions at Stromboli: Timing and dynamics of the April 5, 2003 event. *Earth and Planetary Science Letters*, 243:3-4, 594-606

Stix, J., Torres, C.R., Narváez, M.L., Cortés, G.P.J., Raigosa, A.J., Gómez, M.D, Castonguay, R. (1997). A model of vulcanian eruptions at Galeras volcano, Colombia. *Journal of Volcanology and Geothermal Research*, 77, 285-303.

Universita di Firenze, Dipartimento di Scienze della Terra (UF), Activity Bulletin, January 6, 2011. <http://193.206.127.20/stromboli/>

Walker, G.P.L. (1973). Explosive volcanic eruptions, a new classification scheme, *Geol. Rund.*, 62, 431-446.

Watson, I.M., Prakash, A. (2014). Satellite Systems and Interactions. In: Dean & Dehn eds. *Atlas of volcanic eruptions from Space*, Springer Verlag, New York (in press).

Webley, P. W., Dehn, J., Lovick, J., Dean, K. G., Bailey, J. E., Valcic, L. (2009). Near-real-time volcanic ash cloud detection: Experiences from the Alaska Volcano Observatory. *Journal of Volcanology and Geothermal Research*, 186 (1), 79-90.

Wohletz, K., Heiken, G. (1992). *Volcanology and Geothermal Energy*. Berkeley, University of California Press.

Wright, R., Flynn, L. P., Garbeil, H., Harris, A. J., Pilger, E. (2004). MODVOLC: near-real-time thermal monitoring of global volcanism. *Journal of Volcanology and Geothermal Research*, 135(1), 29-49.

**Personal Communications**

Alaska Volcano Observatory (AVO), 2009, Note on dome growth, *Log Post #30508*, S. Prejean.

Alaska Volcano Observatory (AVO), 2012, Cleveland: Dome 4 Destroyed and Dome 5 Appears, *Log Post #97191*, D. Schneider.





**Chapter Three**  
**Frequency Based Satellite Monitoring of Small Scale Explosive**  
**Activity at Remote North Pacific Volcanoes<sup>1</sup>**

**3.1. Abstract**

Monitoring of volcanoes in the North Pacific can be an expensive and sometimes dangerous task, specifically for those located in Alaska (USA) and Kamchatka (Russia). An active frequency detection method previously used at Stromboli, Italy, uses the thermal- and mid-infrared wavelength bands from the Moderate Resolution Imaging Spectroradiometer (MODIS) satellite data to detect anomalies at a volcano. This method focuses on small scale explosive activity, often referred to as strombolian activity which can produce small spatter fields near a volcano's active vent. In the North Pacific, there are a number of volcanoes which exhibit small scale explosive activity and three are the focus of this study: Chuginadak (Mt. Cleveland) and Shishaldin in Alaska, and Karymsky Volcano in Kamchatka. Satellite images from the Advanced Very High Resolution Radiometer (AVHRR) were used to monitor the frequency of thermal features as well as the occurrence of ash plumes at each volcano. This data was then used to produce a time series spanning 2005-2010 for all three volcanoes. During this time period, each volcano underwent a series of eruptive cycles including background levels of activity, heightened frequency of small explosions (identified as precursory activity), and heightened activity typified by ash plume-producing eruptions. Each location has a unique precursory signal, both in timing and magnitude. The use of a previously developed method on a new sample set of volcanoes has proved the validity of this method as a monitoring tool for volcanoes with small scale explosive activity. This method should be applied to a larger set of volcanoes to continue the development and database production for its use as a volcano monitoring tool.

---

<sup>1</sup> Worden, A., Dehn, J., Webley, P. (2014). Frequency Based Satellite Monitoring of Small Scale Explosive Activity at Remote North Pacific Volcanoes. *Journal of Volcanology and Geothermal Research*. (Submitted to the Journal of Volcanology and Geothermal Research).

### 3.2. Introduction

Monitoring of volcanoes in the North Pacific can be an expensive and sometimes dangerous task, specifically for those located in Alaska (USA) and Kamchatka (Russia). The Northern Pacific region, although often thought of as remote, is both populated and a highly traveled air traffic route with more than 10,000 passengers and millions of dollars in cargo flying over this volcanic region each day (Neal et al., 1997), demonstrating the need for consistent methods of monitoring. Satellite remote sensing offers a safe, relatively inexpensive method for monitoring large areas where field work is logistically unrealistic (Lillesand et al., 2008). A method has been developed (Worden et al., 2014) that uses satellite imagery to review and determine the activity at remote volcanoes. This method focuses on small scale explosive activity, often referred to as strombolian activity (Lacroix, 1904; Walker, 1973; Wohletz and Heiken, 1992), which can produce small spatter fields near a volcano's active vent. These spatter fields are detectable in satellite data as "thermal anomalies", i.e. groups of pixels with a temperature elevated over the background temperature (Harris, 2013). Their frequency and duration can be detected, monitored, and analyzed to give insights into changing volcanic systems.

The frequency detection method developed by Worden et al. (2014) uses the thermal- and mid-infrared wavelength bands from satellite data to detect anomalies at a volcano. Once the number of these 'thermal' anomalies has been determined, then an assessment is made of the weather conditions across the region and a number of other geometric and spectral factors impacting remotely sensed images. The information on thermal anomalies, cloud conditions, and spectral/geographic conditions of data acquisition is then used to calculate an estimated number of explosions that may have occurred on a weekly interval in an effort to normalize the results. This number represents the average frequency of explosions and can give an indication of the typical activity at a volcano. In addition, as the frequency fluctuates, this method can be used to track changes in the volcanic system and used to detect indications of increasing activity.

In the North Pacific, there are a number of volcanoes which exhibit small scale explosive activity that are the focus of this study. The volcanoes of interest are: (1) Chuginadak (Mt. Cleveland) and (2) Shishaldin in Alaska, USA, and (3) Karymsky Volcano in Kamchatka, Russia. All three of these volcanoes have a recorded history of small scale explosive activity, though at varying intensities and frequencies (Cleveland - McGimsey et al., 2007; Shishaldin - Dehn et al., 2002; Karymsky – Izbekov et al., 2004). Changes in the frequency of explosions indicate changes in the systems and can be a useful monitoring tool by analyzing weekly patterns rather than daily fluctuations that can be affected by changes in weather, satellite sensor viewing geometry and the timing of satellite overpasses.

### **3.3. Background**

Volcanism in the North Pacific represents the northern most border of the Ring of Fire (Figure 3.1). This region exists due to the subduction of the Pacific Plate beneath the North American Plate. This subduction environment exists for most of the Aleutian Arc, but switches to a more strike-slip margin in the western portion of the arc (Ryan and Scholl, 1993). This transitions back to a subduction environment in Kamchatka as the Pacific Plate again subducts beneath the North American Plate. The Aleutian Arc meets the Kamchatka Peninsula at a triple junction between the Pacific plate and two lesser tectonic plates - the Okhotsk Plate and the Komandorsky Plate (Scholl, 2007; Volynets et al., 2010) near the location of Shiveluch, Kliuchevskoi, Bezymianny, and Ushkovsky volcanic complexes.

The Aleutian Arc is made up of over 40 volcanoes (Wallace et al., 2000), stretching from Mount Spurr in the northeast to Buldir Island, 1580 miles to the west (Coats, 1962). Activity at these volcanoes ranges from ash plumes reaching 18 km a.s.l. (Waythomas et al., 2010) at Kasatochi volcano, interfering with air traffic and posing threats to populations, to quiescent lava flows in areas far from human habitation, such as the emplacement of lava flows on Yunaska Volcano (Simkin and Siebert, 1994).

Kamchatka, Russia is home to over 70 volcanoes, producing ash plumes, lava flows, and caldera forming explosions (Braitseva et al., 1995; Schneider et al., 2000; Ramsey and Dehn, 2004). The volcanoes of Kamchatka are divided into the Central Kamchatka Depression (including the Kliuchevskoi group of volcanoes) and the Eastern Volcanic Front (including Karymsky and the town of Petropovlovsk-Kamchatsky, located only 30 - 35 km from active volcanoes Avachinsky and Koryaksky).

### *3.3.1 Volcanoes that Exhibit Small Scale Explosive Activity*

Though there is a vast range of volcanic activity types present in the North Pacific, from the ash plumes of Kasatochi volcano in 2008 (Waythomas et al., 2010) to the lava flows of Tolbachik volcano in 2012 - 2013 (BGVN, 2012), this work aims to provide a monitoring and detection tool for small scale explosive activity as a precursor to larger scale explosions and activity. This type of activity, similar to Strombolian type explosions, occurs at many volcanoes in the North Pacific, perhaps most notably Chuginadak (Mount Cleveland) (Reeder, 1990a; McGimsey et al., 1995; McGimsey et al., 2007) and Shishaldin (Reeder, 1990b; Dehn et al., 2002; Siebert and Simkin, 2002; Beget et al., 2003) in the Aleutian Islands, and Karymsky in Kamchatka (Izbekov, 2004). All three volcanoes are near the center of their respective arcs.



**Figure 3.1:** Map of the North Pacific volcanic region (modified from Hansell et al., 2006; Steinbeck and Fuller, 2004). Red triangles indicate the volcanoes chosen for this study. The diamonds are the locations of the regional infrasound arrays in the North Pacific; blue – Fairbanks, yellow – Dillingham, green – Okmok..

### 3.3.1.1 Chuginadak (Mt. Cleveland), Alaska

Mt. Cleveland is a stratovolcano that is located on the western half of Chuginadak Island in the Aleutian Arc of Alaska (Miller et al., 1998) as seen in Figure 3.2. The volcano is roughly 8.5 km in diameter, symmetrically conical and rises to an elevation of 1730 m a.s.l. (Simpson et al., 2002; Dean et al., 2004). Though the volcano is quite distant from large population centers (Anchorage, the largest city in Alaska, is 1500 km (950 miles) away), there are small villages nearby, the closest being Nikolski at 72 km (45 miles) to the east-northeast with a permanent population of 18; and Unalaska at 257 km (160 miles) with a permanent population of 4376 (as of the 2010 census, USCB [2014]) (Figure 3.2). However, the airspace above Mt. Cleveland is the daily home to more than 10,000 passengers and millions of dollars in cargo on numerous air traffic routes (Neal et al., 1997). Mt. Cleveland is the most consistently active volcano in the Aleutian Arc (AVO, 2014a; GVP, 2014a) and has produced ash plumes up to 10 km asl during major

eruptions in 1998 and 2001 (Reeder, 1990a; Dean et al., 2004), with many lower level plumes occurring throughout its eruptive cycles (GVP, 2006a, 2008, 2010a).

The first recorded eruption at Mt. Cleveland occurred in 1893 and though it was a confirmed eruption, there is no available information about the nature of the activity (Reeder, 1989). The first well described eruptive activity took place in 1932 and was comprised of ashy emissions accompanied by minor explosive activity (Jaggard, 1932). Since then, a number of active eruptive periods lasting multiple years have been reported, mainly made up of small explosions and ash emissions, though periods of major activity have occurred at which time large explosions, ash plumes, lava flows, tephra plumes, lahars, pyroclastic flows, and debris avalanches have been reported (McGimsey et al., 2004).

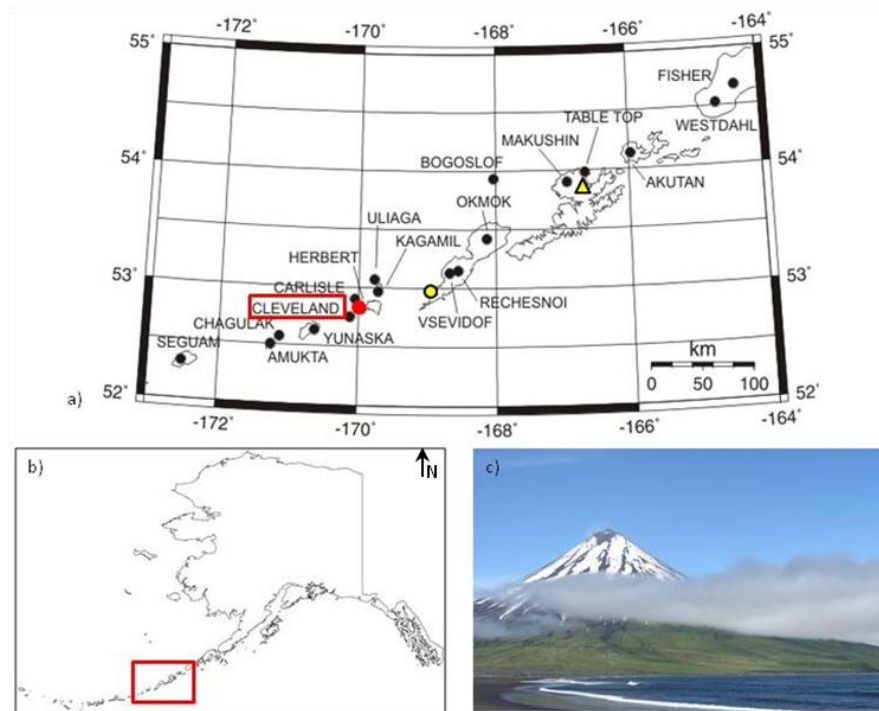


**Figure 3.2:** a) Location map of Mt. Cleveland (red dot) and surrounding volcanoes and towns (Nikolski is indicated with the yellow dot, Unalaska is indicated with a yellow triangle). b) Location of Cleveland inset map in relation to the Aleutian Arc. c) Mt. Cleveland is a stratovolcano in the Aleutian Arc with an elevation of 1720 m a.s.l. and a roughly 8.5 km diameter. The volcano occupies the western half of Chuginadak Island. Photo: S. Smith, USGS/AVO

Despite the active nature of Mt. Cleveland, its remote location has prohibited large amounts of petrologic and geologic research. Unpublished data from field campaigns by K. Nicolaysen and others (personal communication; AVO, 2014a) indicates that most of Mt. Cleveland lavas are basaltic andesite to andesite in composition, with few dacites. There are also a number of satellite cinder cones composed of andesitic material (59-63 wt% silicone dioxide) (Nicolaysen, 2013).

Though there is no seismic network on Mt. Cleveland, there are seismic networks set up on nearby volcanoes - Okmok, Makushin, and Korovin networks range from 140 to 290 km from Cleveland (Brantley et al., 2009). These networks are sometimes able to detect large explosions/eruptions from Mt. Cleveland, though smaller explosions go unseen (Dixon et al., 2012). The seismic network at Okmok Volcano, ~ 140 km from Mt. Cleveland, has been able to detect ground-coupled acoustic signals during periods of heightened activity (larger explosions) (De Angelis et al., 2012). There are a number of infrasound sensors and arrays deployed throughout the Aleutian Arc and on the Alaska mainland as can be seen on Figure 3.1 (Arnoult et al., 2010; De Angelis et al., 2012). Explosions at Mt. Cleveland during the 2011-present eruptive period were detected at the Okmok array (140 km to the east northeast), Dillingham array (1000 km to the northeast), and Fairbanks array (1830 km to the northeast) (De Angelis et al., 2012). These large explosions were the result of the destruction of a number of domes that plugged the summit vent of the volcano (AVO, 2011). Activity at Cleveland is ongoing and, given its location, monitoring this activity and providing assessment of developing hazards are based heavily on the use of satellite remote sensing.

#### *3.3.1.2 Shishaldin, Alaska*

Shishaldin Volcano is located on Unimak Island on the Southwestern tip of the Alaska Peninsula (Figure 3.3). The island is also home to Westdahl volcano (last explosive activity in 1991; McGimsey et al., 1995), Fisher Caldera (last reported activity in the early 1800's; Veniaminov, 1840), Isanotski Volcano (last reported activity in the early

1800's; Veniaminov, 1840; Coats, 1950), and Roundtop (last active in 7600 BC; GVP, 2014d). Shishaldin has shown activity (small explosions, thermal signatures, and fumarolic and steam activity) at frequent intervals as recently as 2008 (Neal et al., 2011), though the last major activity (such as ash plume, lahars, incandescence) was reported in 1999 (AVO, 2014b; GVP, 2014b).

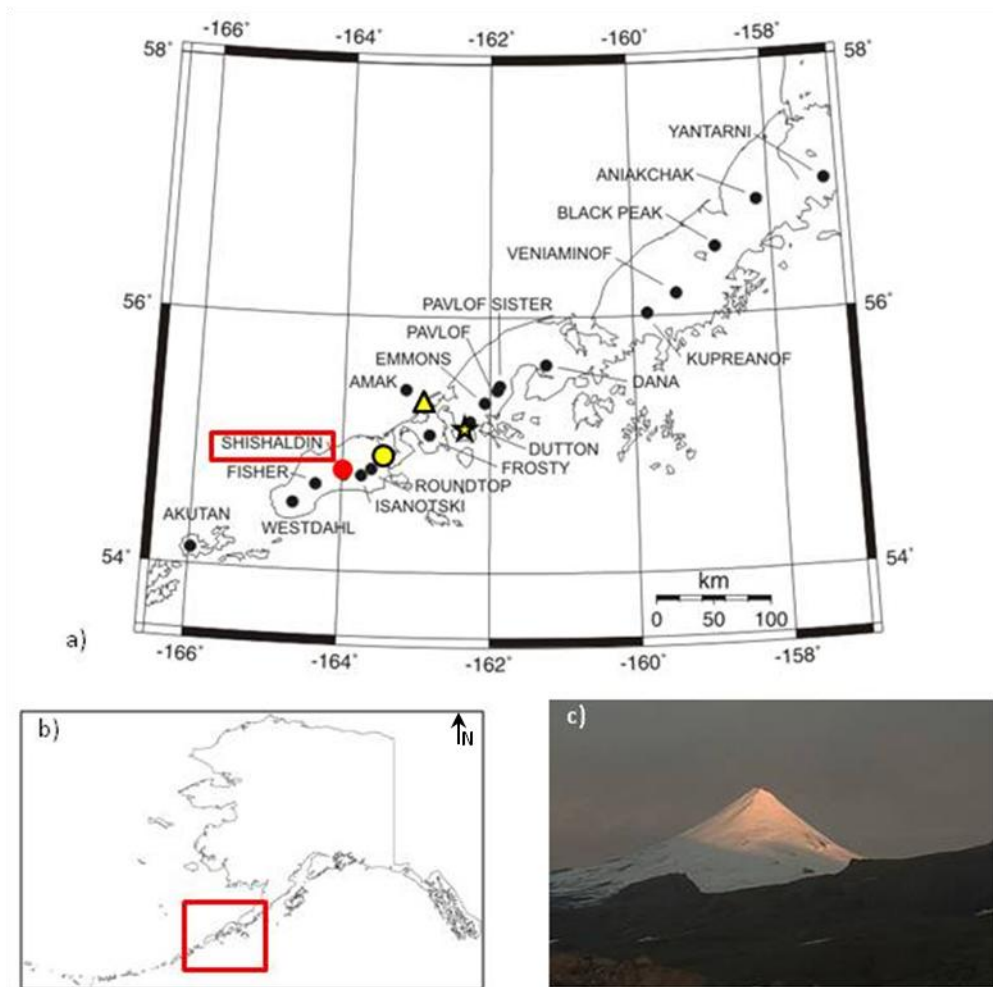


**Figure 3.3:** a) Location map of Shishaldin Volcano (red dot) and surrounding volcanoes and towns (False Pass is indicated with a yellow dot, Cold Bay is indicated with a yellow triangle, and King Cove is indicated with a yellow star). b) Location of Shishaldin inset map in relation to the Aleutian Arc. c) Shishaldin is a stratovolcano in the Aleutian Arc with an elevation of 2857 m a.s.l. The volcano sits on Unimak Island on the Southwestern tip of the Alaska Peninsula. Photo: USGS/AVO.



Shishaldin is a stratocone volcano that is the highest peak (at 2857 m a.s.l.) in the Aleutians as well as one of the most active volcanoes in the arc (Neal et al., 1995). In addition, this volcano also has an especially deep crater compared to other volcanoes with similar eruptive activity, approximately 400 m from the active vent to the crater rim. This depth and the steepness of the walls affects the spatial distribution and overall detection capabilities of small explosions from the volcano (Dehn et al., 2002). Shishaldin volcano has had 27 recorded eruptions since 1775 including 2 dozen in the 20<sup>th</sup> century (Miller et al., 1998; Neal et al., 2004), most of which have involved small scale explosive activity, ash, and steam emissions (Neal et al., 1995). Presently, the volcanic cone (Holocene in age) sits atop the remnants of an older volcanic edifice which remains exposed on the northeastern and southern flanks (Nye et al., 2002). It is tholeitic in nature (Fournelle, 1988) and has produced basaltic andesites (Nye et al., 2002), high alumina and magnesian basalts, as well as some dacites, at 62-67 wt% silica (Fournelle and Marsh, 1991). Older lava flows, possibly associated with the somma on the western flank, are high magnesium basalt, daciterhyodacite, high alumina-titanium basalt and minor andesite (Fournelle, 1988).

Shishaldin is unique in the set of volcanoes being studied here as it is fairly close to a number of population centers, posing a threat to people and infrastructure should a large eruption occur. It is located ~675 miles (1000 km) southwest of Anchorage, Alaska's largest city, between the Alaska Peninsula National Wildlife Refuge and the Alaska Maritime National Wildlife Refuge. Other nearby population centers include False Pass (40 km away, population 64), Cold Bay (95 km away, population 108), and King Cove (110 km away, population 938) (USCB, 2014; Figure 3.3). Shishaldin is also the only volcano in this sample set with permanent and functioning seismic and infrasound networks (Caplan-Auerbach and McNutt, 2003).

### 3.3.1.3 *Karymsky, Kamchatka*

Karymsky volcano is located on the Kamchatka Peninsula (Figure 3.4), about 125 km (80 miles) Northeast of the town of Petropavlovsk-Kamchatsky with a population of 180,000 (FSSS, 2011). There are numerous small towns and airports throughout the Kamchatka Peninsula, each within 600 km of the volcano: Paratunka (150 km southwest with a population of 1,767), Esso (200 km to the north-northwest with a population of 1,965), Palana (550 km north with a population of 3,155) (FSSS, 2011; see Figure 3.4).

Karymsky is the most consistently active volcano in the Kamchatka Peninsula (KVERT, 2013; GVP, 2014c) and is a part of a volcanic complex with Academia Nauk (a vent located on the rim of an intracaldera lake with a single recorded eruption – 1996; Ivanov et al., 1991) and Maly Semiachik (last eruptive activity in the 1950's following 100 years of inactivity; Ivanov et al., 1991). Karymsky is a stratovolcano that occupies most of a 5 km diameter caldera which formed 7900 years ago as the result of a catastrophic eruption that produced 5–7 km<sup>3</sup> of dacite (Braitseva et al., 1995). The summit of Karymsky is at ~1500 m a.s.l. with a summit crater that is approximately 225 - 250 m across (Ivanov et al., 1991).

For the past 500 years, Karymsky has erupted andesites of very uniform composition (Ivanov et al., 1991; Ozerov et al., 2001; Izbekov, 2002; Izbekov et al., 2004). In the last century there have been eruptive periods spanning 1908–1915, 1921–1925, 1929–1935, 1943–1947, 1952–1967, 1970–1982 ((Ivanov, 1970; Tokarev, 1989) from Izbekov et al., 2004 and Izbekov, 2002), 1996-2000, and 2001-present (GVP, 2014c). The typical behavior at Karymsky consists of persistent small scale explosive activity following a paroxysmal onset (Johnson et al., 1998). The ongoing activity has been mostly made up of continuous small scale explosive activity accompanied by periods of effusive activity, pyroclastic flows, and frequent ash emissions (Ozerov et al., 2001). Regular explosions have been seen to send ash and gas to an altitude of 2 – 3 km above the vent (Izbekov et al., 2004). In the case of larger eruptions, ash can travel to heights of up to 10 km asl (KVERT, 2013).

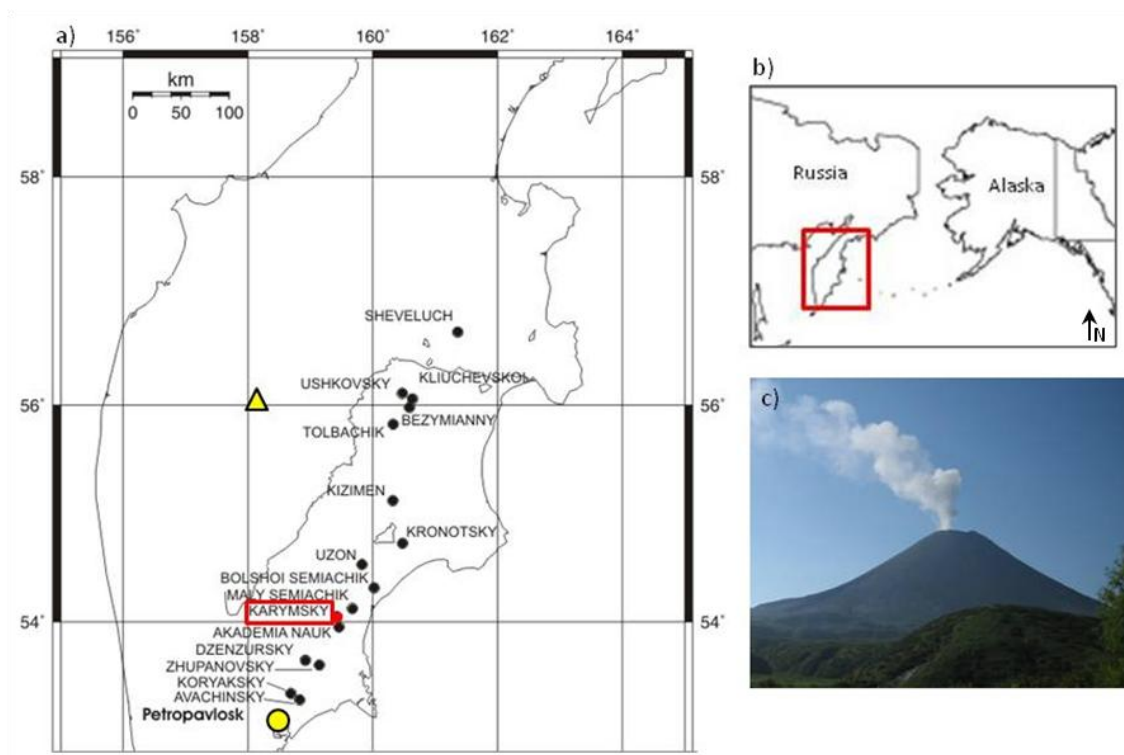


**Figure 3.4:** Location map of Karymsky Volcano (red dot) and surrounding volcanoes and towns (Petropavlovsk-Kamchatsky is indicated with a yellow dot, Esso is indicated with a yellow triangle). b) Location of Karymsky inset map in relation to the North Pacific. c) Karymsky is a stratovolcano on the Kamchatka Peninsula with an elevation of ~1500 m a.s.l. Photo: A. Belousov.

There have been a number of campaign networks set up for both seismic and acoustic studies at Karymsky (see Johnson et al., 1998; Johnson and Lees, 2000; Lees et al., 2004; Johnson, 2007). These campaign networks are typically only in the field for a number of days to weeks, usually during periods of increased activity. The Kamchatka Volcano Eruption Response Team (KVERT) is responsible for a permanent seismic network at Karymsky that is used for daily monitoring of volcanic activity. However, at the time of this research, the quality of, and access to, seismic data is limited and is mainly used by KVERT for daily monitoring of volcanoes (KVERT, 2013).

### 3.3.2 *Thermal Anomalies: Determination of Source and Transient Nature*

#### 3.3.2.1 *Small Scale Explosive Activity*

This type of volcanic activity occurs in many volcanic regions (e.g. Pacaya, Guatemala (GVP, 2007); Etna, Italy (Andronico et al., 2005); Paricutin, Mexico (Pioli et al., 2008); Villarrica and Llaima, Chile (Aguilera, 2005)) and is some of the most common volcanic activity on Earth (Simkin and Siebert, 1994; Siebert and Simkin, 2002). It can occur at almost all types of volcanoes (such as shields, stratovolcanoes, and cinder cones) and can occur along side fissure eruptions, dome building eruptions, and larger volcanic explosions. Often these small explosions are part of a larger eruptive period, such as at Cleveland in 2001 (Dean et al., 2004), but can occur as the sole activity at a volcano, such as the consistent typical activity at Stromboli (Barberi et al., 1993; Rosi et al., 2000). Due to the variance in occurrence, concurrence, and scale of these explosions, it is important to be able to detect and monitor them for the introduction or change in character of small scale explosive activity. These types of changes can lead to heightened levels of volcanism which in turn can pose a threat to populations, communities, environments/habitats, and human infrastructure (Mothes, 1992; Wilson et al., 2007).

#### 3.3.2.2 *Thermal Source*

Small scale explosive activity deposits a spatter field composed of juvenile lava blobs, bombs, and fragmented edifice material (Blackburn et al., 1976; Patrick et al., 2007; Harris and Ripepe, 2007). This debris is significantly hotter than the surrounding area immediately following the explosion, cooling exponentially after it is deposited around the vent and possibly flanks of the volcano (Harris et al., 2013; Worden et al., 2014). Erupted material from these small scale explosive events can be around 700°C (~1200°F). The elevated temperature material relative to its surroundings is the main component of the thermal signal that can be detected by various satellite platforms and their associated sensors (see Dehn et al., 2000). A thermal signal detected in mid infrared satellite data is indicative of a very recent small explosion, due to the rapid cooling of deposits and the

wavelengths available on current sensors. These explosions are most detectable if they are spatter rich, as opposed to being dominated by ash or broken up edifice material (Patrick et al., 2007). A feature is classified as a *thermal anomaly* if it appears to be significantly (or detectably) brighter (and therefore warmer) than the background (see work by Dehn et al., 2000; Dean et al., 2002). For this study, the classification of thermal anomalies was performed manually for each remotely sensed image. When manually analyzing satellite images, considerations must be made for viewing angle, crater geometry, and other factors that can influence the apparent temperature of a feature on the ground (Dehn and Harris, 2014). These factors can influence the spatial extent of the thermal anomaly as well as problems with pixel overlap (Patrick et al., 2005) and over estimation of anomaly size.

### 3.3.2.3 Spatial Distribution

The spatial distribution of the spatter field will play a role in the detection of the thermal anomaly in satellite data. For a satellite sensor with the spatial resolution of 1 km at nadir, such as the National Oceanic and Atmospheric Administration (NOAA) polar orbiting satellite carrying the Advanced High Resolution Radiometer (AVHRR) sensor and the National Aeronautics and Space Administration (NASA) satellites carrying the Moderate Resolution Imaging Spectroradiometer (MODIS) sensor, the thermal radiance of a single pixel will represent the radiant temperature of everything within that area on the ground (NOAA, 2013). This means that all features, hot and cold, will be averaged to provide a single pixel radiance value. Spatter fields from small explosions were seen to be smaller than the pixel size in area and did not have 100% ground cover. In locations like Stromboli Volcano in Italy, a location known for its regular and consistent small scale explosive activity (Judd, 1881; Barberi et al., 1993; Hornig-Kjarsgaard et al., 1993; Rosi et al., 2000), a single explosion can cover an area averaging 475 m<sup>2</sup> with 5 - 15% coverage (Worden et al., 2014). This means that this hot material, making up only a small portion of the (at nadir) 1 km by 1 km pixel will be averaged with cooler, background

material, giving a pixel radiance (converted to radiant temperature) that, while elevated, will be much cooler than the actual erupted material.

The spatial distribution of a single spatter field will depend on: (1) the size and energy of the explosion; (2) the existence or amount of pre-eruptive crater infill; (3) crater geometry; and (4) the type of material erupted. In some cases, these factors can be hard to constrain, as there may not be ground observations of the physical appearance of the volcanic edifice. Small, low-energy explosions may be constrained within the crater and therefore create a very small spatial feature (Dehn et al., 2002). At a volcano with a vent located deep within a crater (similar to Shishaldin volcano), even a large explosion will be unable to deposit material on the outer flanks of the edifice. The type of explosion that has occurred will also produce different amounts of eruptive material. If the energy from an explosion is expended in blasting through a significant amount of crater infill, the resulting energy left to deposit hot material will be diminished.

#### *3.3.2.4 Cooling Rate*

Through lab experiments and observations collected at Stromboli Volcano, Italy, both Harris et al. (2013) and Worden et al. (2014) determined that spatter fields produced by small scale explosive activity tend to cool within seconds to a few minutes after the explosion (Figure 2.3). Similar sized spatter fields from volcanoes that exhibit small scale activity in the North Pacific will likely act similarly, though during the winter months, local environmental temperatures (i.e. much colder ground surface for hot material to be deposited upon) may increase the cooling rate. This short residence time limits the probability of the timing of a satellite overpass corresponding to a new active, hot deposit on the ground. Even at a very active volcano (like Stromboli volcano), say one that experiences about 70 explosions per day, the amount of time that deposits will be hot enough to be detected in the satellite data is only about 70-140 minutes, or 5-10% of the day. For this reason, one is able to infer that not all explosions will be detected in satellite imagery. Fortunately, it may be possible to analyze the number of explosions detected in

satellite data and use this information to estimate the amount of explosions that actually occurred on each day.

The duration of a single explosion is unique for each volcano and each explosion. When observing a single volcano (i.e. Stromboli) explosion durations ranging from 20-90 seconds were noted consecutively from a single vent (Worden et al., 2014). Longer duration explosions will increase the time that hot material is available for possible imaging by the satellite sensor, as hot material will be present both during the eruptive event and then also during the time it takes for the deposits to cool below the detection capability of the sensors. These extended explosions will also deposit a larger volume of hot material onto the flanks. Field observations are often the best way to determine the length of explosions; however, this data is not available at the three volcanoes investigated here, due to their remote location. For this reason, the duration of explosions cannot be directly accounted for in our analysis and the residence time of a single explosion will be designated by an average cooling rate.

### **3.4 Available Data and Methodologies Applied**

#### *3.4.1 Available Data*

##### *3.4.1.1 Satellite Remote Sensing*

The AVHRR sensor is aboard multiple polar orbiting NOAA satellites. There are currently, circa early 2014, five sensors collecting images of the North Pacific (N15, N16, N18, N19 presently collecting images; N17 ended service in April 2013 [where N represents NOAA] but provided information for our analysis; NOAA, 2013). The AVHRR sensors record data in a number of spectral bands, in particular the mid-and thermal-infrared bands of interest for detection of thermal features. Band 3 is a mid-infrared band, collecting imagery from 3.55 - 3.93  $\mu\text{m}$  (NOAA, 2013). Band 4 is a thermal-infrared band, collecting imagery from 10.5 - 11.3  $\mu\text{m}$  (NOAA, 2013). All

bands record circular pixels with a spatial resolution (diameter) of 1.09 km at nadir (Patrick, 2002; NOAA, 2013). The five polar orbiting sensors capture an average of 30 images of the North Pacific region each day (Dean et al., 2002).

This study was carried out with the use of a continuous data set provided by UAF/GI Remote Sensing which includes all AVHRR images captured of the target areas for a period spanning 2005-2010 (Dean et al., 2002). This continuous dataset will provide a near seamless view of the activity of the volcanoes, interrupted only by outages in the satellite systems themselves (which are very rare for the periods and locations of interest).

#### *3.4.1.2 Other Data Available for Study*

For our target volcanoes, we are able to obtain some data from the following additional sources: (1) webcams; (2) infrasound sensors; (3) seismic networks; and (4) first hand observations of activity. Every piece of non-satellite derived data is an important key piece of information in linking activity on the ground to the signals seen in the satellite imagery. Although there are not direct observations at all volcanoes for each eruption, the volcanoes chosen in our analysis exhibit similar patterns of activity and so generalities can be drawn between field observations at one volcano to satellite observations at another volcano.

In July of 1997, a network of 6 short period (SP) and one broadband (BB) sensors was deployed around Shishaldin volcano. All stations were located between 5 and 19 km from the active vent (Caplan-Auerbach and McNutt, 2003). Data is continuously telemetered to the Alaska Volcano Observatory (AVO) to be analyzed, reported on, and stored. Seismic networks are capable of detecting a variety of signals from different sources, such as regional earthquakes, volcanic tremor, and fluid movement (Caplan-Auerbach and McNutt, 2003; De Angelis, 2011; Gottsmann et al., 2011). These instruments are also



capable of detecting ground movement related to small scale explosive activity (Ripepe et al., 2002).

Additionally at the volcano, an infrasonic pressure sensor is co-located with SP seismic station SSLN, 6.4 km from the vent (Caplan-Auerbach and McNutt, 2003). Infrasonic signals are composed of low frequency pressure waves (<20 Hz) below the range of human hearing. In volcanic systems, explosive activity produces pressure waves that can be detected hundreds of kilometers from the volcano (Fee and Matoza, 2013).

Infrasonic arrays can also be found at Okmok, Dillingham, and Fairbanks (Arnoult et al., 2010). These sensors have all proved capable of picking up signals from explosions at volcanoes in the Aleutian Arc, specifically the most recent activity at Cleveland (De Angelis et al., 2012). These sensors can be susceptible to wind noise and other environmental factors, but do serve as a good indicator of the occurrence of an explosion even as a tool used in hindsight (De Angelis et al., 2012; Fee and Matoza, 2013).

Numerous campaign infrasonic arrays have been carried out during heightened eruptive activity at Karymsky, though no permanent stations exist (Johnson et al., 1998; Johnson and Lees, 2000; Lees et al., 2004; Johnson, 2007). No campaign surveys were deployed during the time subset chosen from the satellite image archive. Infrasonic signals seen at distant sites are most likely due to larger explosions and therefore, for our study, the usefulness of infrasonic as a tool for identifying small scale explosive activity is limited.

Seismic networks are located on and around numerous volcanoes in the Aleutian arc and Kamchatka (Brantley et al., 2009; KVERT, 2013). The network at Shishaldin provides a vital data set to be analyzed in conjunction with the satellite data for this study. Seismic signals from Cleveland and Karymsky volcanoes are harder to analyze in comparison to the satellite archive due to availability and distant locations of the stations from each volcano. The nearest arrays to Cleveland are located approximately 140 km away at Okmok volcano (Brantley et al., 2009). Karymsky has a closer seismic network

maintained by KVERT, but this data was not available at the time of this study. Similar to distant infrasound arrays, the distant seismic stations may pick up larger explosions but tend to miss all small scale activity that is the focus here (Fee and Matoza, 2013). For this reason, there will be no seismic component used for the analysis of Cleveland and Karymsky volcanoes.

AVO actively maintains webcams directed towards Shishaldin (located ~10 km from the summit) and Cleveland volcanoes (located in Nikolksi, 70 km from the active vent, Figure 3.2). These webcams have both captured eruptions from the volcanoes, though only larger, ash producing eruptions are seen due to distance from the volcano (in the case of Cleveland) and depth of crater (in the case of Shishaldin). For the period of our study, there was no webcam viewing Karymsky volcano.

#### *3.4.2 Methodology Applied to Satellite Data*

Given the similar mid- and thermal infrared data available on the MODIS and AVHRR sensor, we have adapted the Worden et al. (2014) method for use with AVHRR data for this study at the three volcanoes in question.

##### *3.4.2.1 Description of Satellite Method*

Worden et al. (2014) developed a method for the use of MODIS thermal data for analyzing thermally anomalous activity originally for Stromboli volcano in Italy. Satellite images were sorted, analyzed, and quantified to develop a time series of small scale explosive activity, changes in activity, and indicators of larger eruptive episodes. This method has been proven to be useful in monitoring volcanic activity (Worden et al., 2014) and in our study, the general methodology will be applied to use with AVHRR satellite data. In the case of the North Pacific test locations, AVHRR data is a more abundant and reliable data source, and was therefore chosen for use in this study. Though AVHRR is a different sensor, it collects similar data (both in spatial and spectral

resolution) to produce very similar information when compared to the MODIS sensor across the same spectral range (Table 3.1).

**Table 3.1:** Comparison of the spatial, spectral, and temporal resolutions of the AVHRR and MODIS sensors. (NOAA, 2013). MODIS channels 21 and 22 cover a duplicate spectral range but each has a separate gain setting, allowing better detection of higher temperature targets in channel 21.

<i>Attribute</i>	<i>AVHRR</i>		<i>MODIS</i>	
<i>Spatial Resolution At nadir (km)</i>	1.09		1	
<i>Spectral Resolution (<math>\mu\text{m}</math>)</i>	Band 3	3.55-3.93	Channel 20	3.66-3.84
			Channel 21	3.929-3.989
			Channel 22	3.929-3.989
	Band 4	10.3-11.3	Channel 31	10.78-11.28
	Band 5	11.5-12.5	Channel 32	11.77-12.27
<i>Temporal Resolution (in North Pacific)</i>	Up to 28 overpasses from 5 satellites		Up to 6 overpasses from 2 satellites	

#### 3.4.2.2 Database Retrieval

Satellite data was obtained from the archives maintained by University of Alaska, Fairbanks (UAF) and the Geographic Information Network of Alaska (GINA) (see description of the system in Dean et al., 2002; Bailey et al., 2010; Webley et al., 2013). This archive contains AVHRR, MODIS, and other satellite imagery, mainly centered on the North Pacific region (Dean et al., 2002). The data available for the North Pacific spans a time period of 1993-present, with few periods of data omission and is being added to every day. For this study, a subset of data from 2005-2010 was chosen for Cleveland, Shishaldin, and Karymsky. The number of images included in these subsets throughout the progress of the study is summarized in Table 3.2.

**Table 3.2:** Summary of the available data for Shishaldin, Cleveland, and Karymsky volcanoes through multiple steps in the processing of satellite imagery.

Volcano	Year	Initial Images	Final Image Count	% of Initial Images	Observed Thermal Anomalies
<b>Shishaldin</b>	2005	3881	411	10.59	0
	2006	7305	581	7.95	0
	2007	7005	568	8.1	0
	2008	5296	553	10.44	6
	2009	6329	695	10.98	53
	2010	5335	537	10.06	1
	<b>Total</b>	<b>35151</b>	<b>3345</b>	<b>9.69</b> (average)	<b>60</b>
<b>Cleveland</b>	2005	3496	384	10.98	10
	2006	5351	577	10.78	31
	2007	5113	520	10.17	55
	2008	4952	557	11.25	56
	2009	5960	688	11.54	6
	2010	5032	521	10.35	68
	<b>Total</b>	<b>29904</b>	<b>3247</b>	<b>10.85</b> (average)	<b>226</b>
<b>Karymsky</b>	2005	1617	184	11.38	70
	2006	2497	271	10.85	122
	2007	3276	381	11.63	141
	2008	3227	434	13.44	109
	2009	3789	548	14.46	203
	2010	3583	538	15.02	238
	<b>Total</b>	<b>17989</b>	<b>2356</b>	<b>12.8</b> (average)	<b>883</b>

The data gathered from the archive contained information on all spectral bands available from the satellite as well as a number of special band math products. These include bands that indicate the presence of ash and steam, basic cloud cover, solar influence, and special thermal considerations (Table 3.3). Additionally, metadata was available on the position of the satellite, the satellite zenith angle, and the time and date of data capture. This data was viewed using the online webtools viewer (Bailey et al., 2010). This tool subsets each

image to a 40 km by 40 km area centered on the georeferenced location of the volcano of interest (Dehn et al., 2000; Dean et al., 2002; Webley et al., 2009). In addition to displaying the spectral bands and band math products, this tool also indicates the amount of cloud cover, areas of problematic solar reflection, and thermal anomalies as calculated by the Okmok algorithm (Dehn and Harris, 2014), and areas where corrupted or null data pixels occur.

**Table 3.3:** *Band math products available for AVHRR data. For MODVOLC methods see Wright et al., 2004. For split-window methods see Prata, 1989.*

Name	Band Math/Spectral Range	Purpose
Ch 2	0.725 $\mu\text{m}$ to 1.00 $\mu\text{m}$	Solar reflectance test
Ch 3	3.55 $\mu\text{m}$ to 3.93 $\mu\text{m}$	Thermal feature detection (near infrared)
Ch 4	10.3 $\mu\text{m}$ to 11.3 $\mu\text{m}$	Thermal feature detection (thermal infrared)
Ch 5	11.5 $\mu\text{m}$ to 12.5 $\mu\text{m}$	Cloud cover
3m4	Ch3 – Ch4	Evidence of elevated MIR temperatures above the TIR data
3nd5	Ch3-Ch4/Ch3+Ch4	Equivalent to MODVOLC data
4m5	Ch4 – Ch5	Indicates presence of ash, similar to split-window products

#### 3.4.2.3 Processing Routines Applied to Satellite Data

In our study, multiple steps were applied to the original satellite dataset before the imagery was used for our frequency calculations. These steps were used to remove null data and determine how images were impacted by cloud cover, solar radiation, and unfavorable geometrical characteristics. The bands utilized throughout these steps were AVHRR band 2 (to indicate solar reflection), AVHRR band 3 (to classify thermal features and manually estimate cloud cover), and AVHRR band 4 (used to obtain background temperature information). See Worden et al. (2014) for more details on the processing sets applied here.

Each satellite image has a unique set of characteristics that will impact how features on the surface are detected. One of the most critical characteristics in the satellite scene is the satellite zenith angle, or the angle off of nadir from which the satellite measures the signals omitted by the volcano. At nadir, each pixel of an AVHRR image will be 1.09 km in diameter. As the satellite zenith angle increases, these pixels will be deformed and begin to overlap (Patrick, 2002; Patrick et al., 2005; Lillesand et al., 2008). If there is too much pixel overlap, the retrieved radiance value represented by the pixel will no longer be unique to that single pixel, as it may be shared by neighboring pixels, and a satellite zenith angle of  $40^\circ$  is the cut-off chosen for this method to limit the amount of overlap (Patrick et al., 2005; Dehn and Harris, 2014). All images in the original dataset that have a satellite zenith angle exceeding  $40^\circ$  are removed.

The satellite zenith angle is also important when considering the geometry of a specific volcano and the sensor's capability to detect activity. In order for a satellite view to observe the active vent, it must be able to retrieve signals from below the crater rim. If the volcano is very shallow (such as Stromboli, Italy and Karymsky, Russia) acceptable satellite zenith angle can be as high as  $30^\circ$  and still provide signals from within the crater. As the crater deepens, the satellite zenith angle must be reduced appropriately to still provide a signal that comes from within the crater. The zenith angles chosen for the target volcanoes in this study are: Karymsky -  $30^\circ$ , Cleveland -  $25^\circ$ , and Shishaldin -  $20^\circ$ .

This analysis method requires images to be individually examined to determine the cloud cover (Worden et al., 2014). Cloud cover is determined on an individual image basis because even in an image with 99% cloud cover, the summit of a high elevation volcano can poke above the cloud deck, allowing for the detection of a thermal anomaly. The weather for each image was assigned as clear (95), mostly clear (75), partly cloudy (50), mostly cloudy (25), cloudy (5), and not-a-number or NAN (0). This value is later used to calculate a weather statistic for use in the statistical processing.

The final step in this process is to individually analyze each image to determine if a thermal anomaly is present. Each thermal anomaly was selected by manual analysis and interpretation. It was characterized as a single or group of pixels with a temperature of 5 - 10°C above the background temperature in the MIR data. Finally, images were grouped into weekly periods and the total number of images and observed thermal anomalies were summed across these time periods. For each volcano examined, only 10 - 13% of the original images remained at the completion of the processing routine (see numbers in Table 3.2).

#### 3.4.2.4 Statistical Analysis

After each image had been analyzed and evaluated for geometry, weather, and thermal characteristics, the information was used to produce a statistical matrix to calculate the estimated number of explosions each day and week. This method takes into account weather, observed number of explosions, the number of satellite passes, the residence time of the sensor, and the residence time and cooling rate of the spatter field. The method is described in detail in Worden et al. (2014) and uses a series of statistical calculations to produce an estimated *average number of events per week* value that is reported in *Results* and Figures 3.5, 3.6, and 3.7. These plots also display the color code for each volcano during the period of study. This code is assigned by AVO based on the work of Gardner and Guffanti (2006) and signifies the level of danger posed by the volcano, mainly for the aviation community.

### 3.5 Results

#### 3.5.1 Chuginadak (Mt. Cleveland), Alaska

Mt. Cleveland is the most active volcano in the Aleutian Arc (AVO, 2014a; GVP, 2014a) and this is seen in the data collected from satellite imagery over the 6 year time period chosen for analysis. A total of 226 thermal anomalies were observed during the time span (7% of all images viewed showed evidence of recent small scale explosive activity)

(Table 3.2). There were also 105 manually observed ash plumes relating to heightened levels of eruptive activity.

In multiple instances, there is an increase in the frequency of small scale explosions just prior to a period of ash plume producing eruptions (prior to 2006 - 2008, prior to activity in 2008, Figure 3.5). This means that the small explosion increase is indicative of increasing activity and will likely lead to larger explosions.

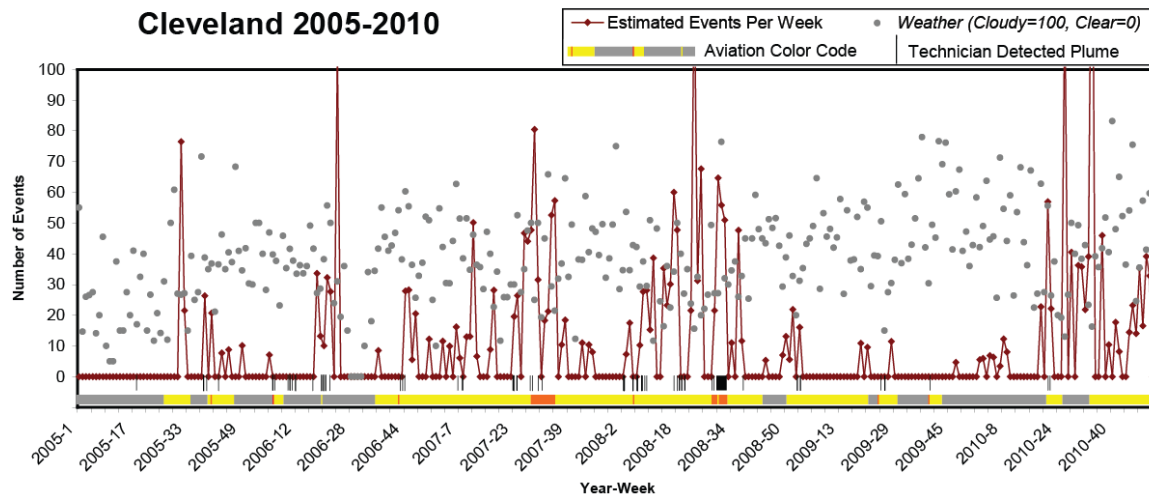


**Figure 3.5:** Plot of estimated number of explosions per week from 2005 through 2010 at Cleveland Volcano. This plot was created with data from 226 thermal anomalies and 105 ash plumes.

### 3.5.2 Shishaldin, Alaska

Though Shishaldin is the third most active Aleutian volcano (AVO, 2014b; GVP, 2014b), it showed the lowest amount of activity using this method; only 60 thermal anomalies seen (under 2% of images had thermal activity) (Table 3.2). It is important to note that this is only the result of this method, and may not be a precise indicator of the activity occurring on the ground. As discussed earlier, the depth of Shishaldin's crater makes viewing the active vent quite difficult. There were also few ash plumes relating to heightened activity, only 14, indicating a much lower level of large scale activity. One final consideration is the distinct lack of detected activity during the 3 years prior to



2008. This provides evidence of the quiet nature of this volcano. Despite the low background activity, this method is still able to detect precursory activity with the short period of quiescence prior to the first detected thermal features in 2008.

At Shishaldin there is only one larger eruptive period occurring during 2009. The first signs of unrest were observed thermal anomalies associated with small explosions early in the year. These explosions increased in frequency until their peak in the 28<sup>th</sup> week of 2009 (Figure 3.6). Soon after this peak there were multiple large ash producing explosions which transported ash to unconfirmed altitudes (McGimsey et al., 2014).

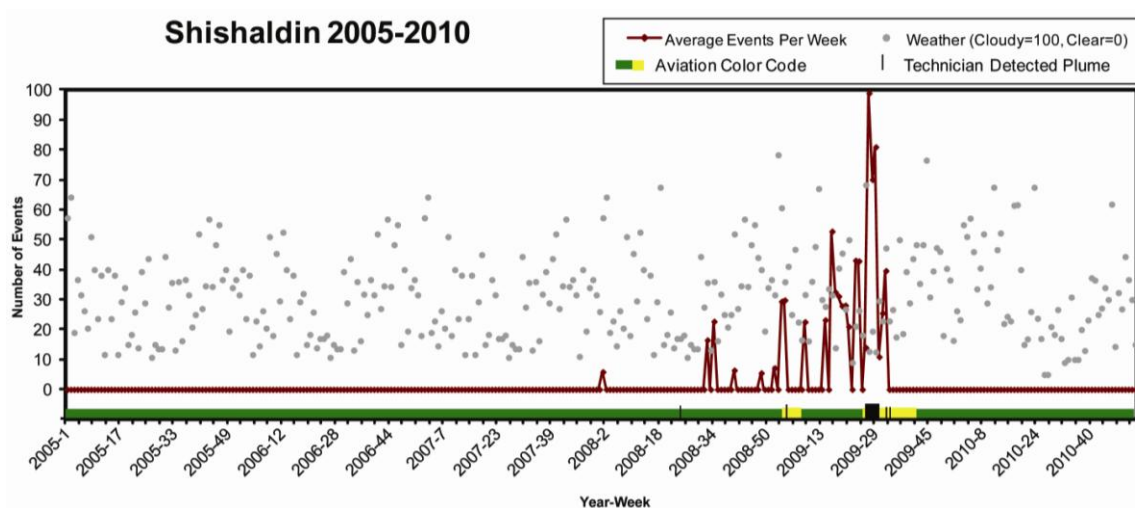


**Figure 3.6:** Plot of estimated number of explosions per week from 2005 through 2010 at Shishaldin Volcano. This plot was created with data from 60 thermal anomalies and 14 ash plumes.

### 3.5.3 Karymsky, Kamchatka

Karymsky is by far the most active volcano in this sample set (Figure 3.7). During the 6 year period chosen for analysis, the volcano had 883 observed thermal anomalies (almost 40% of the images showed recent small scale explosive activity) (Table 3.2). There were also over 200 manual observations of ash producing eruptions during this time period. These large explosions correspond to (changes/increases) in frequency of small explosions.

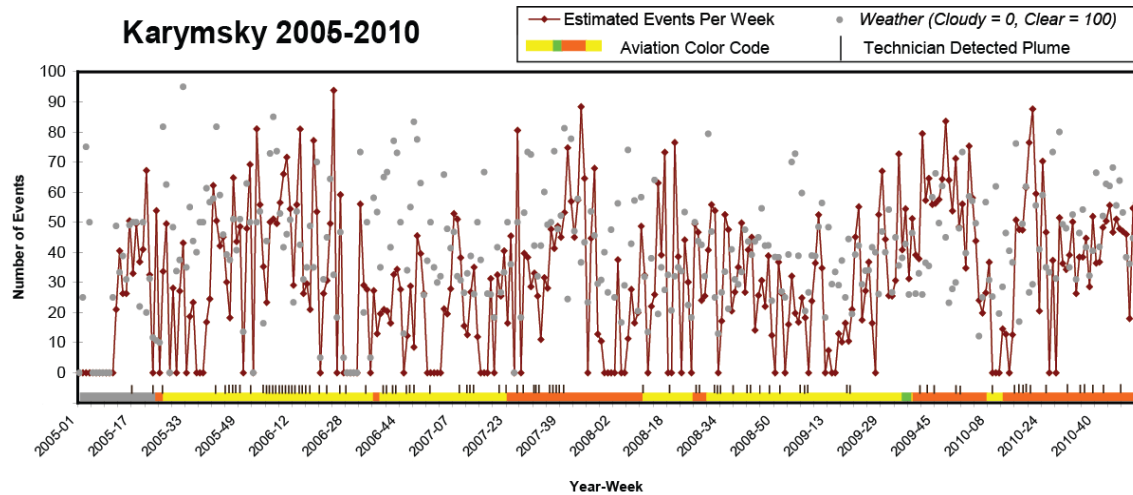


**Figure 3.7:** Plot of estimated number of explosions per week from 2005 through 2010 at Karymsky Volcano. This plot was created with data from 883 thermal anomalies and over 200 ash plumes.

### 3.6 Discussion

#### 3.6.1 Trends in Activity

For each volcano in this study, a distinct trend in activity was observed. In order to determine the timing of precursory activity, the magnitude of plume-producing eruptive periods was calculated and compared to the amounts of thermal activity one, two, three, and four weeks prior to those plumes. This was done based on a Bayesian method of rating the magnitude of the plumes observed at the volcano. Points were assigned to the plumes based on their existence, the length of the plume (or distance from the volcano, if the plume is drifting), if the plume is visible in multiple subsequent images (indicating a sustained plume), if there was more than one plume detected in a day (indicating an extended period of heightened activity), and finally based on the optimal satellite zenith angle ( $40^\circ$ ). Once this rating process was complete, the numbers were summed on a weekly basis producing a weekly plume magnitude (Figure 3.8). The thermal feature ratio (Figure 3.8) was calculated by looking at the number of observed thermal anomalies in the satellite imagery for the week during plume activity and then comparing that to the

number of observed thermal anomalies during one, two, three, and four weeks prior to the plume activity.

In each case, the frequency of small scale explosive activity showed an increase prior to a period of plume producing eruptions (indicating a heightened level of eruptive activity) (Figure 3.8). Though all three volcanoes show a similar general trend, they present at different scales and time periods. At Shishaldin, the increase in activity is quite striking due to the low level of background activity. At Cleveland, and even more so at Karymsky, it is a bit harder to determine the increases in activity prior to plume-producing eruptions, though they are still detectable. These plots also well illustrate the level of activity that can be considered background at the volcano.

The timing and existence of precursory activity can also say something about how the entire volcanic system reacts to an influx of new magma. For each volcano, there is a point (when the plume magnitude is around 8 - 10) below which the small scale explosive activity is not indicative of impending larger eruptive activity. In these smaller cases, the thermal features are functioning at background levels and do not indicate increased magma supply and the plumes produced are low altitude, generally single plumes, and short lived. Above this point, (plume magnitude greater than 10-15), the number of small explosions is more of an indicator that a larger eruption is forthcoming, typically multiple high altitude plumes during an extended period (multiple days) of eruptive activity. This breaks down to mean that the larger eruptive periods are seen by increases in small scale explosive frequency, but the smaller plume periods do not have the same effect on the number of small scale explosions.

#### *3.6.1.1 Cleveland*

At Cleveland, the strongest thermal activity occurs one week prior to a plume-producing period of activity (Figure 3.8). There is also a slight increase two weeks prior to plume activity, but no discernible trend previous to that. At most, Cleveland typically gives one

to two weeks of warning to an increase in eruptive activity. The background activity at Cleveland is very few eruptions per week, near zero, though there are periods of small scale explosive activity, which, while detectable, does not necessarily indicate impending larger plume-producing eruptions.

#### *3.6.1.2 Shishaldin*

Though activity is infrequently detected at Shishaldin there were enough plumes to create 6 data points, with multiple overlapping at a plume magnitude of 1 (Figure 3.8). At Shishaldin volcano the precursory activity begins much sooner, showing the strongest increase in activity three weeks prior to a period of plume-producing activity. The background level of activity is very near zero explosions per week, which makes the detection of precursory activity relatively uncomplicated.

#### *3.6.1.3 Karymsky*

The precursory activity at Karymsky is harder to pinpoint due to a higher background level of activity. However, a slight increase in activity can be seen three weeks prior to a period of plume-producing activity (Figure 3.8). This increase is of a lower intensity than the increases at either of the other volcanoes. The trend line at Karymsky indicates that the background level of activity there is higher than Cleveland and Shishaldin, with activity occurring constantly. This constant level of activity makes the detection of precursory activity more complex.

The activity at Karymsky shows well the split between lower plume magnitudes and higher plume magnitudes. This matches well with work by others that indicates that there are separate shallow and deep systems causing activity (Eichelberger and Izbekov, 2000; Izbekov, 2002; Izbekov et al., 2004; Lopez et al., 2013). The lower plume magnitudes relate to thermal ratios that are very spread out, indicating that this thermal activity is not directly related to plume activity. The higher plume magnitudes correlate quite closely

with the thermal ratios, and indicate that these thermal precursors are due to activity from the deep system, which is more likely to create activity involving plumes (Figure 3.8).

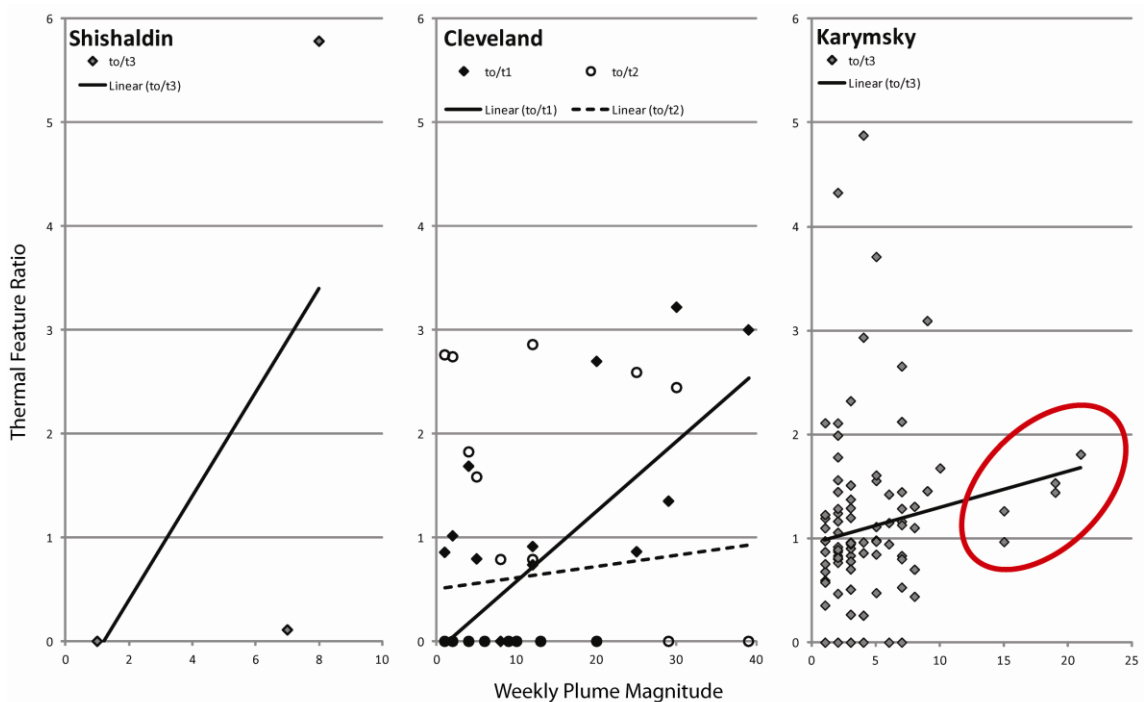


**Figure 3.8:** The strongest trends in activity are highlighted, indicating the period of time prior to large eruptive activity when thermal precursors are the strongest. The time periods represented are denoted as: *to* – the week including the plume activity, *to/t1* – the week prior to plume activity, *to/t2* – two weeks prior to plume activity, and *to/t3* – three weeks prior to plume activity. Linear trends are best fit lines to the data available for weekly plume magnitude. The circled Karymsky data appears to indicate a deeper source mechanism than the lower plume magnitude data.

### 3.6.2 Factors for a Statistically Valid Methodology

As discussed in Worden et al. (2014) there are a number of important factors for having a statistically valid methodology. These factors are a continuous and continually populated dataset, appropriate satellite resolutions (both spatial and temporal), a recorded history of the volcano, and ground based observations and monitoring system(s). While some of these factors are satisfied at these three volcanoes, no location can consistently offer all aspects for creating an ideal system.

**Cleveland:**

- Continuously populated dataset averaging 15 - 20 images per day.
- Satellite resolution that is appropriate for detection of small-scale explosive activity.
- A partial recorded history. Much of the early history was passed down through native oral tradition and is not confirmed elsewhere. There has also not been any carbon dating of deposits.
- There are no ground-based systems located on Cleveland to gather data. There is a webcam that is sporadically functional located about 70 km from the volcano (for location see Figure 3.2).

**Shishaldin:**

- Continuously populated dataset averaging 15 - 25 images per day.
- Satellite resolution that is appropriate for detection of small-scale explosive activity.
- Good confirmed record of historic activity including multiple results from carbon dating of deposits.
- There is a seismic network located at Shishaldin and an infrasound array available for detection of ground movement and eruptive activity. There is a webcam that is sporadically functional located about 10 km from the volcano.

**Karymsky:**

- Continuously populated dataset averaging 5 - 15 images per day.
- Satellite resolution that is appropriate for detection of small-scale explosive activity.
- Good confirmed record of historic activity including multiple results from carbon dating of deposits.

- All seismic networks and infrasound arrays deployed at Karymsky are focused on campaign studies and do not collect data continuously. There is no ground based visual resource at this time.

#### *3.6.2.1 Dataset Population*

In the North Pacific, AVHRR, MODIS, the Multi-Functional Transport Satellite (MTSAT), and the Geostationary Operational Environmental Satellite (GOES) data is collected for the region (Dean et al., 2002). AVHRR and MODIS were used for this study based on their spatial resolution. These two sensors provide anywhere from 5 - 30 images per day, depending on the location of the volcano. This data is collected and stored at UAF/GI, providing a fairly dense dataset for the North Pacific starting in 1993 and that is constantly being added to with few interruptions due to system issues and outages (Dean et al., 2002; Bailey et al., 2010). Data lost during outages of receiving stations is typically added to the database when the system is repaired.

#### *3.6.2.2 Spatial and Temporal Resolution*

As stated previously, the AVHRR sensor was chosen based largely on the spatial resolution of 1.09 km at nadir. Issues can arise from sensors with smaller pixel size, as an active volcano will typically have a consistently warmer summit area. This warmer temperature could potentially overshadow small explosions. Adversely, a too coarse pixel size will hinder the detection of small explosions due to pixel averaging. One sensor that collects data in the North Pacific, the GOES sensor, records images with a pixel size near 5 km by 7 km (Dean et al., 2002). At this pixel size, even a large single explosion (larger than those studied here) can be diminished by cold background temperatures. With the AVHRR sensor chosen, there are likely some explosions that are too small to be detected; but the important choice is to find a sensor that allows the detection of most small explosions without an abundance of sensor saturation.

The temporal resolution of the AVHRR sensors provide about 5 - 30 images each day (depending on volcano location). This is sufficient to provide a good representation of what is occurring at the volcano from day to day. There are sensors that have a more frequent temporal resolution, such as GOES with an image nearly every 15 minutes; however they are all of a much coarser spatial resolution, and are therefore not ideal for the reasons previously highlighted.

### *3.6.2.3 Recorded History*

As discussed earlier, all three volcanoes have a recorded history, though to varying extents. As they are remote volcanoes, they were not observed from the ground easily or frequently, which creates a sporadic historical timeline. Also, much of the information about their history was kept by native groups relying heavily on an oral tradition and who may not have passed the information along in a well documented manner.

There is recorded observed activity at each volcano in this study as far back as the 1700's [Cleveland – 1893 (GVP, 2014a), Shishaldin – 1775 (GVP, 2014b), and Karymsky – 1771 (GVP, 2014c)]. There are also some records of activity obtained through radiocarbon dating of deposits for Shishaldin (7550 BCE (GVP, 2014b)) and Karymsky (6600 BCE (GVP, 2014c)). Unfortunately, Cleveland has no available data from radiocarbon dating, so the first documented activity remains in the late 1800's.

### *3.6.2.4 Ground-Based Observations and Monitoring*

At Cleveland volcano, there are no ground based measurements and the only field observations are possible via a webcam located 70 km from the volcano (near Nikolski), which is often obscured by cloud cover and periodically non-operational. Karymsky is more frequently visited (Johnson et al., 1998; Johnson and Lees, 2000; Lees et al., 2004; Johnson, 2007), but there is no permanent ground-based monitoring system or webcam available (KVERT, 2013). Shishaldin has seismic and infrasound networks (Caplan-



Auerbach and McNutt, 2003) as well as a webcam (AVO, 2014c), making it the most highly monitored volcano of the set.

The extra information gained from the seismic and infrasound networks at Shishaldin allows for cross referencing activity and producing further methods for monitoring the state of volcanic activity. For example, at Shishaldin there was a period of tremor detected by the seismic networks that coincided with the increase in frequency of explosions (Caplan-Auerbach and McNutt, 2003). These two activity types occurred just prior to the plume-producing eruption in 2009. From this information, it can be inferred that an increase in small explosions will also present itself as a period of tremor, especially useful when weather obscures satellite views of the summit vent.

### **3.7 Conclusion**

Small scale explosions from active volcanoes can be observed using remote sensing methods. The method first developed and tested by Worden et al. (2014) provides good results when tested for use on North Pacific volcanoes. As seen on Stromboli, smaller explosions are still likely to be missed, so all results are a lower level estimate. Though this method does miss detection of the fraction of smallest events, the more important aspect is the analysis of changes in the relative frequency. The results shown here indicate that the three volcanoes in question have a detectable signature of activity prior to larger eruptions. Satellite data can be continuously monitored and analyzed for detection of this signature, leading to the possibility of emergency planning and hazard awareness in times when heightened activity is expected.

The importance of a few factors has been highlighted by studying these three volcanoes. A continuous and continually populating database is important in order to have a clear view of the activity of a volcano and to be able to determine what future activity may occur. The spatial and temporal resolution of the sensors chosen must be suitable for detection of small explosions and provide data without long gaps in data acquisition. A

recorded history of the activity at the volcano is important to have a better understanding of the normal background behavior, spanning time periods prior to the era of space-based sensors. Finally, some ground-based monitoring instrumentation is very beneficial to be able to correlate activity seen in satellite images to activity occurring on the ground.

More of these types of volcanoes, with activity similar to Cleveland, Shishaldin, and Karymsky, should be studied using this method to determine how the trends in frequency of smaller explosive activity relates to differing sizes and durations of plume activity. Some other volcanoes to consider would be Sakurajima, Popocatepetl, Etna, Merapi, and Kliuchevskoi. Some of these volcanoes have a very high level of background activity as well as more complex patterns and types of eruptive activity (e.g. lava flows and fountains at Etna, GVP, 2013; lava flows and gas emission at Kliuchevskoi, GVP, 2010b; dome building and pyroclastic flows at Merapi, GVP, 2006b). This would produce a larger database of volcanoes that can be used to assess the applicability of the method to all environments. Until then, the work shown here has illustrated the capability for high-latitude volcanoes, with very different local environmental conditions to the results of Worden et al. (2014).

### **3.8 Acknowledgements**

This project is based on work supported by the United States Geological Survey through the Alaska Volcano Observatory; a NASA Urgent Request Protocol grant for targeting ASTER acquisitions; and National Science Foundation (NSF) Interdisciplinary/Collaborative Research under grant no. CMMI-1131799. Special thanks also to the University of Alaska Fairbanks and the GINA for the use of systems and satellite databases.

J. Dehn and P. Webley aided in data synthesis and analysis for this research.

### 3.9 References

Aguilera, F. (2005). Contrasting styles of volcanic activity as observed by remote sensing: The case of Lascar, Llaima and Villarrica volcanoes, Chile. 6<sup>th</sup> Int. Symposium on Andean Geodynamics (Ext. Abstract), 21-25.

Alaska Volcano Observatory (AVO), (2011). Subsequent satellite images showed that the December 25 (recognized in retrospective data analysis) and 29 explosions had largely removed the dome.

<http://www.avo.alaska.edu/volcanoes/activity.php?volcname=Cleveland&page=basic&eraptionid=692>.

Alaska Volcano Observatory (AVO), (2014a). Key events from Cleveland Volcano: Reported Activity,

<http://www.avo.alaska.edu/volcanoes/volcact.php?volcname=Cleveland>

Alaska Volcano Observatory (AVO), (2014b). Key events from Shishaldin Volcano: Reported Activity,

<http://www.avo.alaska.edu/volcanoes/volcact.php?volcname=Shishaldin>

Alaska Volcano Observatory (AVO), (2014c), Live webcam homepage,

<http://www.avo.alaska.edu/webcam/>

Andronico, D., Branca, S., Calvari, S., Burton, M., Caltabiano, T., Corsaro, R.A., Del Carlo, P., Garfi, G., Lodato, L., Miraglia, L., Murè, F., Neri, M., Pecora, E., Pompilio, M., Salerno, G., Spampinato, L. (2005). A multi-disciplinary study of the 2002-03 Etna eruption: insights into a complex plumbing system. *Bulletin of Volcanology*, **27**, 314-330.

Arnoult, K.M., Olson, J.V., Szuberla, C.A.L., McNutt, S.R., Garcés, M.A., Fee, D., Hedlin, M.A.H. (2010). Infrasound observations of the 2008 explosive eruptions of Okmok and Kasatochi volcanoes, Alaska. *Journal of Geophysical Research*, **115**, D00L15.

Bailey, J.E., Dean, K.G., Dehn, J., Webley, P.W. (2010). Integrated satellite observations of the 2006 eruption of Augustine Volcano, in Power, J.A., Coombs, M.L., and Freymueller, J.T., eds., *The 2006 eruption of Augustine Volcano, Alaska*: U.S. Geological Survey Professional Paper 1769.

Barberi, F., Rosi, M., Sodi, A. (1993). Volcanic hazard assessment at Stromboli based on review of historical data. P. Manetti & J. Keller (Ed.), *Acta Vulcanologica*, **3**, 173-187.

Beget, J. E., Nye, C.J, Schaefer, J.R., Stelling, P.L. (2003). Preliminary Volcano-Hazard Assessment for Shishaldin Volcano, Alaska. Alaska Department of Natural Resources, Division of Geological & Geophysical Surveys.

Blackburn, E.A., Wilson, L., Sparks, R.S.J. (1976). Mechanisms and dynamics of strombolian activity. *Journal of the Geological Society*, **132**, 429-440.

Braitseva, O.A., Melekestsev, I.V., Ponomareva, V.V., Sulerzhitsky, L.D. (1995). Ages of calderas, large explosive craters and active volcanoes in the Kuril-Kamchatka region, Russia. *Bulletin of Volcanology*, **57**, 383-402.

Brantley, S.R., McGimsey, R.G., Neal, C.A. (2009). The Alaska Volcano Observatory – Expanded Monitoring of Volcanoes Yields Results. United States Geological Survey Fact Sheet 2004-3084. <http://pubs.usgs.gov/fs/2004/3084/>

Bulletin of Global Volcanism Network (BVGN), (2012). November 2012 report of Tolbachik volcano: Seismicity precedes onset of dual fissure eruption in November 2012, Report BGVN 37:12.

Caplan-Auerbach, J., McNutt, S.R. (2003). New insights into the 1999 eruption of Shishaldin volcano, Alaska, based on acoustic data. *Bulletin of Volcanology*, **65**, 405-417.

Coats, R. R. (1950). Volcanic activity in the Aleutian Arc: U.S. Geological Survey Bulletin B 0974-B, p. 35-49, 1 sheet, scale unknown.

Coats, R.R. (1962). Magma Type and Crustal Structure in the Aleutian Arc, *Geophysical Monograph Series*, **6**, 92-109.

De Angelis, S., McNutt, S.R., Webley, P.W. (2011). Evidence of atmospheric gravity waves during the 2008 eruption of Okmok volcano from seismic and remote sensing observations. *Geophysical Research Letters*. **38**, L10303, doi:10.1029/2011GL047144.

De Angelis, S., Fee, D., Haney, M., Schneider, D. (2012). Detecting hidden volcanic explosions from Mt. Cleveland Volcano, Alaska with infrasound and ground-coupled airwaves, *Geophysical Research Letters*, **39**, L21312.

Dean, K. G., Dehn, J., Engle, K., Izbekov, P., Papp, K., Patrick, M. (2002). Operational satellite monitoring of volcanoes at the Alaska Volcano Observatory. Monitoring Volcanic Hotspots using Thermal Remote Sensing, AJH Harris, M. Wooster and DA Rothery (Eds), *Advances in Environmental Monitoring and Modeling*, **1**, 70-97.

Dean, K.G., Dehn, J., Papp, K.R., Smith, S., Izbekov, P., Peterson, R., Kearney, C., Steffke, A. (2004). Volcanic Observations from Space: New Results from the EOS Satellite Instruments Integrated satellite observations of the 2001 eruption of Mt. Cleveland, Alaska. *Journal of Volcanology and Geothermal Research*. **135**, 1-2, 51-73.

Dehn, J., Dean, K., Engle, K. (2000). Thermal monitoring of North Pacific volcanoes from space. *Geology*, **28(8)**, 755-758.

Dehn, J., Dean, K.G., Engle, K., Izbekov, P. (2002). Thermal precursors in satellite images of the 1999 eruption of Shishaldin Volcano. *Bulletin of Volcanology*. **64**, 525-534.

Dehn, J., Harris, A.J.L., (2014). Thermal anomalies at volcanoes in satellite imagery. In: Dean & Dehn eds. Atlas of volcanic eruptions from Space, Springer Verlag, New York (in press).

Dixon, J.P., Stihler, S.D., Power, J.A., Searcy, C.K. (2012). Catalog of Earthquake Hypocenters at Alaskan Volcanoes: January 1 through December 31, 2011. USGS Data Series 730. 90 p.

Eichelberger, J.C., Izbekov, P.E. (2000). Eruption of andesite triggered by dyke injection: contrasting cases at Karymsky Volcano, Kamchatka and Mt Katmai, Alaska. *Philosophical Transactions of the Royal Society*, **358**, 1465-1485.

Fee, D., Matoza, R.S. (2013). An overview of volcano infrasound: From Hawaiian to Plinian, local to global. *Journal of Volcanology and Geothermal Research*. **249**, 123-139.

Fournelle, J. (1988). The geology and petrology of Shishaldin Volcano, Unimak Island, Aleutian Arc, Alaska. Ph.D. Dissertation thesis, John Hopkins University, 507 pp.

Fournelle, J., Marsh, B.D. (1991). Shishaldin Volcano: Aleutian high-alumina basalts and the question of plagioclase accumulation. *Geology*, **19**, 234-237.

Federal State Statistics Service (FSSS), (2011). 2010 All-Russian Population Census, vol. 1, (in Russian).

Gardner, C.A., Guffanti, M.C. (2006). U.S. Geological Survey's Alert Notification System for Volcanic Activity, U.S Geological Survey Fact Sheet 2006-3139, Version 1.0, 4p.

Global Volcanism Program (GVP), (2006a). On 23 May, AVO reported that an astronaut aboard the International Space Station observed an ash plume from Cleveland at 1500. A plume was visible on satellite imagery at 1507 that drifted SW and reached a height of 6.1 km (20,000 ft) a.s.l. At 1700, an image showed the detached ash plume 130 km SW of Cleveland. United States Geological Survey, Alaska Volcano Observatory, 17 May – 23 May, 2006. BVGN 31:07.

Global Volcanism Program (GVP), (2006b). On 14 June, a dome-collapse event, lasting approximately 3.5 hours, produced pyroclastic flows that reached a maximum distance of 7 km SE along the Gendol River., Pusat Vulkanologi dan Mitigasi Bencana Geologi (PVMBG) also known CVGHM, 14 June – 20 June, 2006.

Global Volcanism Program (GVP), (2007). INSIVUMEH reported that during 4-5 January, Strombolian eruptions from Pacaya produced incandescent material that was expelled at 2-40-second intervals, up to 100 m above the crater. Gas clouds reached an altitude of 2.7 km (8,900 ft) a.s.l. and drifted S. A lava flow 50 m in length pooled near the NE edge of MacKenney Cone, Instituto Nacional de Sismologia, Vulcanologia, Meteorologia, e Hidrologia (INSIVUMEH), 3 January, 2007. BVGN 30:10

Global Volcanism Program (GVP), (2008). On 24 July, a low-level ash plume and a strong thermal anomaly were noted near the summit. The thermal anomaly suggested the presence of an active lava flow. The thermal anomaly continued to be detected during 26-28 July and possible ash plumes drifted SE, E, and NE at altitudes of 3-6.1 km (10,000-20,000 ft) a.s.l. during 27-29 July., United States Geological Survey, 23 July – 29 July, 2008.

Global Volcanism Program (GVP), (2010a). AVO reported a small ash emission from Cleveland on 30 May. A detached plume seen in satellite imagery rose no higher than 4.9 km (16,000 ft) a.s.l. and drifted SW., United States Geological Survey, Alaska Volcano Observatory, 26 May – 1 June, 2010. BVGN 35:06.

Global Volcanism Program (GVP), (2010b). KVERT reported that during 23-30 July seismic activity from Kliuchevskoi was above background levels and lava flowed down the SSE flank. Strombolian activity and gas-and-ash emissions were observed during 23-24 and 29 July., Kamchatkan Volcanic Eruption Response Team (KVERT), 28 July – 3 August, 2010.

Global Volcanism Program (GVP), (2013). INGV reported on the morning of 23 November the 17th paroxysm occurred from Etna's New Southeast Crater (NSEC), five days after the previous one. The episode was characterized by a rapid evolution from Strombolian activity to lava fountains, an ash plume that rose several kilometers and drifted NE, and lava flows that were significantly less extensive than those emitted during the 16-17 November paroxysm., Sezione di Catania - Osservatorio Etneo (INGV), 20 November – 26 November, 2013.

Global Volcanism Program (GVP), (2014a), Cleveland Eruption History, <http://www.volcano.si.edu/volcano.cfm?vn=311240>



Global Volcanism Program (GVP), (2014b), Shishaldin Eruption History,  
<http://www.volcano.si.edu/volcano.cfm?vn=311360>

Global Volcanism Program (GVP), (2014c), Karymsky Eruption History,  
<http://www.volcano.si.edu/volcano.cfm?vn=300130>

Global Volcanism Program (GVP), (2014d), Roundtop Eruption History,  
<http://www.volcano.si.edu/volcano.cfm?vn=311380>

Gottsmann, J., De Angelis, S., Fournier, N., Van Camp, M., Sacks, S., Linde, A., Ripepe, M. (2011). On the geophysical fingerprint of Vulcanian explosions. *Earth and Planetary Science Letters*. **306**, 98-104.

Hansell, A.L., Horwell, C.J., Oppenheimer, C. (2006). The Health Hazards of Volcanoes and Geothermal Areas. *Occupational and Environmental Medicine*. **63**, 149-156.

Harris, A.J., Ripepe, M. (2007). Synergy of multiple geophysical approaches to unravel explosive eruption conduit and source dynamics – A case study from Stromboli. *Chemie der Erde*, **67**, 1-35.

Harris, A.J., Delle Donne, D., Dehn, J., Ripepe, M., Worden, A.K. (2013). Volcanic plume and bomb field masses from thermal infrared camera imagery. *Earth and Planetary Science Letters*, **365**, 77-85.

Harris, A.J. (2013). Thermal Remote Sensing of Active Volcanoes, A User's Manual. Cambridge University Press, Cambridge: UK.

Hornig-Kjarsgaard, I., Keller, J., Koberski, U., Stadlbauer, E., Francalanci, L., Lenhart, R. (1993). Geology, stratigraphy and volcanological evolution of the island of Stromboli, Aeolian arc, Italy. P. Manetti & J. Keller (Ed.), *Acta Vulcanologica*, **3**, 21-68.

Ivanov, B.V. (1970). Eruption of Karymsky Volcano during 1962-65 and the Karymsky Volcanic Group. Nauka, Moscow, 135 pp. (in Russian).

Ivanov, B. V., Braitseva, O. A., Zubin, M. I. (1991). Karymsky volcano. In: Fedotov, S. A. & Masurenkov, Yu. P (eds) Active Volcanoes of Kamchatka, Vol. 2. Moscow: Nauka Publishers, 181–203.

Izbekov, P.E. (2002). The 1996 eruption of Karymsky Volcano, Kamchatka: Detailed petrological study of a single basalt-triggered eruption cycle. Ph.D. Dissertation thesis, University of Alaska Fairbanks, 220 pp.

Izbekov, P.E., Eichelberger, J.C., Ivanov, B.V. (2004). The 1996 Eruption of Karymsky Volcano, Kamchatka: Historical Record of Basaltic Replenishment of an Andesite Reservoir. *Journal of Petrology*, **45**, 11, 2325-2345.

Jaggard, T. A. (1932). Aleutian eruptions 1930-1932: The Volcano Letter, v. 375, p. 1-4.

Johnson, J.B., Lees, J.M., Gordeev, E.I. (1998). Degassing explosions at Karymsky Volcano, Kamchatka. *Geophysical Research Letters*, **25**, 21, 3999-4002.

Johnson, J.B., Lees, J. M. (2000). Plugs and chugs - seismic and acoustic observations of degassing explosions at Karymsky, Russia and Sangay, Ecuador. *Journal of Volcanology and Geothermal Research*, **101**, 67-82.

Johnson, J.B. (2007). On the relation between infrasound, seismicity, and small pyroclastic explosions at Karymsky Volcano. *Journal of Geophysical Research*, **112**, B08203.

Judd, J.W. (1881). Volcanoes. In: Kegan et al. (eds) What they are and what they teach. London.

Kamchatka Volcano Eruption Response Team (KVERT), (2013). Karymsky volcano: information, hazard synopsis and eruptions list, <http://www.kscnet.ru/ivs/kvert/volc.php?name=Karymsky&lang=en>

Lacroix, A. (1904), Montagne Pelée et ses Éruptions: Paris, Masson et Cie Éditeurs, 1-662.

Lees, J.M., Gordeev, E.I., Ripepe, M. (2004). Explosions and periodic tremor at Karymsky volcano, Kamchatka, Russia. *Geophysical Journal International*. **158**, 1151-1167.

Lillesand, T.M., Keifer, R.W., Chipman, J.W. (2008). Remote Sensing and Image Interpretation, 6th Edition. Hoboken, New Jersey: John Wiley & Sons, Inc.

Lopez, T., Fee, D., Prata, F., Dehn, J. (2013). Characterization and interpretation of volcanic activity at Karymsky Volcano, Kamchatka, Russia, using observations of infrasound, volcanic emissions, and thermal imagery. *Geochemistry, Geophysics, Geosystems*, **14** (12), 5106-5127.

McGimsey, R. G., Neal, C. A., Doukas, M. P. (1995). Volcanic activity in Alaska: Summary of events and response of the Alaska Volcano Observatory 1992: U.S. Geological Survey Open-File Report OF 95-83, 26 p.

McGimsey, R.G., Neal, C.A., Girina, O. (2004). 2001 volcanic activity in Alaska and Kamchatka: Summary of events and response of the Alaska Volcano Observatory: U.S. Geological Survey Open-File Report OF 2004-1453, 53 p.

McGimsey, R.G., Neal, C.A., Dixon, J.P., Ushakov, S. (2007). 2005 Volcanic activity in Alaska, Kamchatka, and the Kurile Islands: Summary of events and response of the Alaska Volcano Observatory: U.S. Geological Survey Scientific Investigations Report 2007-5269, 94 p., available at <http://pubs.usgs.gov/sir/2007/5269/> .

McGimsey, R.G., Neal, C.A., Girina, O.A., Chibisova, M., Rybin, A. (2014). 2009 Volcanic activity in Alaska, Kamchatka, and the Kurile Islands - summary of events and response of the Alaska Volcano Observatory: U.S. Geological Survey Scientific Investigations Report 2013-5213, 125 p., <http://dx.doi.org/10.3133/sir/20135213> .

Miller, T.P., McGimsey, R.G., Richter, D.H., Riehle, J.R., Nye, C.J., Yount, M.E., Dumoulin, J.A. (1998). Catalog of the historically active volcanoes of Alaska. United States Department of the Interior, United States Geological Survey, Open-File Report 98-582.

Mothes, P.A. (1992). Lahars of Cotopaxi, Ecuador: hazard and risk evaluation. In Geohazards, ed. McCall, G.J.H., Laming, D.J.C., Scott, S.C., 53-63.

National Oceanic and Atmospheric Administration (NOAA), (2013). Advanced Very High Resolution Radiometer – AVHRR, <http://noaasis.noaa.gov/NOAASIS/ml/avhrr.html>

Neal, C.A., Doukas, M.P., McGimsey, R.G. (1995). 1994 Volcanic activity in Alaska: Summary of events and response of the Alaska Volcano Observatory. United States Department of the Interior, United States Geological Survey, Open-File Report 95-271.

- Neal, C.A., Casadevall, T.J., Miller, T.P., Hendley II, J.W., Stauffer, P.H. (1997). Volcanic ash: Danger to aircraft in the North Pacific. United States Geological Survey Fact Sheet 030-97. <http://pubs.usgs.gov/fs/fs030-97/>.
- Neal, C.A., McGimsey, R.G., Girina, O. (2004). 2002 Volcanic activity in Alaska and Kamchatka: Summary of events and response of the Alaska Volcano Observatory. United States Department of the Interior, United States Geological Survey, Open-File Report 2004-1058.
- Neal, C.A., McGimsey, R.G., Dixon, J.P., Cameron, C.E., Nuzhaev, A.A., Chibisova, M. (2011). 2008 Volcanic activity in Alaska, Kamchatka, and the Kurile Islands: Summary of events and response of the Alaska Volcano Observatory: U.S. Geological Survey Scientific Investigations Report 2010-5243, 94 p., available at <http://pubs.usgs.gov/sir/2010/5243> .
- Nicolaysen, K. (2013). Information of composition of Mt. Cleveland flows and deposits, Personal communication and unpublished data.
- Nye, C.J., Keith, T.E.C., Eichelberger, J.C., Miller, T.P., McNutt, S.R., Moran, S., Schneider, D.J., Dehn, J., Schaefer, J.R. (2002). The 1999 eruption of Shishaldin Volcano, Alaska: monitoring a distant eruption. *Bulletin of Volcanology*, **64**, 507-519.
- Ozerov, A., Ispolatov, I., Lees, J. (2001). Modeling eruptions of Karymsky Volcano. *Journal of Volcanology and Geothermal Research*, **122**, 3-4, 265-280.
- Patrick, M.R. (2002). Numerical Modeling of Lava Flow Cooling Applied to the 1997 Okmok Eruption: Comparison with AVHRR Thermal Imagery, M.S. thesis, University of Alaska Fairbanks, Fairbanks, 141 pp.

Patrick, M.R., Dehn, J., Dean, K. (2005). Numerical modeling of lava flow cooling applied to the 1997 Okmok eruption: Comparison with advanced very high resolution radiometer thermal imagery. *Journal of Geophysical Research*, **110**, B02210.

Patrick, M., Harris, A., Ripepe, M., Dehn, J., Rothery, D., Calvari, S. (2007). Strombolian explosive styles and source conditions: insights from thermal (FLIR) video. *Bulletin of Volcanology*, **69**, 769-784.

Pioli, L., Erlund, E., Johnson, E., Cashman, K., Wallace, P., Rosi, M., Delgado Granados, H. (2008). Explosive dynamics of violent Strombolian eruptions: The eruption of Parícutin Volcano 1943-1952 (Mexico). *Earth and Planetary Science Letters*, **271**, 359-368.

Prata, A. J. (1989). Observations of volcanic ash clouds in the 10-12  $\mu\text{m}$  window using AVHRR/2 data. *International Journal of Remote Sensing*, **10(4-5)**, 751-761.

Ramsey, M., Dehn, J. (2004). Spaceborne observations of the 2000 Bezymianny, Kamchatka eruption: the integration of high-resolution ASTER data into near real-time monitoring using AVHRR. *Journal of Volcanology and Geothermal Research*, **135(1)**, 127-146.

Reeder, J. (1989). Cleveland. In *Global Volcanism 1975-1985*. Ed. McClelland, L., Simkin, T., Summers, M., Nielsen, E., Stein, T.C., Englewood Cliffs, New Jersey: Prentice Hall. p. 328

Reeder, J. W. (1990a). Cleveland: in *Annual report of the world volcanic eruptions in 1987*, *Bulletin of Volcanic Eruptions*, **27**, p. 41-44.

Reeder, J. W. (1990b). Shishaldin: in Annual report of the world volcanic eruptions in 1987, *Bulletin of Volcanic Eruptions*, **27**, p. 50-51.

Ripepe, M., Harris, A.J.L., Carniel, R. (2002). Thermal, Seismic, and Infrasonic Evidences of Variable Degassing Rates at Stromboli Volcano. *Journal of Volcanology and Geothermal Research*. **118**, 3-4. Pp. 285-297.

Rosi, M., Bertagnini, A., Landi, P. (2000). Onset of the persistent activity at Stromboli Volcano (Italy). *Bulletin of Volcanology*, **62**, 294-300.

Ryan, H.F., Scholl, D.W. (1993). Geologic Implications of Great Interplate Earthquakes Along the Aleutian Arc, *Journal of Geophysical Research*, **98**, P. 22135-22146.

Schneider, D. J., Dean, K., Dehn, J., Miller, T., Kirianov, V. Y. (2000). Monitoring and analyses of volcanic activity using remote sensing data at the Alaska Volcano Observatory: case study for Kamchatka, Russia, December 1997. *Remote Sensing of Active Volcanism*, 65-85.

Scholl, D.W. (2007). Viewing the Tectonic Evolution of the Kamchatka-Aleutian (KAT) Connection with an Alaska Crustal Extrusion Perspective. *Volcanism and Subduction: The Kamchatka Region. Geophysical Monograph Series*. **172**. 3-35.

Siebert, L., Simkin, T. (2002). *Volcanoes of the world: an illustrated catalog of Holocene volcanoes and their eruptions*: Smithsonian Institution, Global Volcanism Program Digital Information Series GVP-3, <http://www.volcano.si.edu/gvp/world/>.

Simkin, T., Siebert, L. (1994). *Volcanoes of the world [2nd edition]*: Tucson, Arizona, Geoscience Press, 349 p.

Simpson, J.J., Hufford, G.L., Pieri, D., Servranckx, R., Berg, J.S., Bauer, C. (2002). The February 2001 eruption of Mount Cleveland, Alaska: Case study of an aviation hazard. *Weather Forecasting*, 17, 691–704. doi: [http://dx.doi.org/10.1175/1520-0434\(2002\)017<0691:TFEOMC>2.0.CO;2](http://dx.doi.org/10.1175/1520-0434(2002)017<0691:TFEOMC>2.0.CO;2).

Steinbeck, C., Fuller, A. (2004). Map In: Atlas of Pacific Salmon: The First Map-based Status Assessment of Salmon in the North Pacific (by . Augerot, X.). State of the Salmon Consortium.

Tokarev, P.I. (1989). Eruption and seismicity of Karymsky volcano in 1965-1986. *Volcanology and Seismology*, 2: 3-13 (in Russian).

United States Census Bureau (USCB), (2014). The United States Census 2010, <http://www.census.gov/2010census/>

Veniaminov, I. (1840). Notes on the islands of the Unalaska district [translated from Russian by Lydia T. Black and R.H. Geoghegan in 1984]: Pierce, R. A., (ed.), Kingston, Ontario, Limestone Press, 511 p.

Volynets, A.O., Churikova, T.G., Worner, G., Gordeychik, B.N., Layer, P. (2010). Mafic Late Miocene-Quaternary volcanic rocks in the Kamchatka back arc region: implications for subduction geometry and slab history at the Pacific-Aleutian junction. *Contributions to Mineral Petrology*, **159**, 659-687.

Walker, G.P.L. (1973). Explosive volcanic eruptions, a new classification scheme, *Geologische Rundschau*, **62**, 431-446.



Wallace, K.L., McGimsey, R.G., Miller, T.P. (2000). Historically Active Volcanoes in Alaska – A Quick Reference. United States Geological Survey Fact Sheet 118-00.

<http://geopubs.wr.usgs.gov/fact-sheet/fs118-00/>

Waythomas, C. F., Scott, W. E., Prejean, S. G., Schneider, D. J., Izbekov, P., Nye, C. J. (2010). The 7–8 August 2008 eruption of Kasatochi Volcano, central Aleutian Islands, Alaska. *Journal of Geophysical Research: Solid Earth (1978–2012)*, **115**(B12).

Webley, P. W., Dehn, J., Lovick, J., Dean, K. G., Bailey, J. E., Valcic, L. (2009). Near-real-time volcanic ash cloud detection: Experiences from the Alaska Volcano Observatory. *Journal of Volcanology and Geothermal Research*, **186** (1), 79-90.

Webley, P.W., Lopez, T.M., Ekstrand, A.L., Dean, K.G., Rinkleff, P., Dehn, J., Cahill, C.F., Wessels, R.L., Bailey, J.E., Izbekov, P., Worden, A. (2013). Remote observations of eruptive clouds and surface thermal activity during the 2009 eruption of Redoubt volcano. *Journal of Volcanology and Geothermal Research*, **259**, 185–200

Wilson, T., Kaye, G., Stewart, C., Cole, J. (2007). Impacts of the 2006 eruption of Merapi volcano, Indonesia, on agriculture and infrastructure. GNS Science Report 2007/07, 69p.

Wohletz, K., Heiken, G. (1992). *Volcanology and Geothermal Energy*. Berkeley, University of California Press.

Worden, A., Dehn, J., Ripepe, M., Delle Donne, D. (2014). Frequency based detection and monitoring of small scale explosive activity. *Journal of Volcanology and Geothermal Research*. (in press).

Wright, R., Flynn, L. P., Garbeil, H., Harris, A. J., Pilger, E. (2004). MODVOLC: near-real-time thermal monitoring of global volcanism. *Journal of Volcanology and Geothermal Research*, **135(1)**, 29-49.

## **Chapter Four**

### **Conclusions**

#### **4.1 Summary of Findings**

Satellite remote sensing has proved to offer a useful, safe, and relatively inexpensive method for monitoring large areas where field work is logistically unrealistic, costly, and potentially dangerous (Harris et al, 1997; Dehn et al., 2000; Harris et al., 2000; Dean et al., 2002; Webley et al., 2009; Dehn and Harris, 2014). It is possible that by using satellite remote sensing the portion of the smallest explosions at these volcanoes is being missed. However, the sensors are able to detect the major portion of explosions; those which appear to be of a size that tends to effect and represent larger scale changes in the volcanic systems, eventually relating to ash producing periods of extended eruptive activity. As new sensors are developed, the ability to detect activity improves so that a system to gauge the frequency of volcanic activity from space provides a useful monitoring tool.

Four volcanoes were chosen for development and testing of a method to monitor activity. The first volcano was chosen to develop a baseline model which was then applied to the final three volcanoes as an assessment of the method. Each volcano studied had a unique signature of precursors that became evident after the processing of three to five years of back-logged data. Though the type and timing of precursory activity was unique for each volcano, it was identifiable when viewing the results obtained during this research. The most useful method of determining the precursory activity was to characterize the magnitude of plume events (weekly plume magnitude) and compare that value to the thermal activity (thermal feature ratio) one, two, three, and four weeks prior to plume activity (Figure 4.1). Stromboli volcano showed a cessation of small scale explosions prior to larger eruptive periods, though because plume data at Stromboli was not available, the plume magnitudes could not be calculated. Cleveland, Shishaldin, and

Karymsky each showed changes in the frequencies of small scale explosions prior to periods of heightened activity, though each volcano had a unique timing (one to two weeks prior for Cleveland; strong increases three weeks prior for Shishaldin; and minor increases three weeks prior for Karymsky).

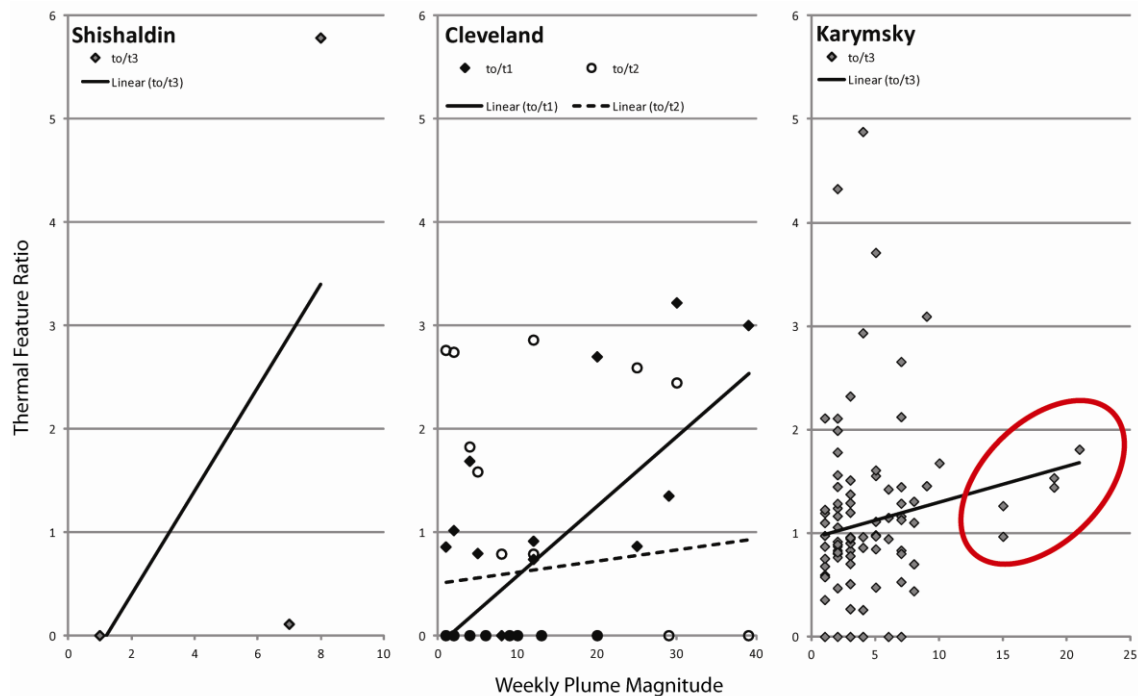


**Figure 4.1:** The strongest trends in activity are highlighted, indicating the period of time prior to large eruptive activity when thermal precursors are the strongest. The time periods represented are denoted as:  $t_0$  – the week including the plume activity,  $t_0/t_1$  – the week prior to plume activity,  $t_0/t_2$  – two weeks prior to plume activity, and  $t_0/t_3$  – three weeks prior to plume activity. Linear trends are best fit lines to the data available for weekly plume magnitude. The circled Karymsky data appears to indicate a deeper source mechanism than the lower plume magnitude data.

## 4.2. Method Development

The method developed on data from Stromboli worked well and was able to produce good results. The basis of choice of location for the development of a monitoring tool was key: a reliably erupting volcano with a comprehensive recorded history and a well maintained system of ground-based measurements. By developing a time series of

activity, it was possible to identify trends in activity prior to larger eruptive periods. By identifying these characteristics, it is possible to have some period of warning for activity in the future.

The method described here could be useful in an operational setting, especially when applied to remote volcanoes that have the potential to impact populations, infrastructure, and the aviation community. A number of important factors will affect the validity of application of this method, and are met to varying degrees by the four volcanoes chosen. They are:

- *The availability of a continuous and continually populated dataset.* For Stromboli Volcano only a partial dataset was available. This covered periods from 2002 – 2010 with significant gaps throughout. For Cleveland, Shishaldin, and Karymsky, a full, continuous data set was available for the period from 2005 - 2010.
- *Appropriate and reasonable sensor resolutions.* The spectral resolution best for identifying thermal features is in the mid-infrared spectrum,  $\sim 3.5\text{-}4\ \mu\text{m}$ . This range is collected by both the MODIS and AVHRR sensors. These two types of sensors also have similar spatial resolution at nadir, 1 – 1.1 km, which was suitable for the detection of small scale explosive activity. AVHRR has a slightly higher temporal resolution than the MODIS sensor, though this is dependent on the region.
- *A recorded history of the volcano's previous activity.* This is an important factor when trying to create a time series for a volcano and characterize background activity. For Stromboli Volcano, the history is very well recorded for the past 2000 – 2500 years (Judd, 1881; Rosi et al., 2000). The volcanoes of the North Pacific are less well reported on. Shishaldin and Karymsky both have confirmed historical activity reported in the late 1700's (GVP, 2014b; GVP, 2014c, respectively). Cleveland, however, does not have an extensive reported history, with the first confirmed eruptions in the late 1800's (GVP, 2014a).

- *If available, some ground-based monitoring system (such as seismic, infrasound, thermal camera, and webcam).* Stromboli Volcano is very well monitored, with seismic, infrasound, digital and thermal cameras, and gas measurements maintained on the summit. The volcanoes of the North Pacific are less monitored. Cleveland and Karymsky have no permanent stations of any kind, with only intermittent webcam footage available (KVERT, 2013; AVO, 2014c). Shishaldin does have a functioning seismic network and infrasound array, as well as intermittent webcam views (Caplan-Auerbach and McNutt, 2003; AVO, 2014c).

### **4.3. Method Application**

When the method developed at Stromboli was applied to volcanoes in the North Pacific it again produced good results. Time series for three volcanoes, Cleveland, Shishaldin, and Karymsky, were produced and at each volcano a trend in small scale explosive activity was detectable a period of time prior to larger eruptive events. A major result when applied in the North Pacific was the realization that the method could help with the identification of different types of precursory activity as well as varying lengths of time prior to larger eruptive activity.

Complications due to the signal to noise ratio at some volcanoes became evident during this process. At volcanoes with a high level of background activity (noise), it will be harder to detect changes in explosive frequency that act as precursors (signal) to larger eruptive events. Karymsky shows a very high level of background activity and so detection of precursors there was difficult. Shishaldin, on the other hand, has an almost null level of background activity, meaning that any sort of precursory activity was very easy to detect with this method.

By using the method on three volcanoes with differing activity, it was proven that this monitoring tool could be applied to a wide range of volcanoes and still produce useful and robust data.

#### 4.4. Future Work

The method developed here and the results that have come from its application to a sample set of volcanoes indicate that it is a useful tool, and should be applied to more volcanoes around the world. Though this method was tested specifically at volcanoes that are remote and not otherwise well monitored, it should be noted that this could also be a very useful tool at volcanoes that are surrounded by populations and infrastructure as well as volcanoes that are heavily monitored with other methods.

A further step towards work in the North Pacific would be to calculate plume magnitudes for all volcanoes with reported plume activity. This could be done using the UAF/GI satellite database, which has plume reports dating back to 2005. This method of plume characterization can indicate types and magnitudes of precursory activity, as well as internal volcanic mechanisms responsible for larger eruptive phases at North Pacific volcanoes.

The method used here deals specifically with the detection of small scale explosive activity. There are many other types of activity that occur as either precursory activity or as activity within an eruptive episode; e.g. lava flows, dome growth and collapse, phreatomagmatic explosions. These types of volcanic activity would be the next step for the development of this method, though preliminary consideration holds some conclusions about the effectiveness. Lava flows are effusive activity which typically continually emit thermal energy. This type of activity does not typically act as a precursor to impending explosive activity (Dehn et al., 2000), with few exceptions (e.g. paroxysms at Stromboli; Barberi et al., 1993; Calvari et al., 2006). Dome growth can be a very clear indication of precursory activity, depending on the volcano. Many volcanoes that undergo dome growth are known to have a cycle of dome growth and dome destruction due to large explosions (van Manen et al., 2010). This activity can be viewed in thermal satellite data as a sustained thermal source leading up to an ash-plume producing explosion. Phreatomagmatic activity would likely not lead to thermal precursors

detectable in satellite images. This type of activity results from a fluid interaction with a volcanic system, typically subsurface. These fluids are very efficient at transferring heat, dissipating it quickly through fluid movement and flash steaming. This would not allow enough heat to transmit to the surface to produce thermal anomalies in satellite imagery. Of course, there will also be volcanoes that do not show any sort of thermal precursory activity. The eruptions of Kasatochi (Waythomas et al., 2010; Neal et al., 2011) and Okmok (Larsen et al., 2009) in Alaska in 2008 were both Plinian eruptions with no thermal precursors. At Kasatochi, there was no active monitoring and seismic warning came from United States Fisheries and Wildlife Services researches on the island one week before the eruption (Waythomas et al., 2008). At Okmok, there was only a short period of seismic precursory activity which was noted in hindsight.

There are dozens of volcanoes with small scale explosive activity at varying intervals and intensities. Some of these volcanoes also have other types of activity coincident with the small explosions, which, while adding another variable to the monitoring method developed, would serve to advance the method for more robust and reliable results. Volcanoes like Sakurajima (Japan), Popocatepetl (Mexico), Etna (Italy), and Merapi (Indonesia) would be informative to begin with as they are known for distinct eruptive activity and fulfill a number of the factors for reliable use of this method (recorded history of the volcanoes previous activity, ground-based monitoring systems, etc.). These volcanoes are also each located in unique volcanic and geologic settings, producing a larger and more diverse database of volcanoes where the method could prove useful. However, until future research is possible, the work shown here has served to illustrate the capability of this method and monitoring tool for use at both Mediterranean (mid-latitude) and North Pacific (high-latitude) volcanoes.



## References

- Alaska Volcano Observatory (AVO), (2014a). Key events from Cleveland Volcano: Reported Activity,  
<http://www.avo.alaska.edu/volcanoes/volcact.php?volcname=Cleveland>
- Alaska Volcano Observatory (AVO), (2014c), Live webcam homepage,  
<http://www.avo.alaska.edu/webcam/>
- Barberi, F., Rosi, M., Sodi, A. (1993). Volcanic hazard assessment at Stromboli based on review of historical data. P. Manetti & J. Keller (Ed.), *Acta Vulcanologica*, **3**, 173-187.
- Bertagnini, A., Di Roberto, A., Pompilio, M. (2011). Paroxysmal activity at Stromboli: lessons from the past. *Bulletin of Volcanology*, **73**, 1229-1243.
- Bertolaso, G., De Bernardinis, B., Bosi, V., Cardaci, C., Ciolli, S., Colozza, R., Cristiani, C., Mangione, D., Ricciardi, A., Rosi, M., Scalzo, A., Soddu, P. (2009). Civil protection preparedness and response to the 2007 eruptive crisis of Stromboli volcano, Italy. *Journal of Volcanology and Geothermal Research*, **182**, 269-277.
- Braitseva, O.A., Melekestsev, I.V., Ponomareva, V.V., Sulerzhitsky, L.D. (1995). Ages of calderas, large explosive craters and active volcanoes in the Kuril-Kamchatka region, Russia. *Bulletin of Volcanology*, **57**, 383-402.
- Calvari, S., Spampinato, L., Lodato, L. (2006). The 5 April 2003 vulcanian paroxysmal explosion at Stromboli volcano (Italy) from field observations and thermal data. *Journal of Volcanology and Geothermal Research*. **149** (1-2), 160-175.
- Caplan-Auerbach, J., McNutt, S.R. (2003). New insights into the 1999 eruption of Shishaldin volcano, Alaska, based on acoustic data. *Bulletin of Volcanology*, **65**, 405-417.

Dean, K. G., Dehn, J., Engle, K., Izbekov, P., Papp, K., Patrick, M. (2002). Operational satellite monitoring of volcanoes at the Alaska Volcano Observatory. Monitoring Volcanic Hotspots using Thermal Remote Sensing, AJH Harris, M. Wooster and DA Rothery (Eds), *Advances in Environmental Monitoring and Modeling*, **1**, 70-97.

Dehn, J., Dean, K., Engle, K. (2000). Thermal monitoring of North Pacific volcanoes from space. *Geology*, **28(8)**, 755-758.

Dehn, J., Dean, K.G., Engle, K., Izbekov, P. (2002). Thermal precursors in satellite images of the 1999 eruption of Shishaldin Volcano. *Bulletin of Volcanology*. **64**, 525-534.

Dehn, J. and Harris, A.J.L. (2014). Thermal anomalies at volcanoes in satellite imagery. In: Dean & Dehn eds. Atlas of volcanic eruptions from Space, Springer Verlag, New York (in press).

Fee, D., Matoza, R.S. (2013). An overview of volcano infrasound: From Hawaiian to Plinian, local to global. *Journal of Volcanology and Geothermal Research*. **249**, 123-139.

Global Volcanism Program (GVP), (2006). On 23 May, AVO reported that an astronaut aboard the International Space Station observed an ash plume from Cleveland at 1500. A plume was visible on satellite imagery at 1507 that drifted SW and reached a height of 6.1 km (20,000 ft) a.s.l. At 1700, an image showed the detached ash plume 130 km SW of Cleveland. United States Geological Survey, Alaska Volcano Observatory, 17 May – 23 May, 2006. BVGN **31:07**.

Global Volcanism Program (GVP), (2008). On 24 July, a low-level ash plume and a strong thermal anomaly were noted near the summit. The thermal anomaly suggested the presence of an active lava flow. The thermal anomaly continued to be detected during 26-28 July and possible ash plumes drifted SE, E, and NE at altitudes of 3-6.1 km (10,000-20,000 ft) a.s.l. during 27-29 July., United States Geological Survey, 23 July – 29 July, 2008.

Global Volcanism Program (GVP), (2010). AVO reported a small ash emission from Cleveland on 30 May. A detached plume seen in satellite imagery rose no higher than 4.9 km (16,000 ft) a.s.l. and drifted SW., United States Geological Survey, Alaska Volcano Observatory, 26 May – 1 June, 2010. BVGN **35:06**.

Global Volcanism Program (GVP), (2014a). Cleveland Eruption History, <http://www.volcano.si.edu/volcano.cfm?vn=311240>

Global Volcanism Program (GVP), (2014b). Shishaldin Eruption History, <http://www.volcano.si.edu/volcano.cfm?vn=311360>

Global Volcanism Program (GVP), (2014c). Karymsky Eruption History, <http://www.volcano.si.edu/volcano.cfm?vn=300130>

Hansell, A.L., Horwell, C.J., Oppenheimer, C. (2006). The Health Hazards of Volcanoes and Geothermal Areas. *Occupational and Environmental Medicine*. **63**, 149-156.

Harris, A.J.L., Butterworth, A.L., Carlton, R.W., Downey, I., Miller, P., Navarro, P., Rothery, D.A. (1997). Low-cost volcano surveillance from space: case studies from Etna, Krafla, Cerro Negro, Fogo, Lascar and Erebus. *Bulletin of Volcanology*, **59**, 49-64

Harris, A. J., Flynn, L. P., Dean, K., Pilger, E., Wooster, M., Okubo, C., Wright, R. (2000). Real-time satellite monitoring of volcanic hot spots. *Geophysical Monograph Series*, **116**, 139-159.

Harris, A., Ripepe, M. (2007). Synergy of multiple geophysical approaches to unravel explosive eruption conduit and source dynamics – A case study from Stromboli. *Chemie der Erde*, **67**, 1-35.

Harris, A.J. (2013). Thermal Remote Sensing of Active Volcanoes, A User's Manual. Cambridge University Press, Cambridge: UK.

Izbekov, P.E., Eichelberger, J.C., Ivanov, B.V. (2004). The 1996 Eruption of Karymsky Volcano, Kamchatka: Historical Record of Basaltic Replenishment of an Andesite Reservoir. *Journal of Petrology*, **45**, 11, 2325-2345.

Judd, J.W. (1881), Volcanoes. In: Kegan et al. (eds) What they are and what they teach. London.

Kamchatka Volcano Eruption Response Team (KVERT), (2013). Karymsky volcano: information, hazard synopsis and eruptions list, <http://www.kscnet.ru/ivs/kvert/volc.php?name=Karymsky&lang=en>

Larsen, J., Neal, C., Webley, P., Freymueller, J., Haney, M., McNutt, S., Schneider, D., Prejean, S., Schaefer, J., Wessels, R. (2009). Eruption of Alaska volcano breaks historic pattern: *Eos, Transactions, American Geophysical Union*, **90** (20), 173-174.

McNutt, S. (1996). Seismic monitoring and eruption forecasting of volcanoes: A review of the state-of-the-art and case histories. *Monitoring and Mitigation of Volcanic Hazards*, 99-146.

Miller, T.P., McGimsey, R.G., Richter, D.H., Riehle, J.R., Nye, C.J., Yount, M.E., Dumoulin, J.A. (1998). Catalog of the historically active volcanoes of Alaska. United States Department of the Interior, United States Geological Survey, Open-File Report 98-582.

Neal, C.A., Doukas, M.P., McGimsey, R.G. (1995). 1994 Volcanic activity in Alaska: Summary of events and response of the Alaska Volcano Observatory. United States Department of the Interior, United States Geological Survey, Open-File Report 95-271.

Neal, C.A., Casadevall, T.J., Miller, T.P., Hendley II, J.W., Stauffer, P.H. (1997). Volcanic ash: Danger to aircraft in the North Pacific. United States Geological Survey Fact Sheet 030-97. <http://pubs.usgs.gov/fs/fs030-97/>.

Neal, C.A., McGimsey, R.G., Girina, O. (2004). 2002 Volcanic activity in Alaska and Kamchatka: Summary of events and response of the Alaska Volcano Observatory. United States Department of the Interior, United States Geological Survey, Open-File Report 2004-1058.

Neal, C.A., McGimsey, R.G., Dixon, J.P., Cameron, C.E., Nuzhaev, A.A., Chibisova, M. (2011). 2008 Volcanic activity in Alaska, Kamchatka, and the Kurile Islands: Summary of events and response of the Alaska Volcano Observatory: U.S. Geological Survey Scientific Investigations Report 2010-5243, 94 p., available at <http://pubs.usgs.gov/sir/2010/5243> .

Ozerov, A., Ispolatov, I., Lees, J. (2001). Modeling eruptions of Karymsky Volcano. *Journal of Volcanology and Geothermal Research*, **122** (3-4), 265-280.

Patrick, M., Harris, A., Ripepe, M., Dehn, J., Rothery, D., Calvari, S. (2007). Strombolian explosive styles and source conditions: insights from thermal (FLIR) video. *Bulletin of Volcanology*, **69**, 769-784.

Rosi, M., Bertagnini, A., Landi, P. (2000). Onset of the persistent activity at Stromboli Volcano (Italy). *Bulletin of Volcanology*, **62**, 294-300.

Siebert, L., Simkin, T. (2002). Volcanoes of the world: an illustrated catalog of Holocene volcanoes and their eruptions: Smithsonian Institution, Global Volcanism Program Digital Information Series GVP-3, <http://www.volcano.si.edu/gvp/world/>.

Simkin, T., Siebert, L. (1994). Volcanoes of the world [2nd edition]: Tucson, Arizona, Geoscience Press, 349 p.

Steinbeck, C., Fuller, A. (2004). Map In: Atlas of Pacific Salmon: The First Map-based Status Assessment of Salmon in the North Pacific (by . Augerot, X.). State of the Salmon Consortium.

Van Manen, S.M., Dehn, J., Blake, S. (2010). Satellite thermal observations of the Bezymianny lava dome 1993–2008: Precursory activity, large explosions, and dome growth. *Journal of Geophysical Research: Solid Earth*, **115**, B08205, doi:[10.1029/2009JB006966](https://doi.org/10.1029/2009JB006966).

Waythomas, C.F., Prejean, S.G., Schneider, D.J. (2008). Small volcano, big eruption, scientists rescued just in time: US Department of the Interior online publication *People, Land, and Water* preprint.

Waythomas, C. F., Scott, W. E., Prejean, S. G., Schneider, D. J., Izbekov, P., Nye, C. J. (2010). The 7–8 August 2008 eruption of Kasatochi Volcano, central Aleutian Islands, Alaska. *Journal of Geophysical Research: Solid Earth (1978–2012)*, **115**(B12).

Webley, P. W., Dehn, J., Lovick, J., Dean, K. G., Bailey, J. E., Valcic, L. (2009). Near-real-time volcanic ash cloud detection: Experiences from the Alaska Volcano Observatory. *Journal of Volcanology and Geothermal Research*, **186** (1), 79-90.

Wright, R., Flynn, L. P., Garbeil, H., Harris, A. J., Pilger, E. (2004). MODVOLC: near-real-time thermal monitoring of global volcanism. *Journal of Volcanology and Geothermal Research*, **135**(1), 29-49.